University of Hertfordshire
Faculty of Science, Technology and Creative Arts

MECHANICAL BEHAVIOUR AND CORROSION OF INTERSTITIAL-FREE STEEL TO ALUMINIUM ALLOY SELF-PIERCING RIVETED JOINTS

JOHN IOANNOU

A thesis in partial fulfilment of the requirements of the University of Hertfordshire for the degree of Doctor of Philosophy

The programme of research was carried out in the School of Engineering and Technology, University of Hertfordshire

September 2009

ABSTRACT

The overall aim of the project is to examine the rivetability of new steels and to investigate the mechanical behaviour of self-piercing riveted (SPR) aluminium-steel hybrid structures for automotive applications. Interstitial Free Steel (I.F.) of 1.2 mm thickness was joined to Aluminium 5754 of 2 mm thickness and Aluminium 5182 (coated and uncoated) of 1.5 mm thickness.

The work began by initially conducting a quality assessment of the various joints that were produced in order to establish the optimum conditions for joining the various sample combinations to be investigated. A relationship was established between the head height and the interlock distance on the one hand and between the interlock distance and the lap shear strength of samples. It was also established that for higher lap shear strength, it is preferable to use the stronger material (I.F. steel) as the pierced sheet and the weaker material (5182) as the locked sheet. However, the results showed that this rule could not be applied for predicting the fatigue behaviour of SPR joints between I.F. steel and 5182. An investigation of the fatigue failure mechanisms was undertaken and possible reasons for this behaviour are discussed. The influence of fretting was also investigated by using scanning electron microscopy and reported.

The fatigue behaviour of Dual Phase (DP600 + 5182) SPR joints was investigated. It was observed that the position of fatigue crack initiation differed with the maximum applied load. An explanation for this observation was provided by considering the failure mechanism of the samples under different load levels. The study also showed how fretting led to the initiation of fatigue cracks.

The corrosion behaviour of (I.F. steel + 5182) samples was investigated by conducting tests in a salt spray according to the ASTM B117-97 standard. Three types of corrosion were observed; galvanic corrosion, differential aeration corrosion, uniform corrosion and are discussed. The weight change with time was monitored and was used to describe the

corrosion behaviour. The lap shear strength was measured as a function of corrosion time. The presence of the corrosion product within the overlap was observed to greatly influence the lap shear strength behaviour. A further study was carried out in order to examine the influence of the individual alloys on the corrosion of the SPR samples. In this part the potential influence of pulse current treatment on corrosion was also investigated and was observed to increase greatly the corrosion resistance of the I.F. steel. Principal findings for this observation are also provided.

This project would not have been possible without the continual assistance and guidance of my project principal supervisor Dr Andreas Chrysanthou and the very cooperative Dr Li Han and Dr Ian McAndrew.

Thanks are also extended to the School of Engineering and Technology, University of Hertfordshire for the financial support. I also express my thanks to the technician officers and computer analyst who offered their help during the experimental work as well as to the Alcan International Limited and Corus UK Limited for supplying the materials used for this project.

I would also like to take this opportunity to thank all my friends and family for the hours spent helping and listening to my stress throughout the writing-up of this project.

I would like to give many thanks to my lovely wife and beautiful daughter for their understanding and support giving me confidence throughout the completion of this project.

Last but not least, I would like to dedicate this dissertation to the memory of Dr Jim O'Sullivan who was one of my project supervisors and has regretfully passed away before the promised completion of this work.

CONTENTS

1. INTRODUCTION

2. LITERATURE REVIEW

3. EXPERIMENTAL PROCEDURE

4. EXPERIMENTAL RESULTS

List of Figures

List of Figures

List of Figures

List of Tables

List of Acronyms

AHSS: Advanced high strength steels

BH: Bake hardening steels

CP: Complex phase steel

DP: Dual phase steel

EDAX: Energy dispersive X-ray micranalysis

E.M.F: Electromotive force

FAM: Field analysis modeller

FE: Finite element

FSW: Friction stir welding

GPa: Giga Pascal

HAZ: Heat affected zone

HSLA: High strength low alloy steel

IF: Interstitial free steel

MIG: Metal inert gas

MPa: Mega Pascal

PEC: Pulse electric current

RSW: Resistance spot welded

SEM: Scanning electron microscopy

SPR: Self piercing riveting

TIG: Tungsten inert gas

TS: Tensile stress

TWI: The Welding Institute

YS: Yield stress

CHAPTER ONE

1. INTRODUCTION

Owing to environmental reasons, the automotive industry is beginning to use lightweight materials like aluminium (2.7 $Mg.m^{-3}$) for vehicle body applications thus replacing the traditional and heavier steel (7.8 $Mg.m^{-3}$). Meanwhile the steel industry has developed new steels that allow their use in thinner gauge, while retaining a high level of stiffness. Lightweight vehicles lead to reduced fuel consumption and fewer emissions. The usage of lightweight materials in place of steel requires new joining methods. Steel auto bodies are generally of monocoque construction, but nowadays manufacturers are introducing spaceframe vehicles made from steel or aluminium to which are attached lightweight panels of aluminium, new steels or plastics [1]. The research programmes of many automotive companies involve the use of a combination of new steels and aluminium for vehicle body applications, thus one of the new challenges concerns the joining of steel to aluminium.

The use of aluminium alloys offers a vehicle of lower weight and may lead to better fuel economy and fewer emissions, whilst the performance, comfort and safety are not compromised. Aluminium alloys have the advantage of high corrosion resistance, good formability and crashworthiness. In addition, the outstanding recyclability of aluminium alloys also poses a considerable attraction to manufacturers. The main benefits that aluminium properties introduce come along with the needs and requirements of the motor industry. Vehicle mass is a major influence on fuel economy and emissions and the vehicle body which is approximately 25-30% of the vehicle mass is a major opportunity for vehicle weight reduction. Aluminium car body structures can be designed and built with the same performance as steel with about one third less weight. In general, fuel consumption can be reduced by 5.5% for each 10% reduction in vehicle weight. Moreover, for every kilogram saved in vehicle weight, a reduction of 20kg CO_2 emissions can be achieved for a vehicle which covers 170,000 km in an average lifetime [2]. Bearing in mind vehicle safety legislation, environment and recycling pressures, emissions legislation, rising fuel and insurance costs, taxation and competition, aluminium and new steels are highly competitive materials for automotive applications.

The technology behind self-piercing rivets was originally designed for the construction industry more than 30 years ago. The first manufacturing application was the assembly of garage doors in Germany. Since then there has been tremendous growth in applications in a wide range of industries. This is directly attributable to the increase in joining dissimilar materials in production processes and the need for fatigue resistant joints in high-cyclical loaded structures. The fasteners have been slowly growing in popularity during the past decade, primarily due to the introduction of new materials, such as aluminium, high-strength steel, plastics and laminate steel [3]. However, the use of aluminium requires not only a different approach in car design, but also a new manufacturing technology including new joining methods [2].

European automotive manufacturers have been more willing to embrace the technology. For instance, automakers such as Audi AG (Ingolstadt, Germany) and Jaguar Cars (Coventry, England) use self-piercing rivets with a combination of adhesive bonding to assemble spaceframes in aluminium intensive vehicles. Audi's A8, the first generation of aluminium spaceframe vehicle first adopted this joining technique in its assembly. Following positive experience with the A8, the use of self-piercing rivets was increased by 40 % to a total of 1800 in the Audi A2, mainly to join sheet metal and extruded sections. At Jaguar, the first aluminium car was the XJ350 which employed 3300 rivets in its assembly. In addition to the application in car-body assembly, self-piercing rivets have also been used in truck assembly. Volvo used 42 self-piercing rivets to improve the fatigue strength of the FH12 cab. Therefore, SPR fulfils the need for an assembly process that meets the modern challenges of light construction required by the auto industry and other industries [2].

The SPR process is increasingly being used in applications requiring economical, high strength and high speed joining in a wide range of sheet materials. Although the process itself is not new [4], SPR has acquired new significance particularly in the automotive industry due to the current growing need to join materials which are inherently difficult to spot-weld [5, 6]. In recent years many manufacturers have moved to using dissimilar sheet and pre-finished metals and in particular aluminium alloys for both structural and non-structural components. As a result, the SPR process is seen as an effective alternative to resistance spot- welding [7, 8, 9]. The assembly speed, ease of automation

and environmental advantages have all assisted in the exploitation of the process into industrial applications.

SPR technology enhances structural reliability without the debilitating and hardening effects of spot-weld heating. Traditional fastening methods are not as advantageous or are impossible to use with some of today's new material joining requirements. SPR has also been identified as a means of joining steel to aluminium. The ability of SPR to join together a wide range of materials offers product designers the latitude to create lighter weight and stronger products with improved quality and increased manufacturing options.

Increasing interest in the fastening process has highlighted the need for research to provide greater information on the fastening behaviour and performance. Increased confidence in joint properties, process tolerance and reliability are required particularly within demanding performance and quality-sensitive industries.

Nowadays, automotive companies want to fasten together Steel with Aluminium but there is little information on the strength and on the corrosion behaviour of these joints. Furthermore there is hardly any reported work setting rules as to how to obtain optimum joints when joining together different alloys or alloys of different thickness.

Therefore, the aims of this project were to join together using SPR automotive steel aluminium alloys and to examine their quality in terms of lap shear strength and fatigue behaviour. In addition, the corrosion behaviour of such joints was also investigated. Three relatively new types of automotive steel sheet materials were used in the study; these were interstitial-free (I.F.) steel, high-strength low –alloy steel (HSLA) and dual-phase (DP) Steel. These steels were joined to two aluminium alloys, 5754 and 5182 (DP steel was only joined to 5182 alloy).

The project objectives were to:

1. Join together using SPR, the above mentioned steels and aluminium alloys.
2. Investigate the potential of measuring the head-height and interlock distance as a means to assess the behaviour of the SPR joints.
3. Investigate the lap shear strength and fatigue behaviour of the SPR joints.
4. Investigate the corrosion behaviour of the SPR joints.
5. Examine the effect of pulse current treatment on the corrosion behaviour of SPR joints.

There are a number of important aspects of the study. First of all there has been very little previous work in trying to understand what constitutes a good quality joint. The present study, therefore, aimed to examine whether there was a correlation between the head-height and the interlock distance. In addition, there has been very little published work on the fatigue behaviour of SPR joints between aluminium and steel alloys. It is well-known that the modelling to simulate the fatigue behaviour of SPR joints does not yield accurate data, primarily because there is a lack of understanding of the failure mechanisms. An investigation like the one presented here that examines the fatigue failure mechanisms is therefore important. Finally, an investigation of the corrosion behaviour of SPR joints was carried out as there has not been any previous published work in the open literature involving steel and aluminium alloys.

1.1 The self-piercing riveting process

Self-piercing riveting is a high-speed cold-forming process of joining together two or more sheets of material by driving into them a semi-tubular rivet. The joining stage consists of two distinct phases; the top sheet is pierced by the rivet which subsequently flares into the bottom sheet to provide an interlock. The entire process takes less than 1.3 seconds, depending on cylinder stroke and feed tube length.

There are four basic processes in setting a self-piercing rivet (Fig.1). First, the rivet is delivered to the placing head. Once detected, the materials to be joined are clamped together by the riveting tool. The rivet is then driven down, piercing the first material and any intermediate materials. The rivet forces the sheet material into a die and radially flares, forming a mechanical interlock. The rivet does not break through the bottom material [10].
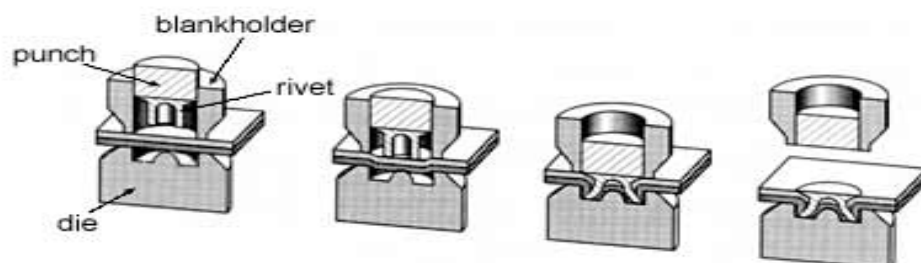
Fig.1 – Schematic representation of the self-piercing riveting process

Initially *setting* takes place where the rivet is forced against the material bringing the sheets together, causing marginal deformation prior to piercing (Fig.2). This is followed by the *piercing* process where the rivet, acting as a punch, shears through the first sheet and partially into the second against the anvil. *Bracing* then takes place. The rivet shank advances under the influence of the anvil and material build up. During this stage of the process the sheet material is deformed into the anvil profile and the hollow rivet shank. Finally, *clinching* takes place where the rivet shank end deforms and expands axially and radially within the lower layer of material against the reaction of the anvil. The rivet head is forced down against the sheet producing a locked, closed shape, fastening [10].
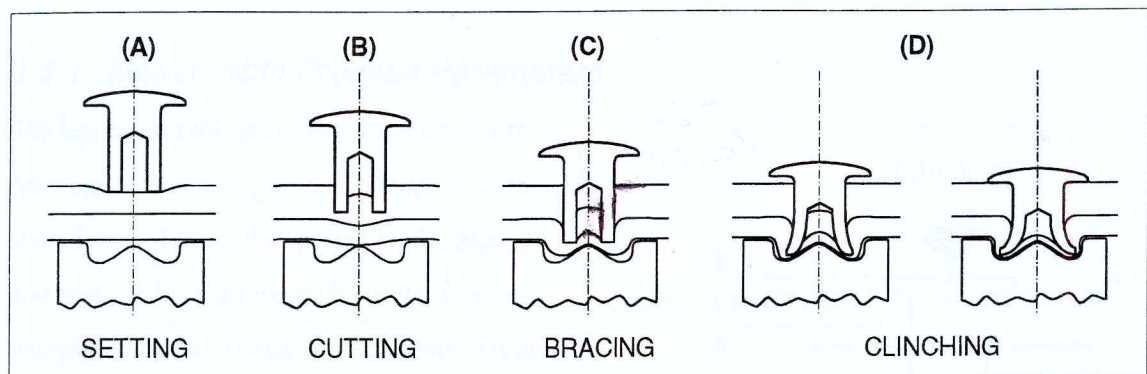
Fig.2 – Self-piercing process

The assembly equipment can be stationary, robotic or integrated into an assembly cell, depending on the production rates and the complexity of parts joined. Typically, equipment is comprised of a support structure engineered to undergo setting forces up to 50 kN, ensuring rivet alignment with the lower anvil or die. The force used to install the rivet is generated either electrically or hydraulically.

High setting forces are essential for rivet installation and critical to the alignment of rivets to the lower anvil. This requires the installation equipment structure to be extremely rigid to prevent excessive bending or deflection during the joining process, which would create a joint of substandard quality. The anvil is a solid cylinder with a cavity whose volume is similar to the material being displaced by the rivet.

Typically, the rivet setter and die are mounted in a C-frame with a hydraulic force application for setting the rivet (Fig.3), which must be large enough to allow access into the areas to be riveted. The placing head and die can operate independently as long as there is alignment during the placement of the fastener. Manual or robotic gun systems are available for relatively short-reach applications, whereas long-reach applications normally use fixed C-frames [11].
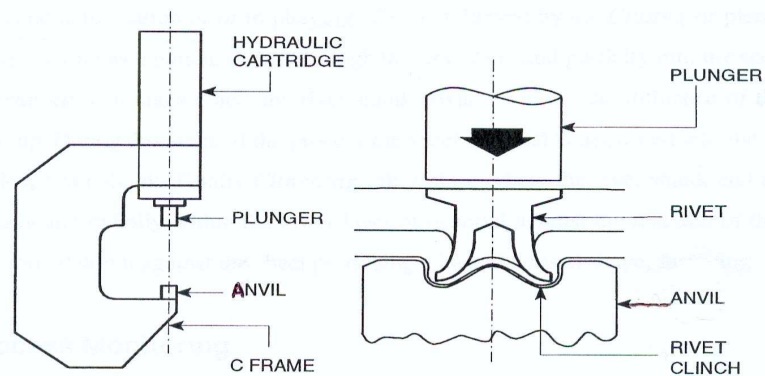
Fig.3 – C-frame with a hydraulic force

1.2 Possible conventional joining methods for aluminium alloys

1.2.1 Spot-welding

Spot-welding and arc-welding are the most popular conventional joining techniques in the automotive industry. Spot-welding has been the principal joining process for decades in steel vehicle structures. However, the quality of spot-welds for aluminium alloys may be poor. In addition, there are other concerns due to the short electrode life and the requirement of higher manufacturing capital.

Aluminium easily reacts with oxygen in the atmosphere and forms an oxide film on the metal surface giving protection to the metal from corrosion. However, according to Patrick [12], the substantially higher melting point of this oxide film requires significantly higher resistance heating to break it down in order to allow weld formation to take place. Coupled with the high electrical and thermal conductivity of aluminium alloys, nearly three times the current and two times the electrode force are required for welding bare

aluminium compared with welding bare steel. Consequently, the electrode life for aluminium alloy spot-welding is 2.5 to 5 times lower, compared with the electrode life for the spot-welding of mild steel. However, the welding time for aluminium alloys is only a quarter to half the time that is required to weld the same thickness of steel, due to the lower melting temperature. In addition, more accurate control of the welding parameters is required compared with steel, due to the effect of the surface oxide and surface roughness as well as the very narrow plastic range of aluminium. Auhl [13] reported that these critical variables led to poor welds that could occur at random and any time. It is obvious that the shorter electrode life requires more investment in the electrode. Apart from this, the different requirements on current and electrode force make the equipment which is used in the automotive production lines for steel spot-welding unlikely to be used for aluminium alloys. The investment in the development of new equipment for spot-welding aluminium alloys is considerable. Therefore, employing the technique for aluminium is likely to be much more expensive. These factors have therefore impelled manufacturers to look for alternative joining techniques.

1.2.2 Arc-welding

Metal Inert Gas (MIG) and Tungsten Inert Gas (TIG) are the two main processes of arc-welding used by industry. In automotive manufacture, the process has been well-automated and has significant advantages in steel structure fabrication. However, the process requirements for welding aluminium are extremely difficult.

The high thermal conductivity of aluminium requires an intensive and localized heat source, while it's relatively large coefficient of thermal expansion demands a high welding speed to minimize the distortion. Polmear [14], Gingell [15] and Barnes [16] reported that the surface oxide film, which has a high melting point, needed to be removed or it might become entrapped and form inclusions in the weld bead. In addition, very low hydrogen content was required due to the high solubility of this gas in molten aluminium, otherwise, weld porosity occurred after solidification. Furthermore, the environmental issues related to oxide fumes, arc-eye and the requirement of intensive energy, presented difficulties for arc-welding of aluminium alloys. Additional costs were thought to be inevitable to improve the process and protect the human operator from the hazardous environment.

Therefore, in order to adapt the process for aluminium, further development is necessary in order to minimise the disadvantages and facilitate the application of the process in service. There is growing interest in other joining techniques for aluminium due to the notable disadvantages of the conventional joining methods. Many studies have examined the suitability of other joining methods and explored new joining techniques. As a result, new joining techniques have been developed.

1.3 New joining techniques for aluminium alloys

Laser welding, friction stir welding and mechanical fastening as well as adhesive bonding are the new joining methods that are considered as candidates for joining aluminium in the automotive fabrication and assembly.

1.3.1 Laser welding

Two main types of lasers can be considered for sheet metal joining. They are CO_2 lasers and Nd: YAG lasers. According to Jones [17], laser welding offered many advantages for joining sheet materials, such as a lower overall heat input which resulted in very little thermal distortion, a higher welding speed and a smaller heat affected zone. Barnes [16] also reported that the potential for automation and the inherent flexibility of the system made laser welding more attractive. However, high surface reflectivity, high thermal conductivity and for some alloys, low melting point constituents, low viscosity in the liquid phase and the presence of the surface oxide layer, are the main difficulties encountered by laser welding process for aluminium. Therefore, Jones [17] suggested that a high power density and a high welding speed are necessary to avoid limited penetration depths, an irregular shape and a rough appearance. Apart from these, the relative expense of capital equipment and the consumable items, such as the shielding gas, must be taken into account. In addition, according to Barnes [16], the risks of accidental injury whilst the laser is in operation and damage to the eye, which can result from exposure to some laser beams, also needed to be considered. Further work on real aluminium components is necessary in order to assess the performance of laser-welded assemblies in service.

1.3.2 Friction stir welding

Friction stir welding (FSW) was invented at The Welding Institute (TWI) in 1991. It is a solid phase process and particularly suitable for joining lightweight sheet materials, such as aluminium, copper, lead and plastics to produce straight-line welds. According to Stephan [18] and Waldron [19], the process has a number of advantages including low cost, low power demand, good appearance of the weld bead and no emission of fumes. In addition, as a solid-phase weld, many of the problems associated with liquid-phase welding aluminium alloys are avoided. The surface oxide layer can be effectively broken and dispersed throughout the weld due to the weld action. However, as a new joining method, FSW limitations still remain. Besides a relatively slow process rate, Stephan [20] also reported that two components being joined together need to be clamped rigidly onto a backing bar due to the high pressure involved in the process in order to avoid the two pieces being forced apart, whilst a hole left at the end of each run has to be filled. In addition, for some aluminium alloys, post-weld heat-treatment is required to optimise the properties in the joint area and this is not a practical solution for many applications. Therefore, further development is necessary.

1.3.3 Adhesive bonding

Adhesive technology can be an alternative method for joining aluminium alloys. Compared with other joining techniques, such as welding and mechanical fastening, adhesive bonding can reduce stress concentrations and is more flexible and versatile, in addition to its ability to seal joints against moisture. Furthermore, according to Tavakoli [21], the process can save weight, reduce cost and is capable of joining dissimilar materials. However, the adhesive joints are inherently weak in peel and vehicle design would need to take account of this, particularly with regard to crashworthiness. Additionally, the long-term durability of adhesive joints and the effects of weathering and eventual water ingress are not clearly understood. Furthermore, the environmental issue in connection with adhesive dispensing is also a significant area of concern. Therefore, Barnes [16] has reported that adhesive bonding is less competitive in the domain of joining techniques for the automotive industry. In spite of this, adhesive bonding has been used by the automotive industry to join together aluminium alloys.

However, the relatively low peel strength that is achieved by adhesive bonding has prompted automotive manufacturers to use SPR as a backup. SPR also help to keep the adhesively joined structure together until the adhesives fully cure as well as in case of failure of the adhesive.

1.4 Benefits of self-piercing riveting

Unlike conventional riveting, self-piercing riveting does not require a pre-drilled hole because the rivet makes its own hole as it is being inserted (Fig.4). This brings great benefits in terms of production cost reduction and ease of use compared to conventional riveting [22].

The increasing use of coated, lightweight and high-strength materials, such as galvanised or pre-painted steel and aluminium has led industries to re-examine traditional methods of assembling components. As welding of these materials is difficult or impossible, and assembly using conventional rivets is slow and costly, the benefits of a process that combines high joint integrity with rapid assembly times become obvious. Joining takes place in one operation, simplifying assembly and reducing costs while providing a strong, reliable joint. Self-piercing rivets also emulate the results and quality of spot welding without many of the risks, such as toxic fumes, sparks and noise. Also, they boast static strengths similar to, or better than, spot welding along with superior fatigue performance. Self-pierce riveting is a clean, simple, fast and consistent cold-forming operation. There is no need for punching, cleaning or special treatment of material substrates, reducing component and installation costs. In a single operation, self-piercing rivets join multiple layers of similar or dissimilar materials with varying thicknesses. These materials include rolled, cast and extruded metals, moulded and sheet polymers, nylon, and other durable types of webbing and fabric. The result is a compact, highly stable, corrosion-resistant bond impermeable to gas, water and other external fluids.

The SPR process offers several benefits to assemblers. It can join dissimilar materials, such as plastics and aluminium, and hard-to-weld materials, such as coated sheet metal. It can also join three or more layers of material. Compared with spot-welding, it produces better joints in both aluminium and high-strength low-alloy steel.

Spot-welding has been the dominant method to join automotive mild steel structures. This method is fully automated and fast and in the case of mild steel structures it gives a joint of high integrity. However, in the case of aluminium, spot-welding has many disadvantages. Spot-welding for aluminium requires very high currents as a result of the high electrical conductivity of the metal. The high reactivity of aluminium tends to result in degradation of the copper electrodes. In addition the oxide layer which forms on the surface of aluminium tends to form a relatively poor spot-weld joint with a poor fatigue resistance. These disadvantages have led to a need for alternative joining processes when using aluminium alloys for automotive body applications. These processes are a combination of adhesive bonding and self-piercing riveting. While adhesive bonding provides a strong joint in comparative terms the peel strength is rather weak. SPR has therefore been introduced to provide a higher peel strength. SPR has two additional functions, to hold the adhesively bonded structure in place while the adhesive cures and to act as a back-up in case of failure of the adhesive bond.

Self-piercing rivets have the same static tensile and peel strength as spot welds, but twice the fatigue life [38]. Process monitoring can be integrated with self-piercing technology to verify that every joint created is of high quality. Longer fatigue life and higher joint quality repeatability can reduce the number of fastening points required over spot welds in certain applications.

Unlike spot welding, self-piercing rivets do not generate heat. This is important when using materials that degrade in thermal processing. Spot-welding also can destroy coatings on steel, leaving it vulnerable to corrosion. Self-piercing rivets do not alter metallurgical properties like welding can. Moreover, the fasteners are compatible with galvanized and coated surfaces, minimizing damage and eliminating recoating or replanting, unlike spot welding. Self-piercing systems do not require extensive monitoring equipment or smoke exhaust equipment associated with welding. High joint strength allows the end user to reduce the number of fastening points, further reducing manufacturing cost while maintaining a consistent quality product.

Fig.4 – High speed sheet joining process in which a semi-tubular rivet is set using a punch & die to flare the rivet within the lower sheet, no pre-existing hole is required

Typically, a self-piercing rivet is more expensive than a similar size squeeze or buck rivet. However, because the rivet insertion is an automated process, whereas for bucking and squeezing is a manual process, the in-place cost is generally less. Compared with threaded fasteners and pin-and-collar fasteners, self-piercing rivets are less expensive. Coupled with the automated insertion, they result in a lower cost assembly method.

The cycle time for a self-pierce riveting system is generally the same as spot-welding steel and the same, or less, than spot welding aluminium. It takes 1.3 seconds for a complete rivet and feed cycle at a 30 millimetre tool opening.

Self-piercing rivets are also environmentally friendly. The joints are cleaner and quieter compared with other ways of joining metals, such as welding. The process does not produce any harmful fumes or smells.

Despite the potential advantages of self-piercing riveting, there are number of barriers to widespread exploitation of the technology. These include low awareness, limited joint performance data, restricted design and application information and a need to develop equipment and quality procedures for high volume production [23].

1.5 Assembly applications

A typical steel-body automobile has 3,000 to 5,000 spot welds. But the increasing use of high-strength, thin-sheet steels, aluminium and composites has led to alternative joining processes in applications where fatigue strength and joint reliability are required. Self-pierce riveting fulfils the need for an assembly process that meets the modern challenges of light construction required by the automotive and other industries.

The growing use of mixed materials has made the automotive industry think beyond traditional spot-welding in structural parts. Automotive applications planned or in production include hoods, doors, trunk lids, tailgates, seat rails, side-impact bars, window and sunroof frames, truck cabs, car body frames, A and B-pillars (Fig.5) [106].

Fig.5 - The Chevrolet Corvette Z06 aluminium structure uses self-piercing rivets for assembling some stamped pieces together, for example the B-pillar

1.6 Self-piercing rivets

The use of SPR and Self-piercing rivets made of medium-carbon steel, boron-treated steel, stainless steel and other materials are attracting more and more attention from the auto industry (Fig.6). Rivets made of steel are used to join together aluminium alloys and stainless steels and to join aluminium or steels to plastics [24] Rivets often provide joints that are stronger than conventional spot welds used to fabricate auto bodies, which means that fewer joints are required. The fact that the metal does not have to be perforated prior to riveting means fewer production steps and greater economies. Like welding riveting also

can be combined with adhesive bonding for improved jointing. The rivets themselves come at a cost, however, their use can create small projections in the substrate materials that may be of concern to the designer or product engineer.

Semi-tubular				Split
Split		Full-tubular		
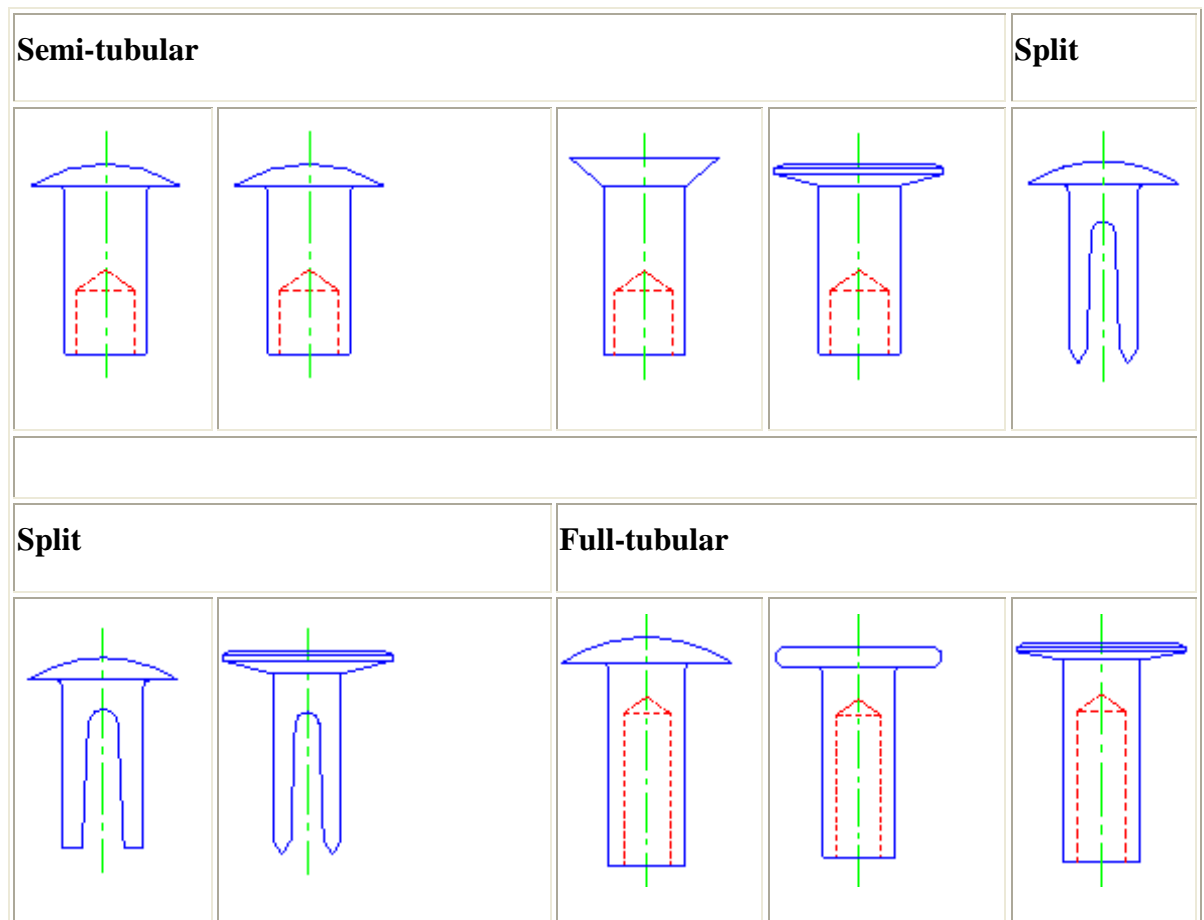
Fig.6 – A range of different types of rivets

A semi-tubular type is the basic form of a self-piercing rivet, which is made of wire material by a multi-blow cold-forming process. The material for rivet manufacture is limited by its ability to be cold-formed, but it can be hardened up to 550 Vickers. A standard specification BS EN 10263 of wire material is used for the formation of the rivets, which are then heat-treated to achieve the required properties. The proportions of the head diameter poke diameter and poke depth are dependent on the rivet shank diameter [2].

Shank Length: The length of the rivet shank is selected based on the thickness of the material to be joined. As the joint thickness increases the rivet length also has to increase in proportion. However, the rivet shank must not break through the lower sheet because of the requirement of good visual quality.

Surface Coating: The external surface of the rivet was protected by a coating to prevent galvanic corrosion.
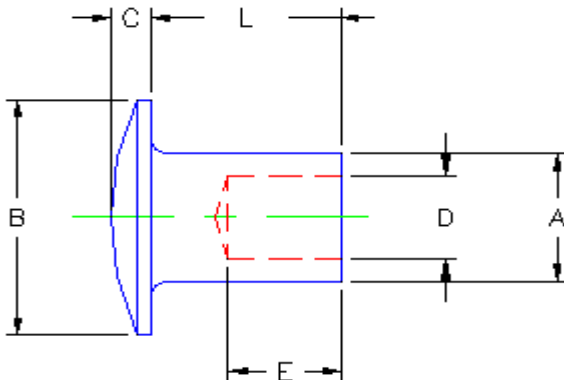
Fig.7 - Body diameter(A), head diameter(B), head height(C), hole

diameter(D) and hole depth(E) of the rivet

A self-piercing rivet is tubular by design with a partially hollow shaft (Fig.7) .This allows the rivet to pierce through the material it is going to join without pre-drilling any holes. After piercing the top panel, the rivet radially expands into the bottom panel.

Fig.8 – Various types of special rivets

Special rivets and cold-formed parts are available to meet nearly any application requirement, including non-fastening applications such as pins, pivots, axles, contacts and knobs as well as other applications. As with standard rivets, these parts are available in a variety of materials and finishes (Fig.8).

All rivet lengths, except countersunk head rivets, are measured from the underside of the head to the end of the shank. In applications involving countersunk head rivets, overall length is measured from the top of the head to the end of the shank. The length under the head must also be specified (Fig9).
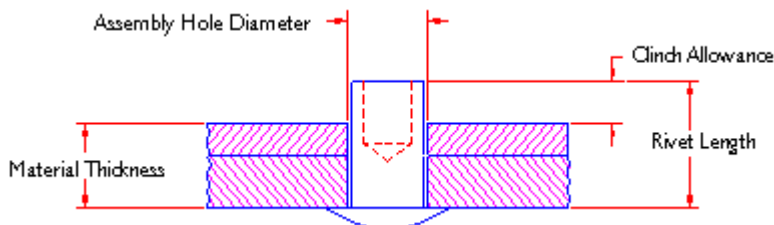
Fig.9 – A typical self-piercing joint measurement between two sheets of material

1.7 Anvil tooling

The purpose of the anvil is to provide a shaped cavity to accommodate the extent of deformation and to cause the rivet shank to flare during joint formation. The anvil shape affects both the piercing force and the flaring in the rivet shank and therefore, the joint strength. The selection of the anvil profile is dependent on the rivet dimensions and the material specifications. Therefore, a specific anvil design should be adopted for each different fastening application [2].

For experimental purposes, a number of standard anvils have been used that work effectively for the complete range of conditions selected.

1.8 Automotive steels

Mild steel has traditionally been the dominant material for automotive body applications. The main reason has been the low cost and availability of the material. In addition the joining, finishing and design technology of steel is well known. Furthermore, steel has an excellent combination of strength, stiffness, ductility, good sheet formability and a clear fatigue limit. However, steel has high density and poor corrosion resistance [25]. The need for lightweight materials has led to the automotive car makers to consider the use of aluminium in place of mild steel. The steel industry has as a consequence responded by developing new automotive steels including (HSLA, DP steels, I.F. steels). The advantage of HSLA and DP steels is that they exhibit superior mechanical properties to mild steel as shown in Fig.10 and Fig.11 and can therefore be used in thinner gauges, thus, reducing the weight of the car body without compromising its mechanical performance [25]. These steels are more expensive than mild steel and their relative costs are shown in Fig.12. The potential weight savings that can be achieved are shown in Fig.13 [25].

Some examples of new automotive steels include High Strength, Low Alloy (HSLA) or Microalloyed Steel, Dent Resistant Steels (Bake Hardening Steel, Rephosphorised Steel), Dual Phase (DP) and Complex Phase (CP) Steel (Fig.14). These mentioned high strength steels have a higher strength (YS and TS) than mild steel and are used for increased dent resistance (outer panels), thinner gauges (outer panels), increased structural performance (reinforcements), increased crash performance (front and end structures but lower formability and weldability)[25].

1.9 Useful worldwide information for steels
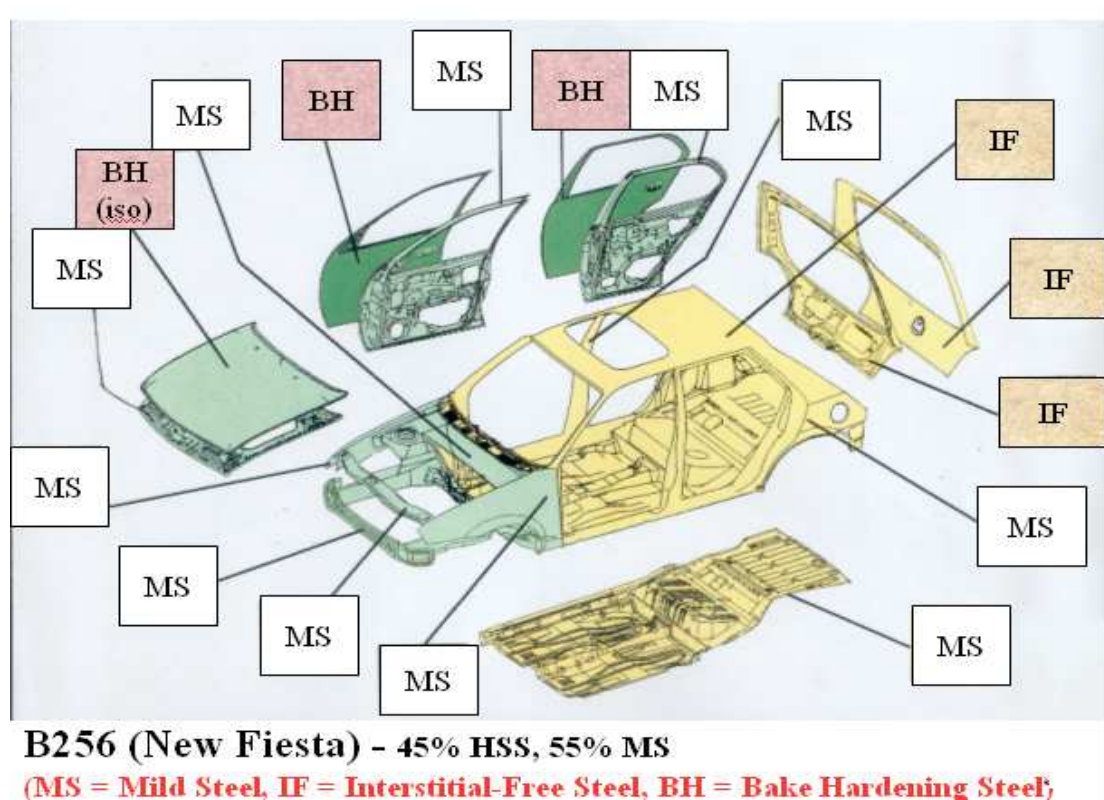
Fig.10 – A typical modern usage of high strength steels
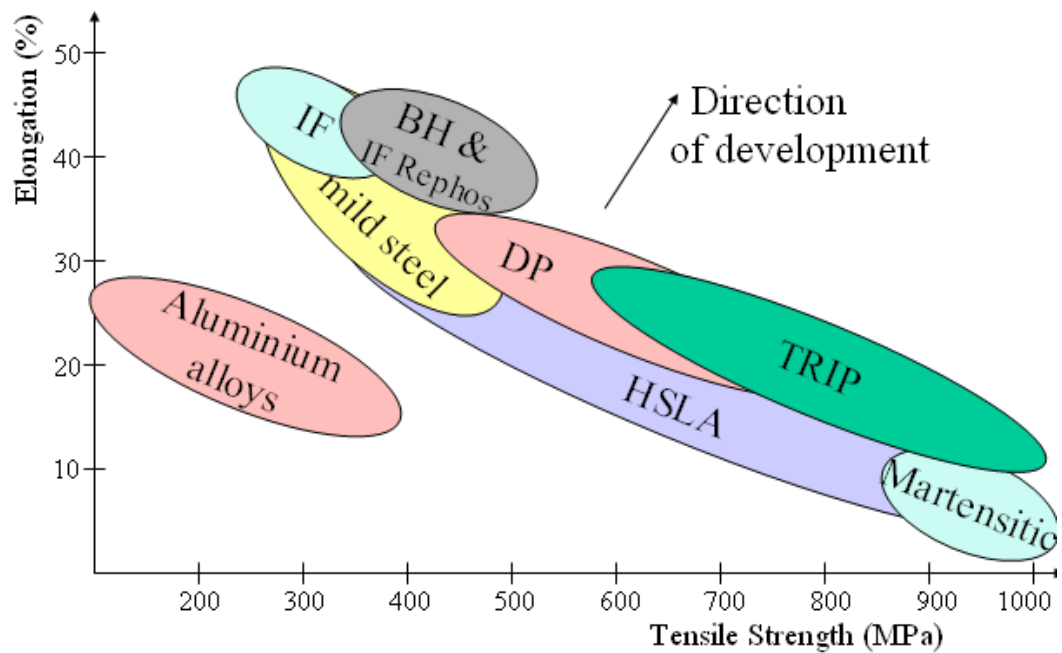
Fig.11 – Relationship between ductility and strength in automotive steels
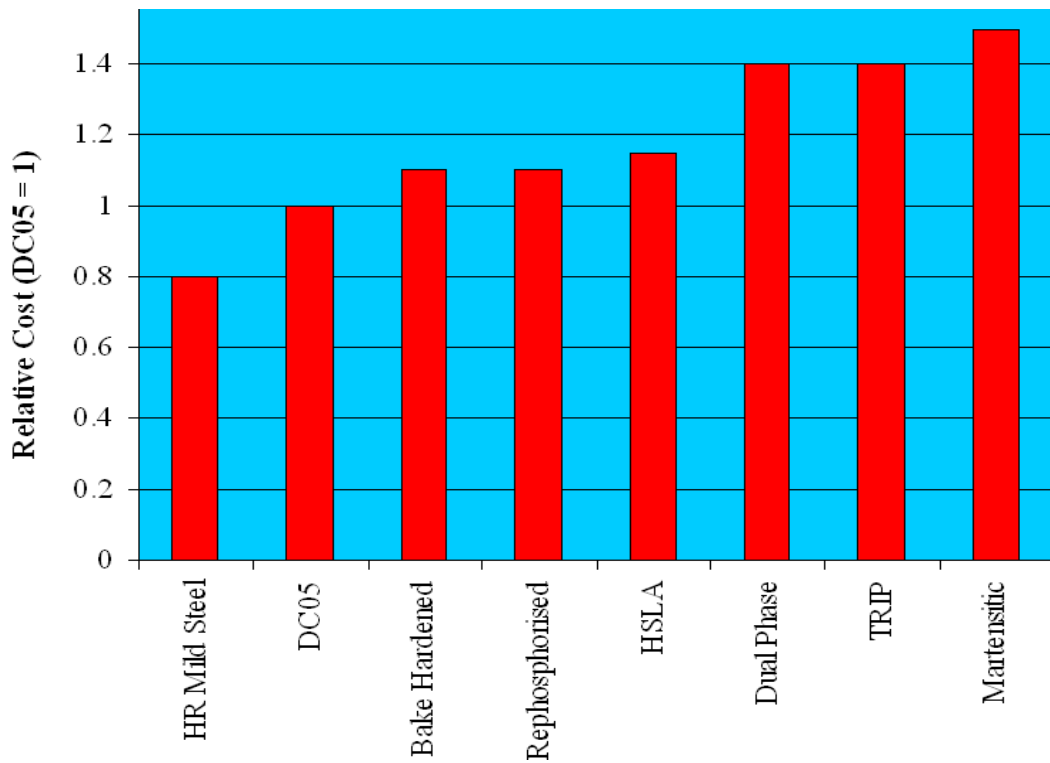
Fig.12 – Relative costs of automotive steels
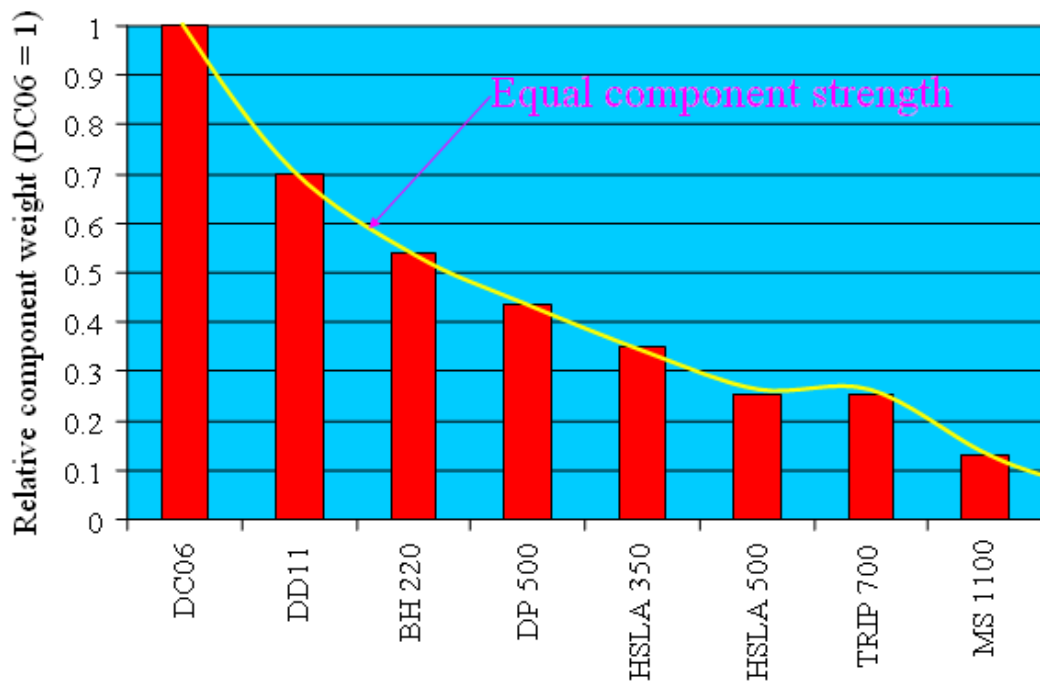
Fig.13 – Potential weight savings through the use of high strength automotive
steels
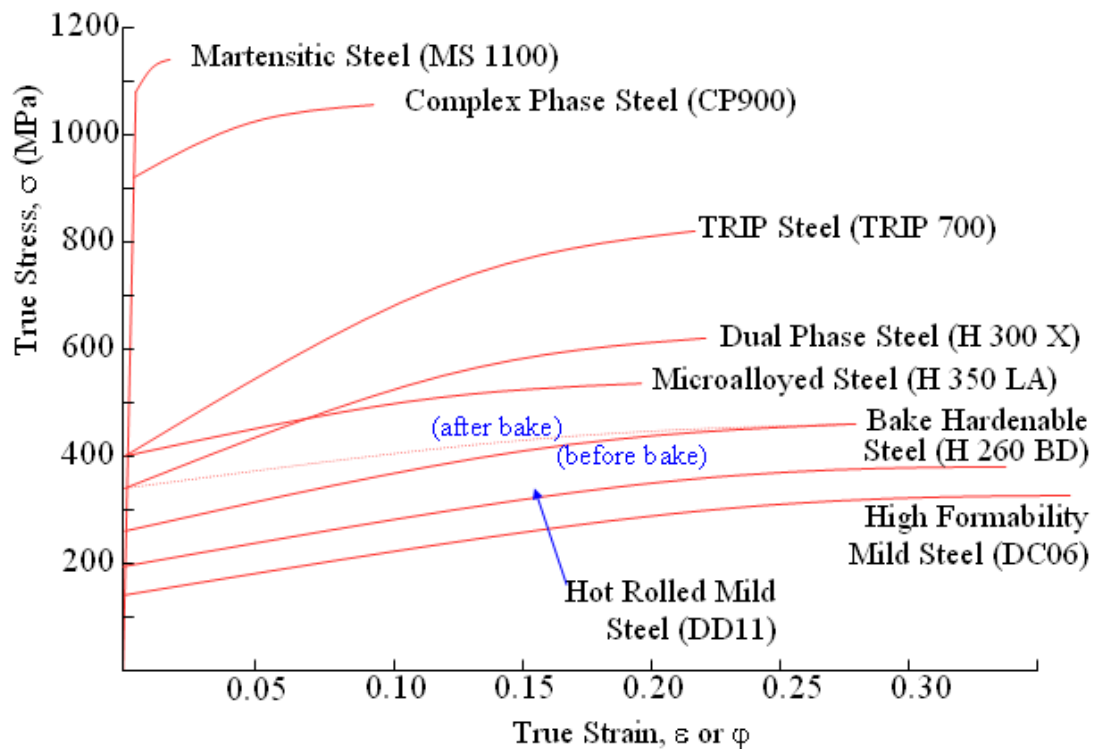
Fig.14 – Properties of automotive steels

1.10 Interstitial-free steels (I.F.)

In Interstitial-free steels, the interstitial elements (in this case carbon) are not allowed to dissolve in the iron (Fig.15). This is achieved by the addition of a small amount of titanium which reacts to form titanium carbide (TiC) thus preventing the carbon from dissolving in the iron. I.F. steels are highly formable and weldable with no yield point phenomenon with time and are suitable for hot-dip coatings. Furthermore, they can be applied to mild steel or high strength steels. Products include not only traditional hot and cold rolled steel sheets, but also coated steel sheets (for example, by zinc) for the automotive industry. Moreover, new versions of I.F. steels have been created, for example: high strength I.F. steel, stainless I.F. steels and so on [26].
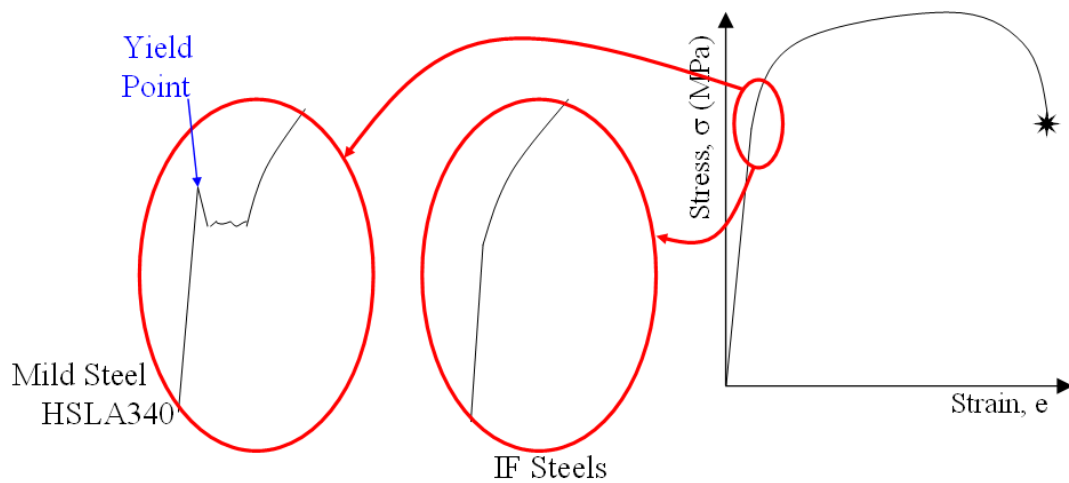
Fig.15 – Interstitial free steel yield stress line

The I.F. steel has an interstitial-free body-centred cubic ferrite matrix. After cold rolling with high level of deformation and annealing, this matrix transforms in a structure with a strong re-crystallization texture. This kind of texture is the reason for the high values of the average plastic strain ratio r, which is associated with a good formability [27].

1.11 HSLA (High strength low alloy steel)

High strength low alloy (HSLA) steels, or microalloyed steels, provide increased strength to weight ratios over conventional low carbon steels for only a modest price premium. Because HSLA alloys are stronger, they can be used in thinner sections, making them particularly attractive for transportation equipment components where weight reduction is important. HSLA steels are available in all standard shaped forms such as sheet, strip, plate, structural shapes, bar size shapes and special shapes [28].

These steels have high yield strengths, in the range of 300-700 MPa (with a corresponding range of formabilities) and are weldable   but are less ductile and formable and therefore suffer from more springback after forming.

However, their formability is sufficiently high to permit the application of these steels to many moderately simple press formed structural parts. These are the preferred steels for applications such as chassis parts (suspension arms, jacking brackets, subframes) and wheels, where weight savings of up to 25% have been managed. Their cost and availability are similar to rephosphorised steels [25]. Also a typical HSLA steel will include additions

of other elements such as Copper (0.2-1.5 %) which improves atmospheric corrosion resistance, Nickel (at least half the copper content), Nitrogen (0.003-0.0012 %) which contributes to strength and can improve weldability and finally Vanadium (up to 0.12 %) which increases strength without reducing weldability through grain refinement.

These steels (also known as microalloyed steels) have the similar ferrite plus (a small amount of) pearlite structure as normal low carbon steels, but they rely on the refining of their grain structure and formation of precipitates to strengthen them.

Since parts made from HSLA steels can have thinner cross sections than equivalent parts made from low carbon steel, corrosion of an HSLA steel can significantly reduce strength by decreasing the load bearing cross section. While additions of elements such as silicon, nickel, chromium, and phosphorus can improve atmospheric corrosion resistance of these alloys, they also increase cost. Galvanizing, using zinc rich coatings, and other rust preventive finishes can help protect HSLA steel parts from corrosion.

HSLA steels have yield strengths up to 552 MPa and cost about 24% more than a typical 234 MPa plain carbon steel. Because these alloys must compete with other structural metals they must be as inexpensive as possible. However, formulating and rolling steel that meets this cost requirement is not easy and the finished product presents a number of tradeoffs. For example, the increase in strength from 241 to 552 MPa may be accompanied by a 30 to 40% loss in ductility [28].

Improved formability HSLA steels were developed primarily for the automotive industry to replace low carbon steel parts with thinner cross section parts for reduced weight without sacrificing strength and dent resistance.

For some grades, formability and impact strength vary significantly depending on whether the material is tested longitudinally or transversely to the rolled direction. For example, bends parallel to the longitudinal direction are more likely to cause cracking around the outside, tension bearing surface of the bend. This effect is more pronounced in thick sheets. This directional characteristic is substantially reduced in HSLA steels that have been treated for sulphide shape control.

The strength of a cold-rolled steel increases as its grain size decreases, so a fine-grained product is desirable. Niobium additions of between 0.06 and 0.1% are capable of developing yield strengths up to about 350 MPa. Typical automotive applications

for these cold-formed HSLA steels include various chassis components such as suspension arms, cross members, bumpers, bracketry, side members and wheel discs, where weight savings of up to 25% have been managed [25].
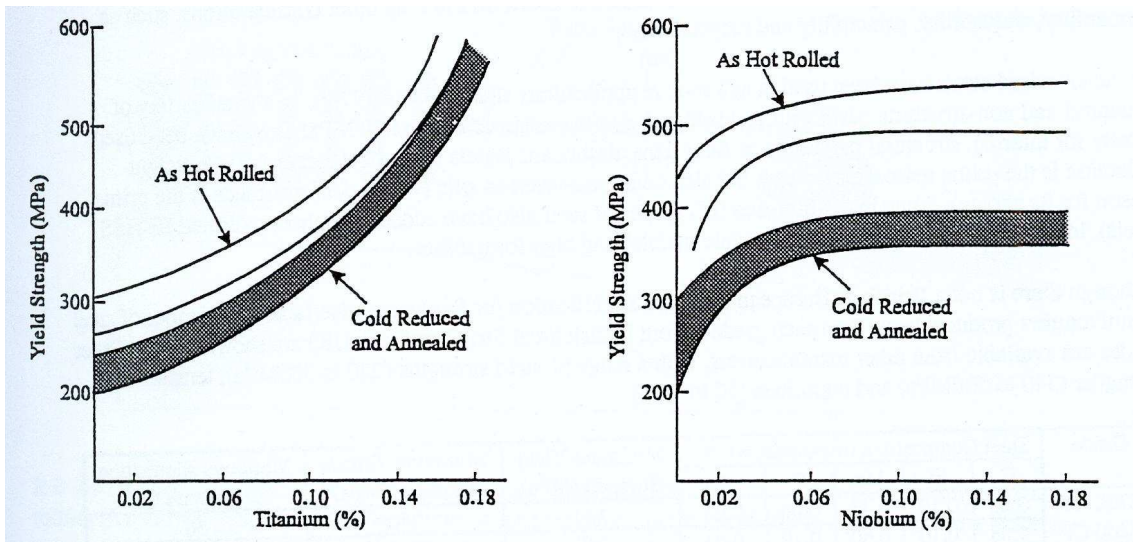
Figs.16 and 17 – Titanium and niobium % vs yield strength of HSLA as cold/hot rolled

HSLA steels are also supplied to the automotive industry as hot rolled products. Here, the strength comes from a combination of fine grain size and (to a much greater extents than with cold reduced steels) the dispersion of very fine precipitates. In these cases, the addition of between 0.04 to 0.1% Nb and careful control of the hot mill processing can generate yield strengths of up to 600 MPa. The formability of these hot rolled products is sufficient to allow their application in many press formed automotive parts, mainly internal structural parts such as suspension mountings and seals. The main problem with HSLA steels is their higher cost and lower formability, which has restricted their use up to now to brackets and chassis parts (Figs.16 and 17).

1.12 Applications of HSLA steels

Applications of HSLA steels include oil and gas pipelines, heavy duty highway and off road vehicles, construction and farm machinery, industrial equipment, storage tanks, mine and railroad cars, barges and dredges, snowmobiles, lawn mowers, and passenger car components. Bridges, offshore structures, power transmission towers, light poles, and building beams and panels are additional uses of these steels. The choice of specific high strength steel depends on a number of application requirements including thickness

reduction, corrosion resistance, formability, and weldability. For many applications, the most important factor in the steel selection process is the favourable strength to weight ratio of HSLA steels compared with conventional low carbon steels. This characteristic of HSLA steels has lead to their increased use in automobile components.

Typical passenger car applications include door intrusion beams, chassis members, reinforcing and mounting brackets, steering and suspension parts, bumpers and wheels. Trucks, construction equipment, off highway vehicles, mining equipment, and other heavy duty vehicles use HSLA sheets or plates for chassis components, buckets, grader blades, and structural members outside the body. For these applications, sheets or light gage plates are specified. Structural forms (alloys from the family of 310 to 345 MPa minimum yield strength HSLA steels) are specified in applications such as offshore oil and gas rigs, single pole power transmission towers, railroad cars and ship construction. In equipment such as power cranes, cement mixers, farm machinery, trucks, trailers and power transmission towers, HSLA bar, with minimum yield strengths ranging from 345 to 483 MPa is used. Forming, drilling, sawing and other machining operations on HSLA steels usually require 25 to 30% more power than structural carbon steels do.

1.13 Microstructure of HSLA steels

THE FCC TO BCC TRANSFORMATION IN HSLA STEELS
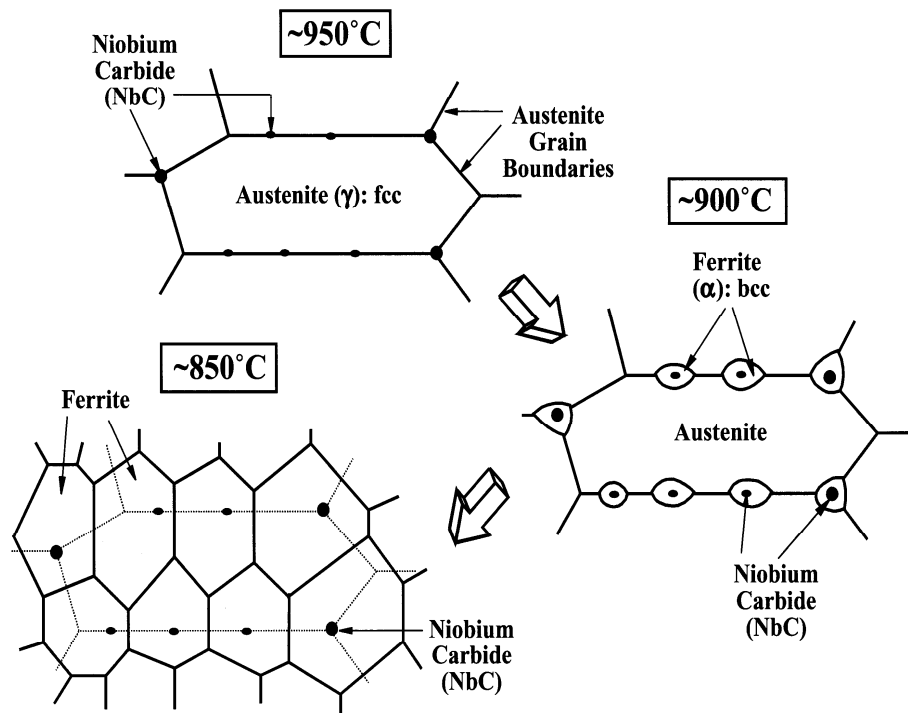
Fig.18 - Microstructure of HSLA steels

HSLA steels have a low carbon (0.15%C) content with around 1.3% Mn added, along with smaller additions (less than 0.1%) of carbide and nitride forming elements such as Nb, Ti and Ta. The resulting precipitates (typically NbCN, TiC) restrict the growth of ferrite grains during processing (slab reheating, hot rolling and annealing) to produce fine-grained and therefore stronger steel. Fig. 18 displays the grain refinement of HSLA steels as they are cooled down from the austenitic phase down to room temperature.

1.14 Dual phase (DP) steels

The microstructure of dual phase (DP) steels is comprised of soft ferrite and, depending on strength, between 20 and 70% volume fraction of hard phases, normally martensite.

Fig.19 displays the micro-structure of DP Steel with 600 MPa yield strength. The soft ferrite phase is generally continuous, giving these steels excellent ductility. When these steels deform, however, strain is concentrated in the lower strength ferrite phase, creating the unique high work hardening rate exhibited by these steels. The work hardening rate along with excellent elongation combine to give DP steels much higher ultimate tensile strength than conventional steels of similar yield strength. Fig. 20 illustrates this, where the quasi-static stress-strain behaviour of high-strength, low alloy (HSLA) steel is compared with that of a DP steel of similar yield strength. The DP steel exhibits higher initial work hardening rate, uniform and total elongation, ultimate tensile strength, and lower YS/TS ratio than the similar yield strength HSLA. DP and other AHSS also have another important benefit compared with conventional steels. The bake hardening effect, which is the increase in yield strength resulting from prestraining (representing the work hardening due to stamping or other manufacturing process) and elevated temperature aging (representing the curing temperature of paint bake ovens) continues to increase with increasing strain. Conventional bake hardening effects, of BH steels for example, remain somewhat constant after prestrains of about 2%. The extent of the bake hardening effect in AHSS depends on the specific chemistry and thermal histories of the steels. DP steels are designed to provide ultimate tensile strengths of up to 1000 MPa.
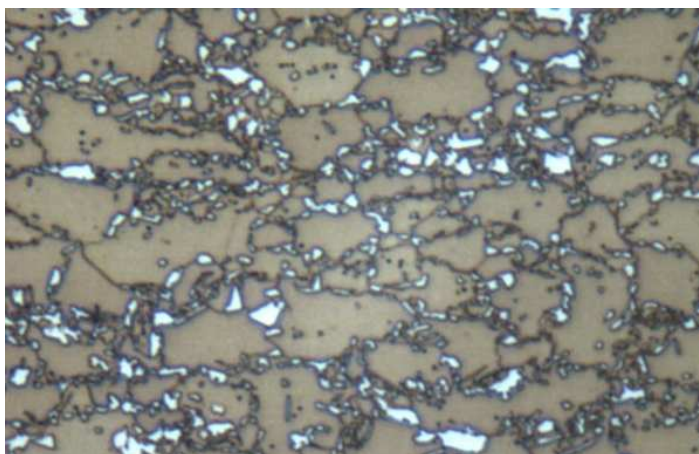
Fig.19 - Microstructure of the DP Steel of 600 MPa yield strength
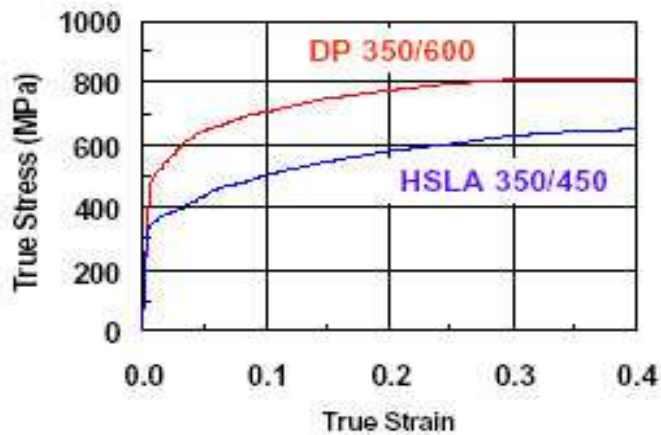
Fig.20 - Comparison of quasi-static stress-strain behaviour of HSLA 350/450

   and DP 350/600 steels

1.15 Aluminium for automotive body applications

The main properties which make aluminium a valuable material are its low density, good strength, recyclability, corrosion resistance, durability, ductility, formability and conductivity. Due to this unique combination of properties, the number of applications of aluminium continues to increase. The metal has become an essential in our daily lives. Aluminium has been used for automotive body applications for several years. This is in addition to its occasional use as bumpers, wheels and trim. There is now an average of 60-70kg of aluminium in new European cars, around 5% of a typical vehicle's weight. Roughly 30% of this is used in the chassis and engine, 50% in gearboxes and 15% in bodywork. In larger more luxurious cars the aluminium fraction tends to be higher.

Aluminium extrusions are used for bumper beams, side impact bars, seat and window frames, heat exchangers, aerodynamic spoilers, oil and hydraulic pipes and intakes manifolds. Aluminium sheet is used for water radiators and inner and outer panels. Forgings are less widespread, but applications include pistons, suspension components and wheels. The majority (85%) of automotive aluminium is at present to be found in the form of castings, for engine blocks and cylinder heads, manifolds, pumps, housings, transmission cases, wheels, hydraulic cylinders and subframes [25].

The main advantage of aluminium as compared to low-carbon steel is its lower density (aluminium = 2700kg/m^3, steel = 7800kg/m^3). However, the lower inherent Young's modulus (aluminium 70 GPa, steel = 205 GPa) of aluminium alloys make it necessary to increase its thickness in order to achieve comparable stiffness with steel. This offsets some of this weight advantage and has limited its use to mainly bolt-on applications. In addition its formability (by drawing, pressing, etc.) is not as good as that of steel and aluminium parts exhibit high springback. This has lead to the need to use tools specifically designed for use with aluminium, making the parts more expensive. An attraction of the use of aluminium is its corrosion resistance without paint, which makes it a good choice for vehicles operating under rough conditions where paintwork can be seriously damaged. The corrosion resistance of aluminium offers up to twice the lifetime of a conventional steel body, but contact with steel components in the structure can lead to galvanic corrosion and so must be avoided. The cost of aluminium is six to seven times that of steel, and is one of the main drawbacks to the increased use of aluminium in future vehicles. This is mainly due to the large amount of energy required to extract it from bauxite ore, 233 MJ per kg of aluminium compared with 25.6 MJ/kg for a medium strength steel. With any future increased impetus to improve the fuel economy of vehicles the use of high strength aluminium alloys to replace steel in structural situations would certainly be considered. As a general guide it has been found that the replacement of steel by aluminium halves the weight at double the cost [25].

The acceptance of aluminium as a candidate material for reducing car body weight does not lie in the material itself, but rather in the designs which meet the criteria of structural performance. The choice for the vehicle manufacturer is whether an all- aluminium design should be based on the conventional unitary (monocoque) structure or a spaceframe of extrusions with exterior panels attached to it. The theoretical weight savings possible with a pure spaceframe (around 40%) are slightly lower than with a monocoque structure (around 50%). The spaceframe approach offers lower tool costs for the extruded sections and fewer parts and joints [25].

A difficulty with the use of aluminium is in its fastening. The oxide layer that forms on its surface contributes to its corrosion resistance but also means that special procedures must be adopted for welding. Spot-welding is often inadequate with high strength aluminium alloys as the stress concentration it creates leads to cracking, and the material is more

easily marked by the welding electrodes. Improvements in spot-welding techniques have gone a long way to overcome this difficulty, but even more significant is the development in the application of structural adhesives based on heat-curing toughened epoxy resins. An adhesively bonded structure is stiffer than riveted or spot-welded ones as the adhesive covers and holds a much greater area of metal. By using a combination of spot-welding and epoxy adhesive bonding (spot-welding for initial part fixing and to provide peel stoppers, adhesive bonding to provide the majority of the fastening strength) it is possible to achieve large improvements in torsional stiffness [25].

Consideration of the properties of the main automotive aluminium alloys shows that their strengths are comparable to that of mild steel. The aluminium- magnesium wrought alloy series (5xxx series A1uminium alloys) containing 2.5 to 3.5% Mg have been the alloys most commonly used by the automotive industry over the past years (Land Rover panels). They have relatively good formability and weldability, good corrosion resistance but are not as strong or ductile as other aluminium alloys. Their formed surface finish is also rather poor.

Aluminium alloys can be divided into two major groups: wrought and casting alloys, depending on their method of fabrication. Wrought alloys which are shaped by plastic deformation (hot- and/or cold- working), have compositions and microstructures significantly different from casting alloys, reflecting the different requirements of the manufacturing process. Within each major group we can divide the alloys into two subgroups: heat-treatable and nonheat-treatable alloys. The 5xxx alloys contain two phases at room temperature, a solid solution of magnesium in aluminium, and Mg_2Al_3, a hard, brittle intermetallic compound. The aluminium-magnesium alloys are strengthened by a fine dispersion of Mg_2Al_3 as well as by strain hardening, solid solution strengthening and grain-size control. However, because Mg_2Al_3 is not coherent, age-hardening treatments are not possible [29].

CHAPTER TWO

2. LITERATURE REVIEW

2.1. Process monitoring

Methods of in process monitoring have been developed by universities and industrial companies where research has provided a greater understanding of the process and the development of computer-based process monitoring package Hill [30],Budde and Lappe [31], Budde [32], Bokhari [33], King [34], King [11], Taylor [35], ETI [36], Henrob Group [37]. The SPR process monitoring system usually comprises a PC with bespoke software and intelligent signal conditioning and communications hardware and transducers. The system records various process parameters (input speed, force etc.) and equipment conditions (desired input speed or force etc.). For "in-process" monitoring it is necessary to establish measurable parameters, which will give an overall picture and producible quality process whereas force-displacement has been established as a credible means of quantifying process quality. By measuring force and displacement directly at the riveting mechanism, it is possible to produce a characteristic curve relating to the joint formation through all of its phases. Fig.21 shows a typical four-step setting force/displacement curve for the SPR process Hou [38]. Since the shape of the force/displacement curve will alter with variations in the process parameters, the curve in effect becomes a fingerprint for all fastenings produced under the same process conditions. The fingerprint curve from an acceptably formed joint can be compared to every joint formed under the same process conditions King [11] and deliver 100% inspection as well as partial control of the fastening quality.
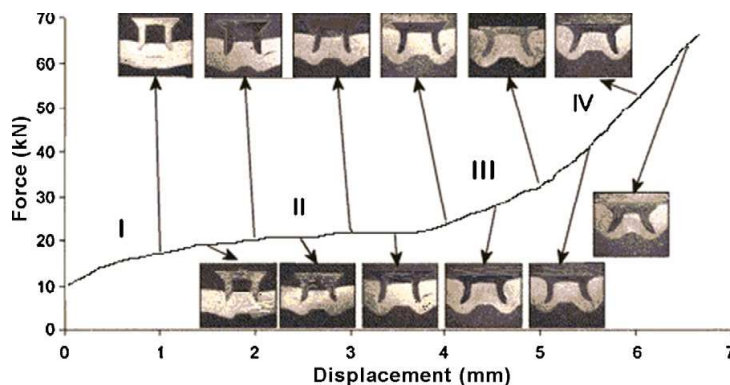
Fig.21 – A typical four-step setting force–displacement curve for a SPR process

2.2 Joint failure mechanics

SPR joints display similar failure modes to all other mechanically fastened joints. Five separate static modes of failure were established by King [11] who showed that the strength and flexibility of SPR joints were dependent on the failure mode of the joint. Westgate and Razmjoo [39] found that steel and aluminium joints exhibited different failure modes. On the same topic, Fu and Mallick [40] emphasised that fracture of the pierced sheet was the only failure system to occur during fatigue testing.

Recent investigations Chen [42] and Han [43] indicated that both rivet fracture and sheet material failure can occur during fatigue testing and this is influenced by fretting behaviour. The effect of secondary bending (an inherent feature of lap joint geometry) on single lap SPR joints was examined using strain gauge measurements by Han [43] and concluded that secondary bending contributed to the failure mechanism and led to a significant reduction in the fatigue strength. Razmjoo and Westgate [44] carried out a study by using so called "H" section specimens to eliminate the effect of the secondary bending. The results showed that the fatigue strength of "H" section specimens was much higher than the single lap SPR joints. With any joining technique, there is the potential for inherent corrosion problems and surface irregularities or crevices will exacerbate the problem. Crevice corrosion is a severe form of highly localised corrosion attack and results from the presence of an electrolyte in a crevice. Galvanic corrosion occurs when dissimilar, conductive materials are joined and the ingress of water forms an electrolytic cell. In this type of corrosion, the material is uniformly corroded as the anodic and cathodic regions moves and reverses from time to time. Howard and Sunday [45] presented extensive data comparing the amount of corrosion in SPR joints to commonly used resistance spot-weld joints and suggested that the amount of corrosion could be reduced significantly by using a polyester coating or cadmium plating. The same authors also found that the ultimate shear strength for both SPR joints and spot-welded joints showed no significant degradation after being subjected to a 90-day alternate immersion test. Galvanic corrosion can be avoided if the rivet is manufactured from the same material as sheets being joined. Preliminary work has been made on aluminium self-pierce rivets for use in the construction of aluminium vehicles Bazdresch [46]. The rivets were produced by sintering as this method readily allows the use of different alloys or mixtures of alloys. In addition, production of the rivets can be made in-house with control over the

whole manufacturing process. It also allows small batch production quantities, required for the initial stage of the research.

2.3 Static and fatigue behaviour of SPR joints

As SPR is considered to be an alternative to spot-welding, most research studies have focused on comparisons of the mechanical behaviour of joints manufactured by these techniques. Research in this area has shown that self-pierce riveting gives joints of comparable static strength and superior fatigue behaviour to spot welding, whilst also producing promising results in peel and shear testing Krause and Cherenkoff [47], Riches [48], Miller [49], Stegemann [50], Sun [51], Sun and Khaleel [52], Lennon [53] have carried out shear tests on four types of mechanical connections, these are self-pierce riveting, press joining, pop riveting and self-tapping screws, with sheet thicknesses 1.0, 1.2, 1.6, 2.0mm. Fig. 22 shows that self-pierce riveting produces a high-peak load, a high initial stiffness and high ductility compared to the other processes. A number of authors have shown that the static strength of SPR joints is some degree lower than that of resistance spot-welded (RSW) joints (Bonde and Grange-Jansson [54], Olivier [55], Booth [56], reported that for steel-to-steel joints the RSW joints exhibited failure loads more than 25% higher than those for corresponding SPR joints. However, when testing aluminium to aluminium joints in lap shear and T-peel configurations, no clear pattern was observed Booth [56]. For joints made with equal thickness substrates of 3mm, the strength of RSW joints was 10–20% higher than that of SPR joints. For joints made with equal thickness substrates of 1.2mm thick and for joints with unequal thickness substrates of 1.2mm and 3.0mm, the SPR joints were approximately 10–20% stronger than the RSW joints.
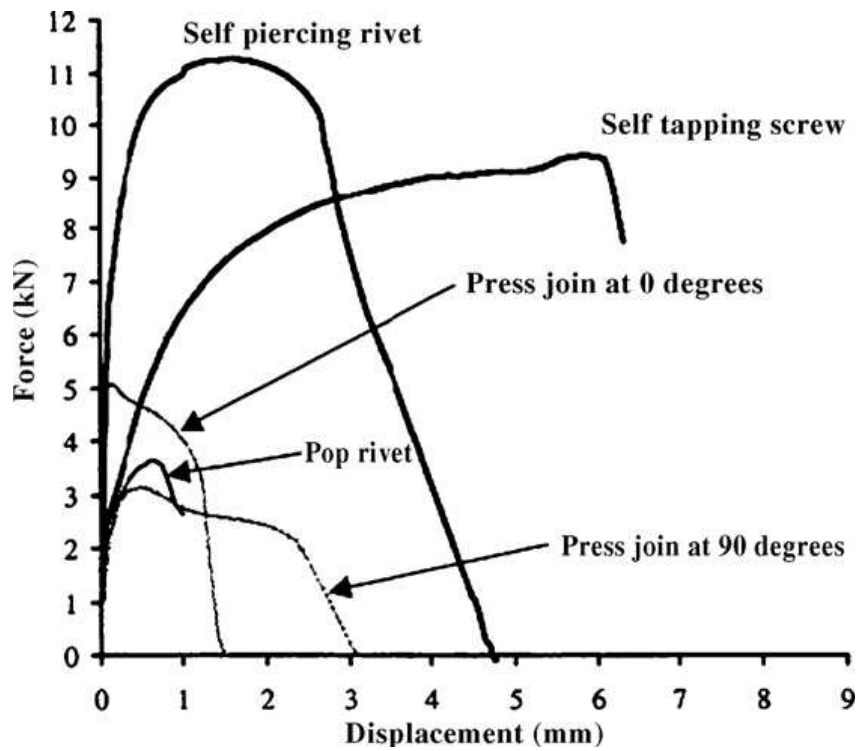
Fig.22 – Average load displacement paths of connections in 2.0 mm thick steel
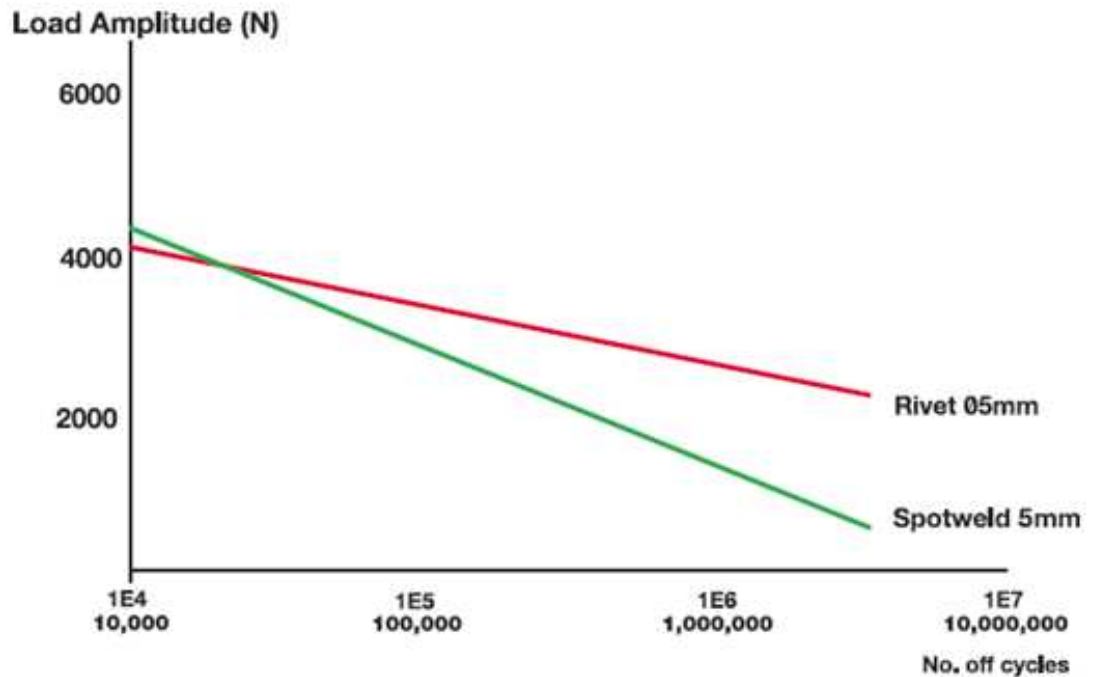
Fig.23 – Fatigue resistance comparison of spot-weld and SPR joints

Although the static strength of SPR joints is probably lower than that of spot-welded joints, it is generally believed that a satisfactory static strength could be achieved for SPR joints through suitable design of rivet and die (Westgate and Razmjoo [39], Riches [48]. The fatigue strength of the SPR joints has been investigated by a number of authors for a number of materials favoured by the automotive industry. All agree that the fatigue strength of SPR joints is superior to that of the spot-welded joints (Henrob Group [37], Fu and Mallick [40,41], Razmjoo and Westgate [39], Krause and Cherenkoff [47], Bonde and Grange-Jansson [54], Booth [56], Cai [57], Hahn [58], Sunday [59], Bonde [60], Litherland [61], Tileli [62], Li and Fatemi [63], Agrawal [64]. Fig. 23 compares the fatigue behaviour of different joining techniques. Mizukoshi and Okada [65] performed fatigue tests on SPR joints, clinched joints and spot-welded joints for some aluminium automotive body sheet materials, such as GC45-O, GC55-O and SG112-T4. The SPR joints were made by using 5mm long steel rivet, which were zinc or tin-coated. They compared joints by what they termed 'Fatigue Ratio' (defined as fatigue strength/tensile strength). The results show that SPR joints obtained higher fatigue strengths and generated fatigue ratios around 0.4, twice those of resistance spot-welded joints. The results also showed that although fatigue strengths of SPR joints decreased by about 30% after exposure to salt spray for 2000 hours, they were still equal to those of spot-welded joints and this was regardless of base materials. Researchers attributed these results to the fact that in spot-welded joints, the metal around the joint has been softened by the heat affected zone (HAZ) but in SPR joints, the substrate adjacent to the rivet has been work-hardened. Efforts have also been focused on enhancing the fatigue life of SPR joints through process optimisation. Jin and Mallick [66] found that ring coining improved the fatigue life of SPR joints in aluminium alloys and the degree of improvement may be dependent on the coining condition and the sheet thickness combination. A new method combining hydroforming and SPR was proposed by Neugebauer [67]. In contrast to the standard method, the riveting process is achieved without a solid die, instead high pressure fluid acts as the die during joining. The advantages of the Hydro-Self Pierce Riveting processes are the reduction of the number of processing steps and new design possibilities are feasible as joining in complex hydroformed units becomes possible and it also allows SPR to be used in inaccessible places Neugebauer [67]. Han [43] reported the influence of sheet prestraining on the static and fatigue behaviour of self-piercing riveted aluminium alloy sheet. Iyer [68] found that both the fatigue and static strength of double-rivet SPR joints to be strongly dependent on the "orientation combination" of the rivets and Hahn [58] have

carried out fatigue performances of a combination of SPR and adhesive bonding in 6016 aluminium alloy with various surface pre-treatments and coatings. Their study showed that the combination produced a much stronger joint than the rivets themselves in both static and fatigue testing. Some other researchers (Olivier [69], Madasamy [70, 71]. Weber [72], Hahn and Wibbeke [73], Anon [74], Whitworth [75] also showed additional benefits from hybrid SPR joints such as: (1) continuous, leak-tight joints, (2) higher strength joints, (3) increased joint stiffness, (4) improved peel and impact resistance, because crack growth away from the joint is arrested by the adhesive bond. In addition, it should be mentioned that neglecting 'hidden' factors such as secondary bending etc, as indicated by Razmjoo and Westgate [39], may result in the joint being under-strength.

2.4 Fretting wear in SPR joints

The presence of fretting can significantly degrade the fatigue life of mechanical fasteners. From tests on three different joints, Iyer [76] concluded that the fatigue crack initiation in SPR joints was accompanied by fretting wear at: (1) the rivet to sheet and (2) the sheet to sheet interfaces. The severity of fretting wear was found to increase with sheet thickness. Optical and scanning electron microscopy (SEM) was used by Chen [42] to investigate the fretting behaviour of SPR aluminium alloy joints. The fretting patterns at the interface between two sheets are shown in Fig.24. It was noted that fretting wear was initially patchy and layers of compacted debris were created as fretting continued. In a recent study, Han [43] report that the fatigue life of a joint was observed to be dependent on the fretting behaviour under different interfacial conditions.
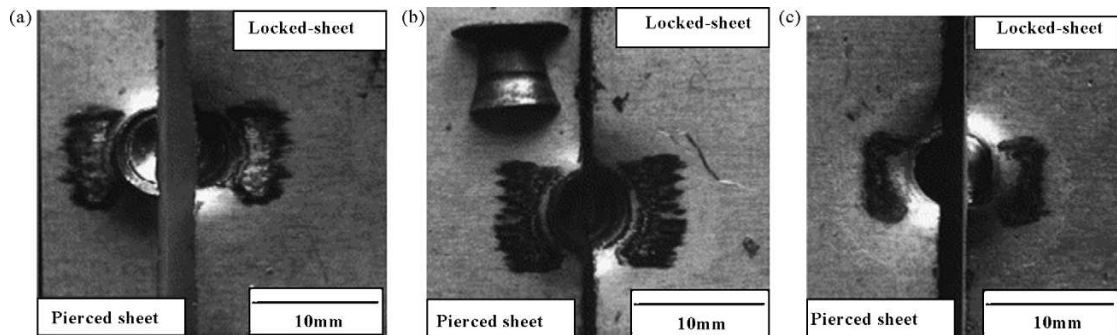
Fig.24 – Fretting regions at the interface between two sheets for: (a) 2.1×10^4 cycles at 4.5 kN, (b) 8.9×10^4 cycles at 4.5 kN and (c) 8.5×10^5 cycles at 2.7kN

2.5 Finite element analysis of SPR joints

The mechanical behaviour of SPR joints is not only influenced by the geometric characteristics of the joint but also the process parameters. It is very difficult to predict the static and dynamic properties of SPR joints although numerical modelling may provide a means to overcoming these problems He [77]. A basic FE model of the indentation of an SPR process was created and analysed using DEFORMTM-2D King [11]. This enabled initial calculations of the setting forces, displacements and component deformations to be compared with that of actual fastenings. The numeric simulation of the SPR process was extensively covered by Hahn and Dolle [78] in which a numerical model of the SPR process was made using the FE programme MSC.AutoForge. Good agreement was found between the experimental force/deformation curves and the corresponding simulations. Westgate [79] developed lightweight self-piercing riveting equipment using FE meshes of C-frames. These were generated using field analysis mod-eller (FAM) and analysed using the general purpose FE code ABAQUS. They suggested that 2D models were sufficient for the early design assessment, and 3D models were required to predict the stresses accurately and to refine the design. Crash testing of SPR of deep drawing and re-phosphorized sheet steels was simulated by Khezri [80] using the FE method. Westerberg [81] carried out FE simulations of SPR peel specimens. In a similar context, Stromstedt [82] performed FE analysis of SPR lap shear joint specimens. Iyer [68, 76] performed 3D FE analysis to evaluate the load induced local distributions of relative slip, contact pressure and bulk stress in joints.

This approach did not consider the residual stresses due to piercing. A FE method has been developed by Tang [83] for modelling the characteristics of SPR in the aluminium parts and structures subjected to impact. It relies on a combination of baseline curves and the universal formulation that predicts the SPR performance by considering the effects of different parameters. The method was applied to a full vehicle side impact analysis and achieved a good correlation with deformed mode and SPR separation. Sui [84] built a non-linear FE model to study the SPR process and found that the hoop residual stress has the greatest influence the mechanical properties of a joint. Kim [85] tried to evaluate the structural stiffness and fatigue life of SPR joint specimens, experimental and numerically (by FEM modelling in according with the FEMFAT guidelines) and found that even though the structural stiffness of an SPR joint specimen is roughly the same as other types of joints (e.g. RSW), the fatigue life is increased and reliant on substrate material and thickness. Atzeni et al. dealt systematically with numerical and experimental investigations of SPR joints Atzeni [86,87,88], producing detailed suggestions for the numerical modelling of SPR process parameters such as friction coefficients of the different interfaces and the value of the kinetic energy used in a quasi-static analysis. The riveting process has also been numerically simulated using the FE method, in particular LS-Dyna Porcaro [89, 90, 91] where a 2D axisymmetric model was generated. Additionally an implicit solution using r-adaptivity has been utilised. An extensive experimental programme on specimens made of 6060 aluminium alloy with two different temper conditions (T4 and T6) generated a database for the validation of numerical simulations. The results proved the feasibility of simulating the riveting process for different combinations of substrate material and rivet geometries Porcaro [91]. Following the success of the 2D model, an accurate 3D numerical model of different types of riveted connections (overlap or coach) subjected to various loading conditions was generated based on the results of the numerical simulation of the riveting process (Porcaro [90]. An algorithm was generated in order to transfer all the information from the 2D numerical model of the riveting process to the 3D numerical model of the connection. The model was validated against experimental results in order to prove the correct deformation modes and the force/displacement characteristics Porcaro [90].

2.6 Cost effects of SPR technique

The SPR process is extremely robust, simple and cost-effective even with the rivet consumable cost Patrick and Sharp [92]. Examples of this can be found in references Bonde and Grange-Jansson [54] and TWI [93]. In order to meet market demand for lower operating costs and higher payloads, the Volvo FH12 truck cabs have made extensive use of high strength steel to achieve a reduction of weight. However, traditional spot-welding techniques were disappointing when used to join these steels, in that the fatigue life of the RSW joint did not increase with the increased yield strength of the substrate. By using the SPR technique, fatigue life of the cab structure was improved greatly. With 42 rivets per cab and 150 cabs produced per day, the tooling investment costs (for the SPR equipment) were $43,000 higher than for spot-welding, but production savings of $244,000 per year were achieved. It is clear that the advantages and savings that Volvo achieved by adopting SPR technology far outweighed the initial increase in equipment cost. Following the success of this project, Volvo considered extending use of SPR to other applications in their range of heavy trucks. Varis [94] introduces a possibility of calculating and analysing the cost effects of joining techniques with and without an additional joining element (like rivets) during product manufacture. Varis compared clinching to SPR and concluded that (1) the additional joining element unit costs of the technique (including the cost of the joining element) was constant and (2) the additional tooling costs for riveting was insignificant and could be ignored. The total costs increased directly in proportion to the amount of joints for those techniques using an additional joining element. Fig.25 shows the basic cost difference between batch specific costs for clinching and SPR. By taking a size batch of 200,000 joints, lines a1 and a2 indicate that the tool service life for clinching and SPR is the same (55,555 joints). However, the author [94] took as the service life of the clinching tools to be 19,000 joints (line b). Under this situation, the total costs for clinching were calculated to be almost three times more expensive than SPR.
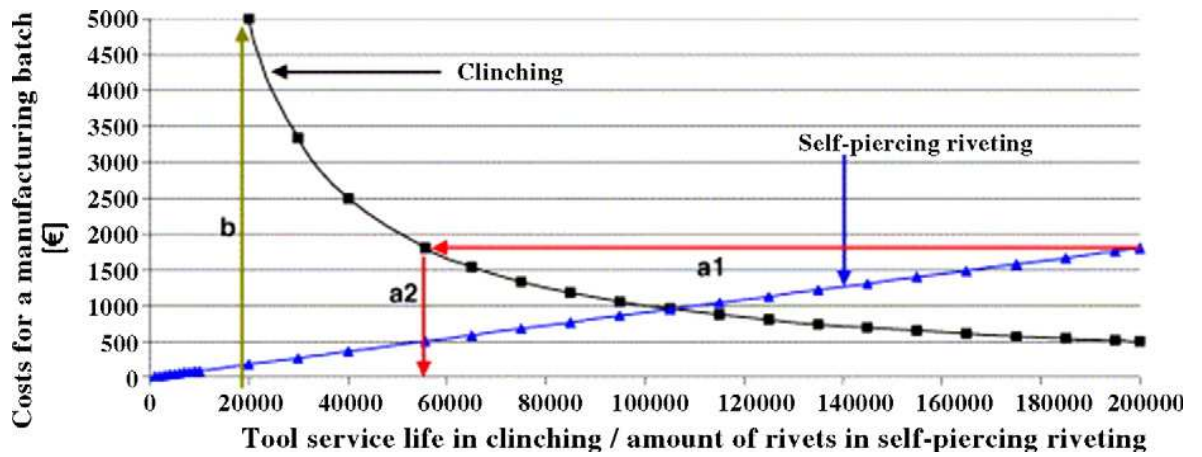
Fig.25 – Costs of a manufacturing batch comparing clinching tool service life and the
amount of rivets required for SPR

CHAPTER THREE

3. EXPERIMENTAL PROCEDURE

3.1 Preparation of the samples

The most important issue for any standard specimen is to be representative of the structural feature which is to be simulated. The lap-shear joint, which has a 0° angle, represents almost 50% of the total joint length in vehicles [2]. Additionally, there are no standards for the self-piercing riveted specimen geometry, therefore it was chosen to follow a specific specimen geometry in order to have the opportunity to compare the results of the experiments with work conducted in other groups like the University of Warwick, Jaguar and Landrover. All the fastenings were created between two sheets of material only, as this is the most common application in auto-body assembly. In order to be able to prepare the samples there was a need to cut all sheets in dimensions of 100 mm x 40 mm using a guillotine machine.

3.2 Materials used for the research study

The chosen materials were Aluminium 5754 with a thickness of 2mm and 1.5mm coated with a thin Cr-free wax, Aluminium 5182 (coated and uncoated) with a thickness of 1.5mm, IF (interstitial free) steel with a thickness of 1.2mm coated with a thin protective zinc and Dual Phase 600 Steel with a thickness of 2mm coated with a thin protective zinc. All of the materials were riveted at the International Automotive Research Centre of Warwick University. The usage of interstitial-free steel is likely to be used in the near future in automotive applications. The usage of aluminium 5754 and aluminium 5182 is currently used in automotive applications. Some of the properties of these materials along with their compositions are shown in Tables 1, 2, 3 and 4.

Table 1: Composition and mechanical properties of aluminium 5754

MECHANICAL PROPERTIES			
Yield Strength (MPa)	Tensile Strength (MPa)	Elongation	Hardness (Hv)
110	240	22%	63.5
%NOMINAL COMPOSITION			
Si	Fe	Cu	Mn	Mg	Al
0 – 0.40	0 – 0.40	0 – 0.10	0 – 0.50	2.60 – 3.60	Balance

Table 2: Composition and mechanical properties of aluminium 5182

MECHANICAL PROPERTIES			
0.2 % Proof Stress (MPa)	Tensile Strength (MPa)	Elongation	Hardness (Hv)
135	290	22%	65
%NOMINAL COMPOSITION			
Si	Fe	Cu	Mn	Mg	Al
<0.2	<0.35	<0.15	0.2 – 0.50	4.0 – 5.0	Balance

Table 3: Composition and mechanical properties of GA260 Interstitial free steel

MECHANICAL PROPERTIES		
Yield Strength (MPa)	Tensile Strength (MPa)	Elongation
260	400	36%
%CHEMICAL COMPOSITION		
C	Mn	Ti	Fe
0.02	0.25	0.30	Balance

Table 4: Mechanical properties of Dual-Phase 600 steel

MECHANICAL PROPERTIES		
Yield Stress (MPa)	Ultimate Tensile Strength (MPa)	Elongation
400	651	27%

3.3 Electrical self-piercing machine

The joining of the specimens was performed at the International Automotive Research Centre of Warwick University using a servo-electric machine, provided by Henrob UK Limited. The rivet setter and die were mounted in the C-frame which was designed to withstand the riveting loads and to allow access into the areas to be riveted. The machine could provide joints under different setting velocities. The setting velocity during the fastening process was recorded by a computer. The machine was equipped with various anvils and a setting platform which could target the position of the joint on the sheets. Moreover, the machine had a maximum nose to die gap of 170 mm, a total stroke of 250 mm and an electronic unit which could automatically or manually adjust the settings of the piercing. Fig.26 shows the servo-electric SPR equipment that was used to prepare the samples.

Fig.26 – Servo-electric self-piercing machine used for piercing the materials

3.4 SPR parameters used to prepare steel to aluminium joints

During the procedure of joining, different types of self-piercing rivets were used, combined with the appropriate die profile in order to optimize the characteristics of the joint. The selection of the anvil profile is dependent on the rivet dimensions and the material specifications [2]. After a number of trials the 36MnB4 type rivets were chosen to fasten together the sheets. These rivets have a countersunk head with shank diameter of 4.8 mm, a shank length of 7.0 mm and a mechanically deposited zinc-tin alloy surface coating.   The code of the anvil that was used was DZ0902050. The setting velocity, which was chosen after many trials with respect to material specification, material hardness and thickness as well as the rivet and anvil design, was 340 mm/min.

3.5 Quality assessment of selected joints

The quality of self-piercing riveted structures has to fulfil some "standards". The method that was used to assess the quality of the joints involved cross-sectioning of the joints at the middle and mounting them for microscopic analysis where a Leitz Metallux 11 optical microscope was used. The microscopic analysis include measurements of the interlock distance, head height etc.

The characteristics which represent a good quality joint are as follows:

1. Flushness of the rivet head
2. Symmetrical and properly flared rivet shank
3. No large gaps between the riveted sheets
4. Little distance between the top surface of the rivet and the upper surface of the sheet material
5. No breakthrough
6. No cracks in the rivet or the sheet material

3.6 Sample mounting and polishing sequence

The samples were hot mounted by placing them on the mounting machine chamber with 20g of coloured phenolic resin powder. The mixture was pressed under 20 MPa for 6 min at a temperature of 160^0 C and cooled inside the mounting machine chamber for 20 min. The product was a mounted sample in cylindrical form of 31.75 mm diameter. The polishing of the samples was achieved by a semi-automatic grinding/polishing machine Motopol 2000. The polishing had four stages and each stage needed the use of different polishing disc of different material and hardness combined with different polishing liquid, time of polishing, rotating speed of the disk, rotating speed of the adaptor which was carrying the samples and pressure that the samples were pushed on the polishing disk. These mentioned parameters of the polishing were chosen bearing in mind that the joints are hybrid (steel and aluminium), the rivet was made from steel and the portion of the material that should be removed from the top surface in order to have an effective shiny surface for microscopy observations. At the end of the process, the samples were ultra sonically cleaned in still water, swabbed with acetone for 3 minutes to

remove the unnecessary materials from the top surface and blow dried. The same procedure was followed for all samples and is shown in Table 5.

Table 5 – Sample polishing sequence used for the research study

SURFACE	SLURRY	PARTICLE SIZE	TIME (MINS)	FORCE (lbf)	WHEEL SPEED (RPM)	HEAD SPEED/ DIRECTION (RPM)
Silicon Carbide Paper (S.I.C)	H_2O	320 grit (46.2 μm)	4	12	220	120/ COMP.
Perforated Chemotextile Napless Cloth	-	9 μm Diamond	5	12	250	60/COMP.
Chemotextile Napless Cloth	-	3 μm Diamond	4	12	250	60/COMP.
Synthetic Rayon Short Soft Nap Cloth	-	0.06 μm Colloidal Silica	2.2	9	80	60/COMP.

3.7 Lap-shear tests

The lap shear tests were performed using the Avery Denison Testing Machine with a load capacity of 500 kN in Tension or Compression. For each fastening condition six samples were tested. The ultimate shear load was recorded to determine the shear strength of the joints. The failure mode was also assessed in order to establish the failure mechanisms of the self-piercing riveted joint. The geometry of a single-riveted lap joint specimen for the shear test is illustrated in Fig.27.

Load Capacity – 500 kN (Tension or Compression)

Type of specimen accommodated:

-Flat specimens: Max width =100 mm

Max thickness = 25mm
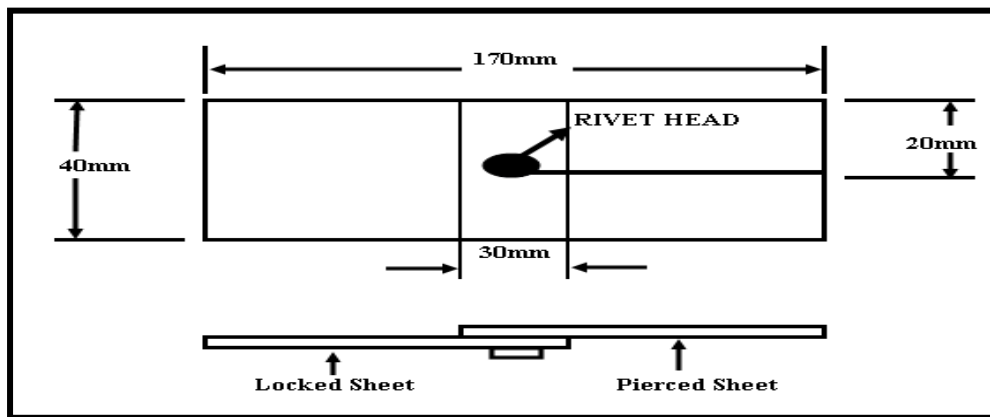
Fig.27 – Geometry of a single-riveted lap joint

The strain rate was calculated approximately at 10 mm/min.

3.8 Fatigue tests

The fatigue tests were performed in a closed-loop servo-hydraulic universal fatigue test machine with a load capacity of 200 kN. A constant amplitude sinusoidal waveform in tension-tension was chosen as the applied load with a frequency of 20 Hz. The maximum load (kN) vs number of fatigue life cycles was plotted on graphs. The maximum applied load ranged from 50% to 70% of the average ultimate shear load. The R ratio, which is the ratio between minimum and maximum load, was 0.1 throughout (ex: 0.45/4.5=0.1). Scanning Electron Microscopy was carried out using a CamScan CS44 microscope and a JEOL 57 microscope equipped with energy dispersive X-ray micranalysis (EDAX).

3.9 Corrosion tests

Single layers of IF steel of 1.2 mm thickness, aluminium alloys 5182 of 1.5 mm thickness and aluminium alloys 5754 of 2 mm thickness (dimensions of all samples were100 x 13 mm) were used to construct the SPR joints. They were joined together by rivets with a countersunk head supplied by Henrob Ltd. Both the I.F. sheets and the rivets had a zinc surface coating. Furthermore, four combinations of dissimilar sheet materials and multilayer were used such as: Aluminium SG-6111 (0.9 mm thickness) + Aluminium NG-5754 (1.5 mm thickness) + Aluminium NG-5754 (2 mm thickness), Aluminium

SG-6111 (0.9 mm thickness) + BH 300 Steel (1.5 mm thickness) + Aluminium NG-5754 (2 mm thickness), DP Steel 600 (2 mm thickness) + Aluminium NG-5754 (2.5 mm thickness) and Aluminium NG-5754 (0.6 mm thickness) + HSLA Steel (1.5 mm thickness) + Aluminium NG-5754 (2 mm thickness).

The samples were cleaned using a soft nail brush followed by treatment in an ultrasonic bath filled with acetone to remove any grease. The samples were then thoroughly dried by blowing hot air at them for 5 minutes. They were subsequently left to rest for 48 hrs before weighing to an accuracy of four decimal places. Corrosion was performed at $35°C$ ($±1.5°C$) in a salt-spray chamber using a 5% NaCl solution in distilled water (Fig. 28). The total time of exposure was 1000 hours. This treatment was carried out in hourly cycles. This involved the samples being subjected to a fog spray (salt spray) for 10 minutes at a flow rate of 0.8 litres/hr followed by 50 minutes of hot air (drying). The sequence was repeated every hour. Samples were removed at approximately 1000 hour for weight measurement and analysis after they were cleaned in an ultrasonic bath using distilled water to remove NaCl deposits and being washed with propan-2-ol and dried at $70°C$ in an oven.
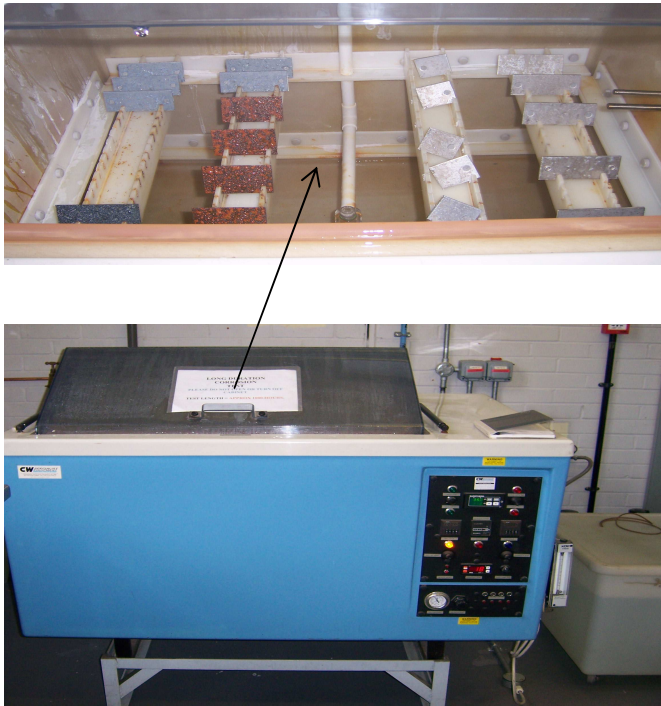
Fig.28 – Corrosion machine used for the research study

3.10 Pulse current treatment

Results of corrosion tests of some structure metals previously treated using pulsed electric current of high density are presented. According to the data obtained the treatment substantially influences the corrosion of metals. In the case of I.F. Steel and aluminium 5182 an increase of the corrosion resistance occurs.

The problem of corrosion of structural metals remains real because it is connected with considerable economic costs. According to various estimations, 10% to 30% of the annual production of iron is irreversibly lost due to corrosion every year [95]. Corrosion leads not only to loss of metal, but also to degradation of mechanical and physical properties and plasticity. This is the reason for the decrease in the lifetime of components sometimes leading to catastrophic failure. For example, 90% of failures in oil-field pipes take place due to corrosion damages; a similar situation occurs in ships [96, 97] and other structures. Taking into account the repair-and-renewal operations and anti-corrosion measures, the losses from corrosion in highly developed countries reach 10% of the national income [95].

Existing methods of metal and alloy protection from corrosion include coatings deposition, electrochemical methods of protection (e.g. cathodic method) and others. It is therefore understandable that there is considerable interest to develop new and more effective corrosion protection methods.

One of the common types of metal and alloy corrosion is electrochemical corrosion, which leads to damage in conductive environments (electrolytic solutions). In general, the electrochemical corrosion mechanism involves the appearance of short-circuited micro-galvanic elements on the metal surface with different values of e.m.f. as a result of the formation of anodic (with low electrode potential) and cathodic (with high electrode potential) zones [98]. These zones are generated because of differences in metal structure, surface roughness, existence of protective films and other factors. The difference in metal structure (difference of grain size and composition, crystal anisotropy, emergence of dislocations on the surface, existence of impurities, inclusions, non-uniform mechanical stresses) is one of the reasons activating corrosion processes. The role of mechanical stresses is important because under the influence of tensile stresses in the metal, anode zones can appear. These zones become the reason of development for corrosion centres [99]. It is known that pulsed electric current (PEC) treatment causes relaxation of mechanical stresses in metals [100-102], and also homogenization of their structure [103]. Based upon common considerations, these circumstances can serve as a basis for the creation of new technology of corrosion protection of metals.

PEC treatment of the samples was fulfilled using a pulsed current generator. Three electric current pulses were passed through each sample with a variety of amplitude such as 19, 24, 29, 34, 35, 41, 52, 53 and 75 kA. The amplitude of the electric current was chosen with the aim to compare the specimens with the same current density taking into account their different thickness (approximately 1.3 kA/mm^2, 2 kA/mm^2 and 3 kA/mm^2, respectively for each specimen group). Specimens were treated using three pulses with 1 min. interval and three pulses with 3 min. interval.

CHAPTER FOUR

4. EXPERIMENTAL RESULTS

4.1 Quality assessment of the joints

The work began by initially conducting a quality assessment of the various joints that were produced. This work was carried out in order to establish the optimum conditions for joining the various sample combinations to be investigated.

4.2 Tensile tests to examine the strength of the as-received materials

Tensile tests were carried out to measure the properties of some of the sheet materials used in the study. The specimen shape of the materials is shown in Fig.29. By using these data, stress/strain curves have been created and are shown in Figs. 30, 31, 32 and 33. The strain rate was 10mm/min.
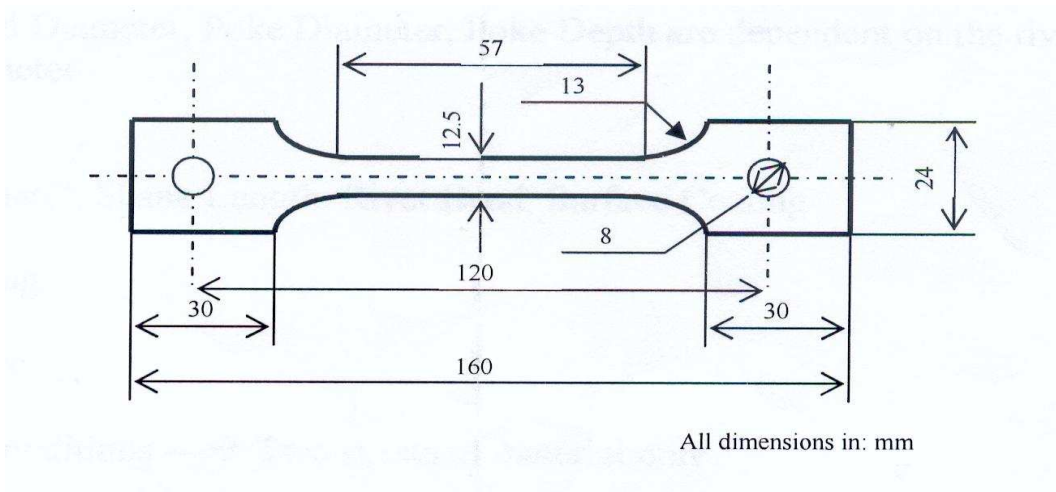
Fig.29 – Specimen shape of the materials used for the research study
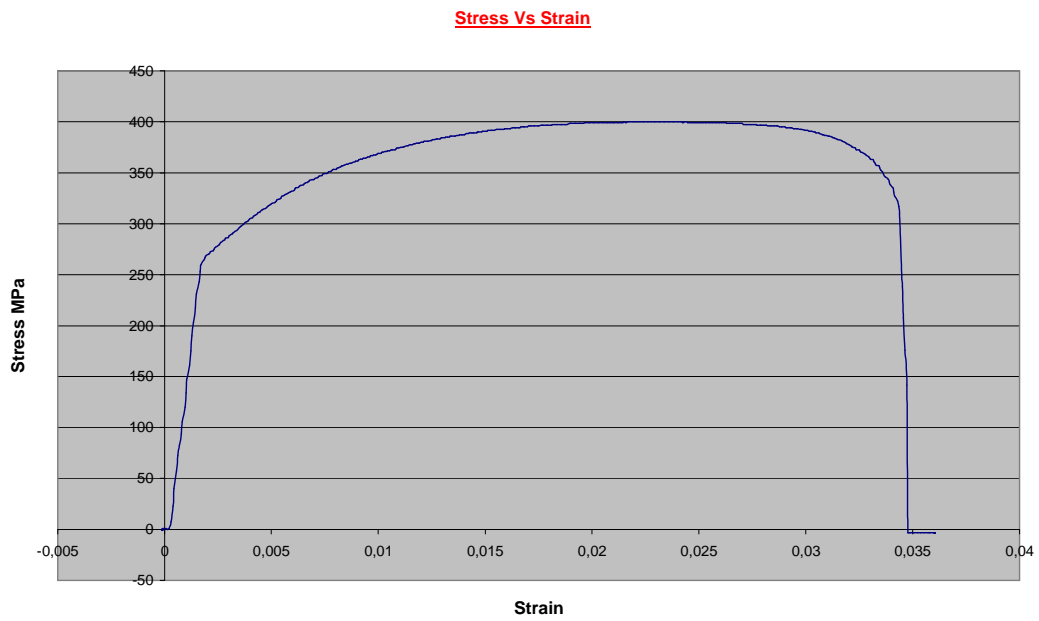
Stress Vs Strain

Fig.30 – Stress/strain curve for I.F. Steel
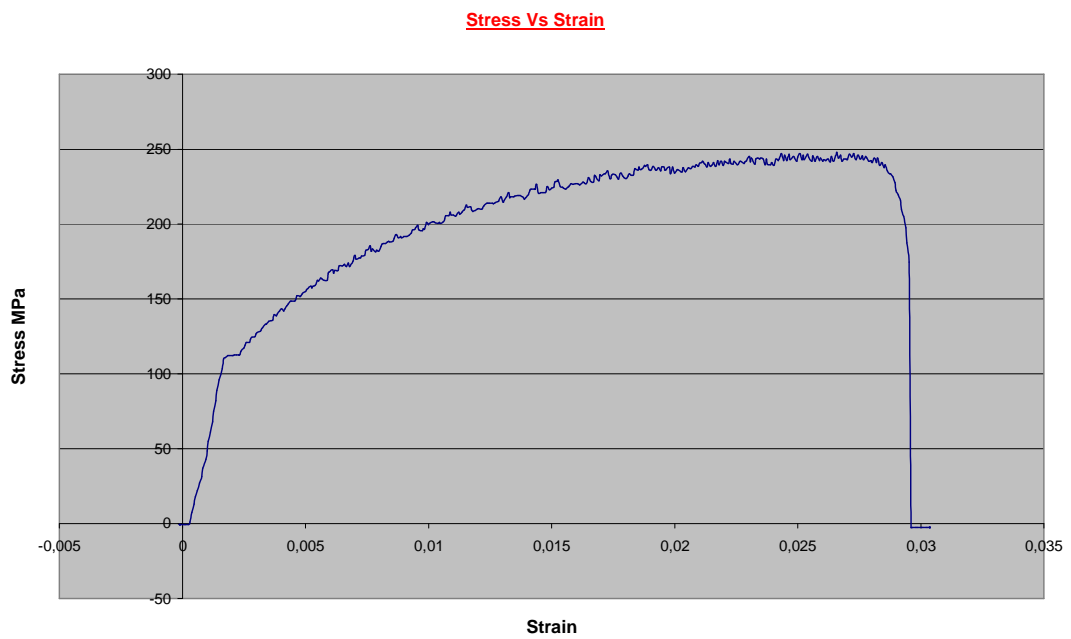
Stress Vs Strain

Fig.31 – Stress/strain curve for Aluminium 5754
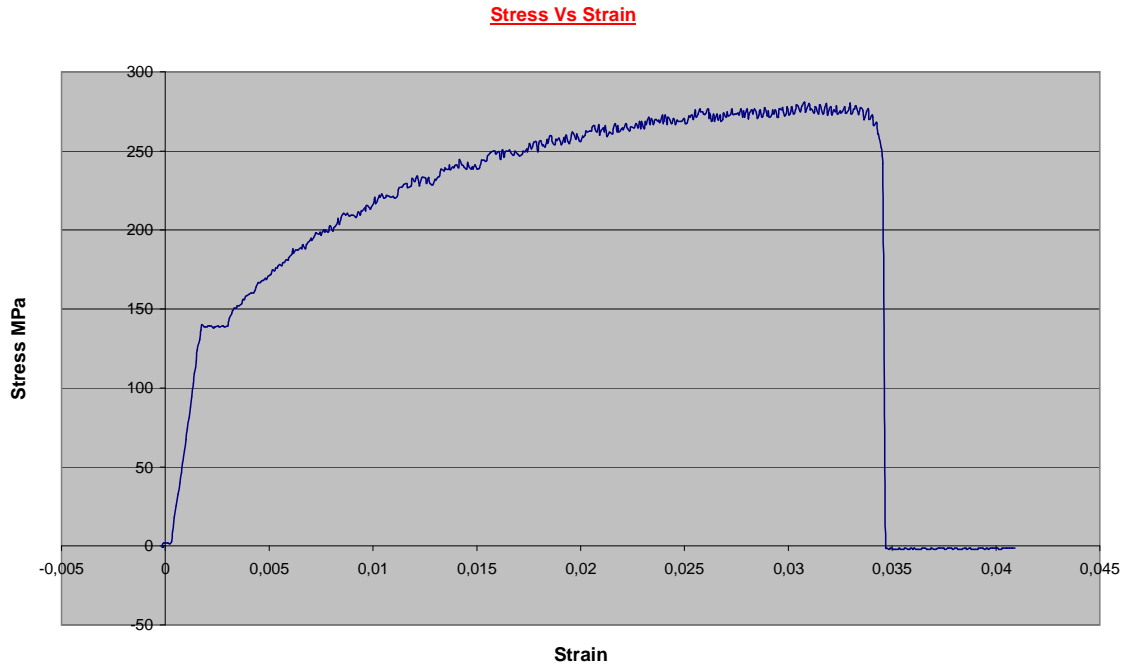
Stress Vs Strain

Fig.32 – Stress/strain curve for Aluminium 5182 (coated)
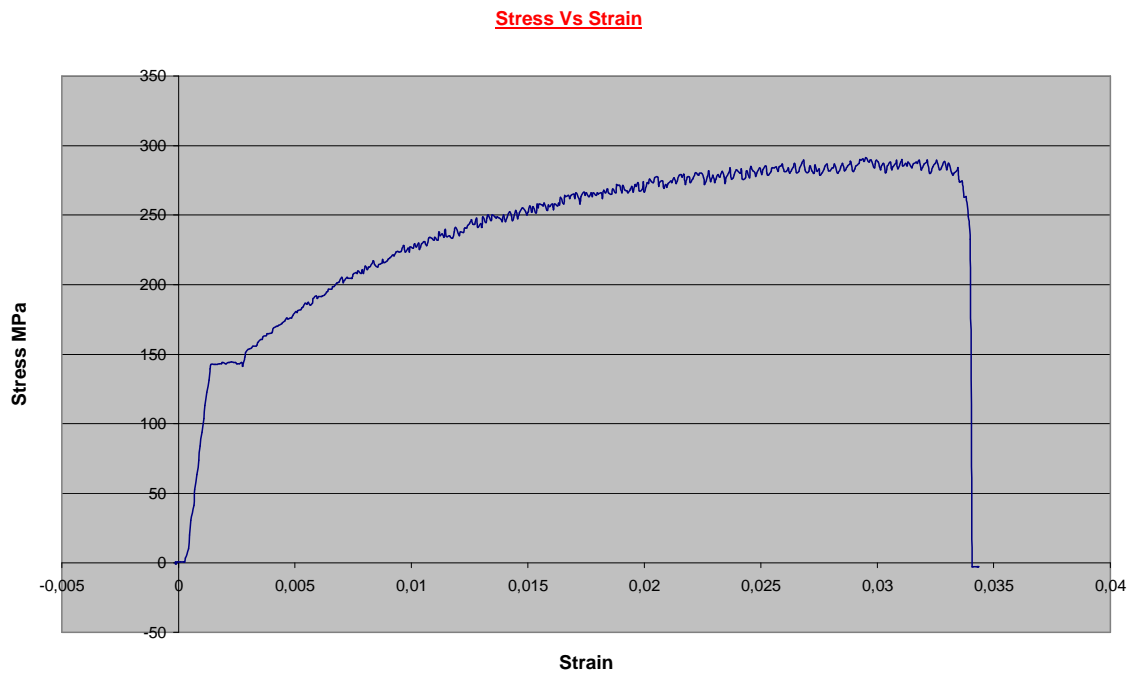
Stress Vs Strain

Fig.33 – Stress/strain curve for Aluminium 5182 (uncoated)

Table 6 shows a summary of the results of the tensile tests of the materials used in this study. These tests were carried out to confirm the mechanical property data provided by the manufacturers. The experimental results were in good agreement with the results provided by the manufacturers.

Table 6 – Tensile tests results and manufacturers data of the materials used

Materials	Yield Stress (MPa)	Ultimate Tensile Stress (MPa)	Strain at failure
Dual Phase 600	405	645	0.28
Manufacturers Data	400	651	0.27
IF Steel	263	400	0.35
Manufacturers Data	260	400	0.36
Aluminium 5754	112	248	0.23
Manufacturers Data	110	240	0.22
Aluminium 5182	142	291	0.20
Manufacturers Data	135	290	0.22

4.3 Effect of setting force on the rivet head-height

Generally a relatively high force is required by a self-piercing rivet to deform and compress the sheet material until the rivet is set fully down. A rivet with a flat countersunk head normally requires a higher setting force than a rivet with an oval head in order to flush with the top sheet. The value of the setting force depends on the material specification, material hardness and thickness as well as the rivet and anvil design. Therefore different setting force values are normally required for joining different alloy combinations.

For the purpose of this investigation, all fastenings were created between two sheets of material only, as this is seen as the most common application in auto-body assembly. Various samples were joined under different conditions and the rivet head height was measured using a special head height measuring device. The advantage of using this is that it is a non-destructive test.

Table 7 shows the results of the relationship between the setting velocities and rivet head height where head height is defined as the distance between the top of the rivet head and the top sheet (Fig.34).
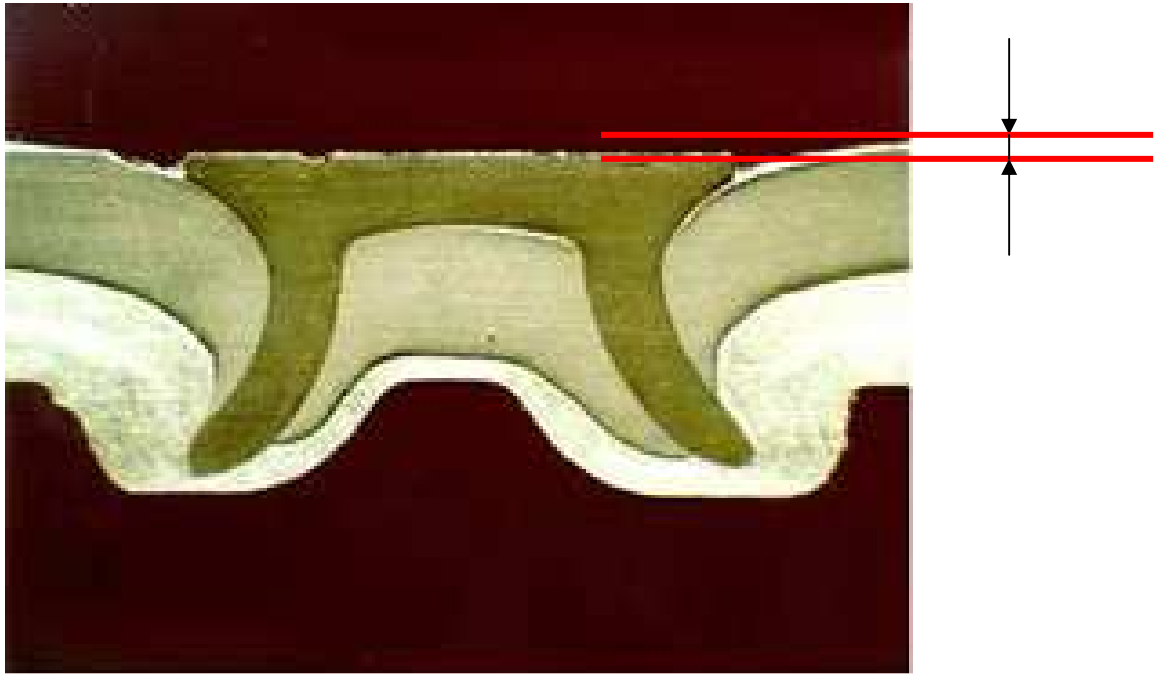
Fig.34 – Distance between the top of the rivet and the top sheet

Table 7 – The relationship between the setting velocities and rivet head height

SPR JOINT CONFIGURATION	Setting Velocity (mm/min)	Rivet Head Height (mm)
A. I.F. Steel on top + Al 5182 on bottom	280	0
I.F. Steel on bottom + Al 5182 on top	280	0.17
B. I.F. Steel on top + Al 5754 on bottom	320	0.14
I.F. Steel on bottom + Al 5754 on top	320	0.31
C. I.F. Steel on top + Al 5182 on bottom	340	0.12
I.F. Steel on bottom + Al 5182 on top	340	0.14
D. I.F. Steel on top + Al 5754 on bottom	340	0.1
I.F Steel on bottom + Al 5754 on top	340	0.27

The results show that the higher the setting velocity the lower the head height. Furthermore, the results are average values of three samples for each joint configuration. From the above results it is obvious that with setting velocities of 320 and 340 mm/min for samples B and D respectively, the rivet head stood closer to the upper surface of the joined material for sample D. For samples A and C the values are almost the same. It was therefore decided to prepare samples for the study using a setting velocity of 340 mm/min as the resulting rivet head value was higher implying that the quality of the rivet was better.

Fig.35 shows the Time vs Force measurement during the self-piercing riveting process. It can be seen that the maximum force used to pierce the Aluminium 5754 (on top) + I.F. Steel (on bottom) was 50024.4 N or 50 kN. This maximum force was approximately the same for all the pairs of sheets used for piercing.
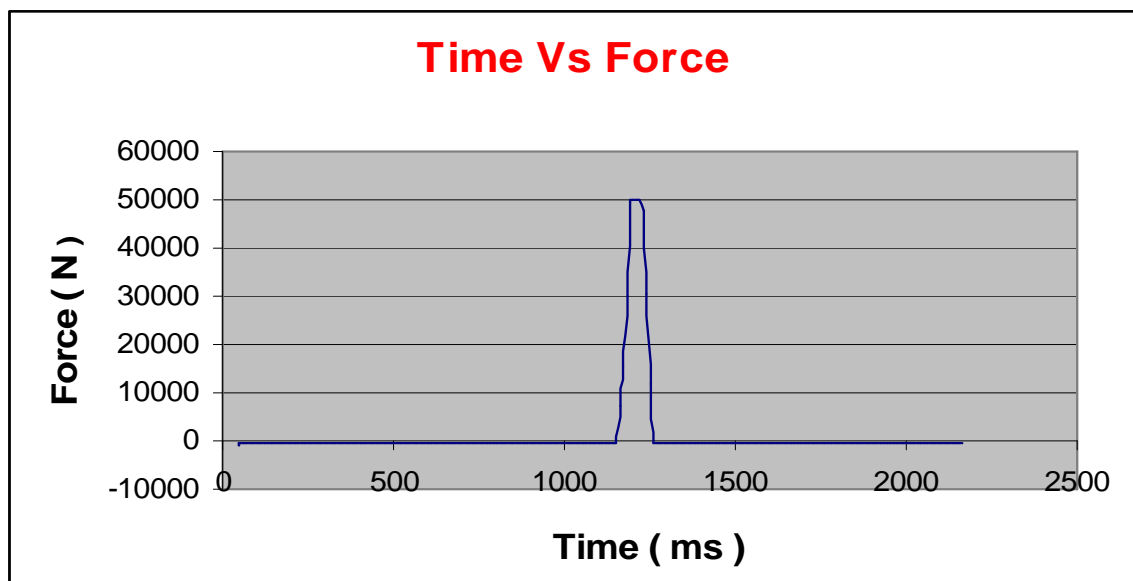
Fig.35 – Time/force graph for the piercing process

4.4 Relationship between setting force, rivet head height, interlock distance and strength of joints

Table 8 shows the measurement of the rivet head height, average interlock distance by applying different setting velocities for the selection of SPR joint configurations as well as the strength of joints configurations. The values presented are averages of three samples per configuration.

Table 8 – Rivet head height, average interlock distance, setting velocity and strength of joints for a selection of SPR joint configuration

SPR JOINT CONFIGURATION	Rivet Head Height (mm)	Average Interlock Distance (mm)	Setting Velocity (mm/min)	Strength of Joints (kN)
A. IF Steel on top + Al 5754 on bottom	0.36	0.84	240	4.94
IF Steel on top + Al 5754 on bottom	0.36	0.83	240	4.94
IF Steel on top + Al 5754 on bottom	0.16	0.92	280	5.45
IF Steel on top + Al 5754 on bottom	0.15	0.89	280	5.45
IF Steel on top + Al 5754 on bottom	0.04	0.94	340	5.95
IF Steel on top + Al 5754 on bottom	0.05	0.92	340	5.95
B. IF Steel on top + Al 5182 on bottom	0.1	0.85	340	6.26
IF Steel on bottom + Al 5182 on top	0.07	0.49	340	4.85
C. Al 5754 on top (1.5mm) + Al 5754 on bottom (2mm)	0.07	0.95	340	4.10
Al 5754 on top (2mm) + Al 5754 on bottom (1.5mm)	0.06	0.63	340	4.41

From the above results it can be clearly seen that for the A joint configuration, as the setting velocity increases, the rivet head height decreases whereas the interlock distance and strength of the joints are increasing. The results of the B joint configuration were used to determine which of the two configurations exhibited the higher strength. The results indicated that the configuration with IF steel on top and 5182 on the bottom had a higher

strength than the configuration with 5182 on top and IF steel on the bottom. It was therefore concluded that for a stronger SPR joint the harder material should be on top (to be pierced) and the softer material on the bottom (to be locked into) as this configuration will normally result in a higher interlock value. The results for configuration C were intended to examine which material should be placed on top and which on the bottom when joining two sheets of the same alloy but of different thickness. Placing the thinner sheet on top resulted in a higher interlock distance, but the SPR joint strength was unexpectedly weaker. Further investigation was conducted to understand this observation which is further discussed in section 4.5.

4.5 Choice of pierced and locked sheets for joints between different materials and between like materials of different thickness

The lap shear strength data for the different joint configurations that were investigated during the study are presented in Table 8. The results indicated that when joining two different sheet materials together, the choice of sheet material to be used as the top sheet (i.e., to be pierced) and bottom sheet (i.e., to be locked) could result in a significant difference in the SPR joint strength. For example, the average lap shear strength for the (1.2mm I.F. steel top + 1.5mm 5182 bottom) configuration was 6.26kN, while the samples for the (1.5mm 5182 top + 1.2mm I.F. steel bottom) configuration failed at an average load of 4.85kN. The average data of a quantitative examination measuring the rivet head height and the rivet interlock are also listed in Table 8.

As mentioned above, the head height is defined as the distance between the top of the rivet head and the top sheet, while the rivet interlock distance is the distance between the outermost point of the rivet leg and the interface between the rivet and the two sheets. Fig.36 illustrates how these measurements were obtained. It presents a (1.2mm I.F. steel top + 1.5mm 5182 bottom) configuration where the head height was 0.1mm, while the interlock distance was 0.85mm.
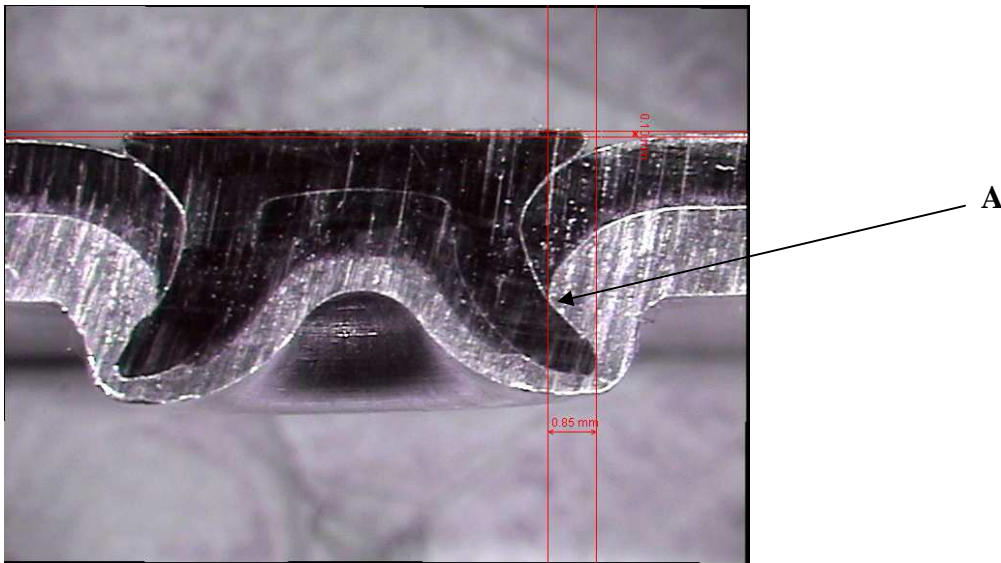
Fig.36 - A typical measurement of the interlock distance and rivet head height

For the (1.5mm 5182 top + 1.2mm I.F. steel bottom) sample, the values for the head height and the interlock distance were 0.07mm and 0.49mm respectively. On the basis of the results from the present study, using the stronger of the two alloys, i.e. the I.F. steel, as the pierced sheet resulted in obtaining a higher interlock distance and a higher head height when compared to the configuration where the I.F. steel was the locked sheet. The I.F. steel, being harder and stronger than the 5182 aluminium alloy, provided a higher resistance to the rivet during the piercing stage giving rise to a higher head height. On the other hand, the 5182 alloy being softer allowed the rivet to lock deeper into it. The rivet was therefore expected to exhibit a higher level of mechanical interlocking when the softer, weaker and thicker 5182 aluminium alloy acted as the locked sheet. The (1.2mm I.F. steel top + 1.5mm 5182 bottom) samples produced stronger joints because the interlock distance for this configuration was greater in comparison to that for the (1.5mm 5182 top + 1.2mm I.F. steel bottom) configuration. During shear testing of a lap joint, the component sheets are subjected to a tensile stress with a non-uniform distribution along the discontinuous cross-section. In addition to this, the lap shear joint is likely to be introduced to plastic deformation and secondary bending that tends to pull the rivet out of the bottom sheet by overcoming the interlock strength. When a conventional riveted lap joint is subjected to a shear load, the shear load is mainly transferred by the rivet and the sheet material by means of shear and bearing after overall slip of the joint takes place.

For a self-piercing riveted lap joint, shearing of the rivet and bearing of the riveted sheets are also expected to occur during the shear test. In addition, for a rivet with a countersunk head, tilting of the rivet also took place during shear testing. When a shear force *S* was applied, two components, *S_1 and S_2,* were created and formed a couple that acted on the rivet as shown in Fig.37. As a result, the rivet tended to tilt up by overcoming the frictional force between the rivet and the two riveted sheets. Some bending of the two sheets was observed and in particular of I.F. Steel. As the loading process proceeded, the bottom sheet suffered localized yielding leading to a large contact area between the riveted sheet and the rivet. Failure therefore occurred by the rivet being pulled out with some deformation of the riveted sheets.
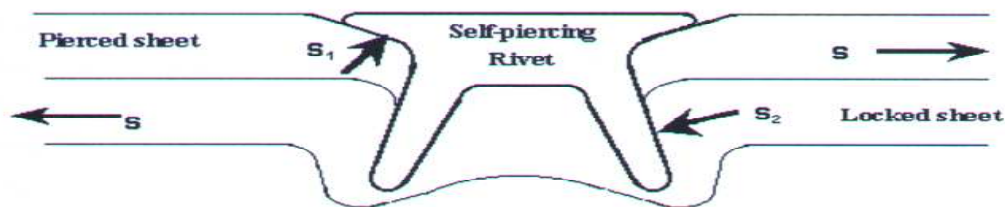
Fig.37 – The two components which are acted on the rivet by applying a shear force

The sheet material adjacent to the rivet is also subjected to a bearing stress since the rivet is in bearing against the side of the two sheets. Therefore the shear strength of a self-piercing riveted joint is dependent on a combination of parameters that include the sheet material tensile strength, the rivet material strength, plastic deformation of the sheet and rivet, the bearing resistance and the interlock strength of the joint. If the tensile strength of the sheet materials that are joined is higher than the bearing resistance and the interlock strength, the dominant lap shear failure mode would be a combination of the interlock and bearing failure. In this type of failure, the rivet is expected to be pulled out of the bottom sheet with some plastic deformation of the bottom sheet adjacent to the rivet. The failure mode for both the (1.2mm I.F. steel top + 1.5mm 5182 bottom) and the (1.5mm 5182 top + 1.2mm I.F. steel bottom) samples was by means of rivet pull-out as shown in figures 38 and 39 respectively. Therefore the lap shear strength was primarily determined by the size of the contact area at the interlock between the rivet and the locked sheet. Since the lap shear failure mechanism was by means of rivet pull-out, the greater the interlock distance, the greater the amount of friction that needed to be overcome in order to facilitate the pull-out of the rivet. Consequently in the case of joining 1.2mm thick I.F. steel to 1.5mm thick 5182 alloy, the present work has shown that for optimum strength, the I.F.

steel should act as the pierced sheet and be placed on top, while the 5182 alloy should be the locked sheet. It is also evident that deformation of the button-hole has taken place as a result of the rivet and the two sheets being in bearing. The 5182 aluminium alloy button-hole, being softer and weaker, has undergone more deformation than the I.F. steel button-hole.

Fig.38 – Rivet pull-out of 1.2mm I.F. steel on top + 1.5mm Al5182 on bottom

Fig.39 – Rivet pull-out of 1.5mm Al5182 on top + 1.2mm I.F. steel on bottom

Table 8 also lists the head height and interlock distance for joints joining two sheets of NG5754 aluminium alloy of different thickness. The configurations that were prepared were (2mm top + 1.5mm bottom) and (1.5mm top + 2mm bottom). The latter configuration exhibited a lower head height and a greater interlock distance than the former one. The reason for this observation is the fact that for the (1.5mm top + 2mm bottom) sample, the rivet had a lower distance (1.5mm) to pierce into and a larger sheet thickness to lock into. Since both the top and bottom materials undergo plastic deformation, this led to the

reference point marked A, in Fig.36, from where the interlock distance was measured, to be further away from the extreme point or tip of the flaring rivet leg, thus making the interlock distance larger. However, contrary to what was expected, the average lap shear strength of 4.10kN for the (1.5mm top + 2mm bottom) configuration was lower than that for the (2mm top + 1.5mm bottom) configuration of 4.41kN. Examination of the samples from the two configurations revealed that they failed by two different mechanisms as shown in Fig.40. The samples for the (1.5mm top + 2mm bottom) configuration (upper photo) failed by means of fracture of the pierced sheet in the area around the rivet. On the other hand, the (2mm top + 1.5mm bottom) configuration (lower photo) failed by means of failure of the button-hole.   In the case of the (1.5mm top + 2mm bottom) configuration, the tensile strength of the 1.5mm top NG5754 sheet was lower than the bearing resistance and the interlock strength. The higher interlock distance for this joint led to a very strong interlock and to a SPR joint that was capable of resisting a greater load than the 1.5mm thickness pierced sheet could and therefore, the pierced sheet failed at an applied load of 4.10kN. On the other hand, the low thickness of the locked sheet for the (2mm top + 1.5mm bottom) configuration led to a low bearing resistance and failure of the button-hole took place.

Fig.40 – Failure mechanism of Aluminium 5754 both configurations

In order to understand the implications of the results of this study, the setting stages of the SPR process need to be considered. The rivet initially pierces the top sheet and then flares into the bottom sheet. The choice of rivet is of particular importance because the rivet must be strong and hard enough to pierce the top sheet. If this condition is not fulfilled, there is

likelihood that the piercing into the top sheet may be incomplete. Following the piercing stage, the rivet must have sufficient ductility to deform and then flare to form an interlock with the bottom sheet. It is understandable that for a good-quality joint, it is better if the rivet would deform and flare symmetrically so that the interlock and the resulting strength of the joint can be balanced. It is also preferable that there are no large gaps between the two sheets within the vicinity of the joint as this would make the joint relatively loose. For the same reasons, large gaps between the rivet and the riveted sheets are also undesirable. Provided a sufficient load has been applied during the SPR process, sufficient flaring may be facilitated in order to achieve an acceptable joint.

The maximum flaring distance that can be achieved (i.e., the distance between the two outermost points or tips of the rivet legs) during the SPR process is dictated by the die size and geometry. For a fixed die design and rivet size, the maximum possible flaring distance that can be achieved will always be the same irrespective of the sheet configuration. Thus the flaring distance cannot be used as a parameter to assess the quality of a SPR joint. Instead, measurements of the interlock of the rivet into the locked sheet can be used for quality assessment of the joint. The interlock distance is determined by the deformation characteristics of both the rivet and the sheets to be joined. The deformation characteristics of the rivet can be quasi-quantified by measuring the rivet head height above (or below) the surface of the pierced sheet and the interlock distance. Both of these criteria are normally interconnected in that insufficient rivet deformation will generally result in a relatively high rivet head height and a very low interlock distance. As a guideline, for the configurations investigated in this study, head height values in excess of about 0.25mm may be considered as too high and therefore unsatisfactory. Ideally, the rivet head height above the pierced sheet should be around zero, while the greater the interlock distance the higher the strength of the joints. One of the crucial requirements is the fact that large gaps between the rivet head and the top sheet need to be avoided in order to prevent the penetration of water or moisture into the gap as this will lead to galvanic corrosion and degradation of the joint. Head height measurements may thus provide a good indication of the deformation characteristics of the alloy sheets and the rivet and can therefore act a useful means of a non-destructive test for assessing the quality of SPR joints. The reference point from where the interlock distance can be measured is the upper "triple" point of intersection between the two sheets and the rivet, i.e., the point of the upper part of the rivet leg that meets the two sheets and marked A, in Fig.36.

The greater the distance between the reference point and the outermost part of the rivet leg, the greater the interlock distance. The strength of a SPR joint is determined by the resistance the rivet legs experience during rivet pull-out. This resistance is manifested in the form of a frictional force between the rivet legs and the sheets of the SPR joint. The higher the interlock distance the larger the rivet leg to sheet contact area and therefore the higher the area of frictional resistance that needs to be overcome for rivet pull-out. The resulting position of the reference point is determined by the piercing and locking characteristics of the rivet and the local deformation of the two sheets relative to each other and to the rivet. In cases where sheets of different thickness are to be joined together using SPR (and assuming good deformation characteristics for both top and bottom sheets), it is obvious that using the thinner sheet as the pierced sheet, the reference point will shift slightly upwards and this will result in a greater interlock distance. However, as indicated by the results of this study, when joining like materials of different thickness, situations arise where the interlock is very strong and the design may fail by fracture of the pierced sheet. The design with the greater interlock distance may therefore not always be the best possible design in terms of strength.

A possible criticism of the methodology that has been used in the study to assess the interlock strength may be the fact that it only takes into account the interlock distance with reference to the upper intersection point between the rivet leg and the two sheets. The technique therefore gives consideration only to the area above the rivet leg and completely ignores the situation below it. However, as the main failure mechanism of SPR joints under lap shear conditions is by means of rivet pull-out, the greatest resistance to failure to be met by the rivet is going to be the friction at the upper interface between the rivet legs and the locked sheet. While substantial interlocking into the locked sheet with respect to both the part above and below the rivet leg may be desirable, the upper part plays a far more significant role in determining the strength of the joint. An important factor that needs to be taken into consideration is the remaining thickness of the locked sheet below the rivet. In some cases, this thickness can be extremely low or the rivet might even break through the locked sheet. A low resulting bottom sheet thickness below the rivet is likely to create a high stress concentration at that area. In such cases, the failure of the joint may also involve failure of the rivet button hole. It is also undesirable for the rivet to break through the bottom sheet because this may lead to water or moisture penetration into the joint and to corrosion problems.

4.6 Lap shear failure mechanisms

A selection of pierced samples was tested using lap shear tests at a strain rate of 10mm/min. The results are shown in Table 8.

Aluminium 5754 on top + IF Steel on bottom:
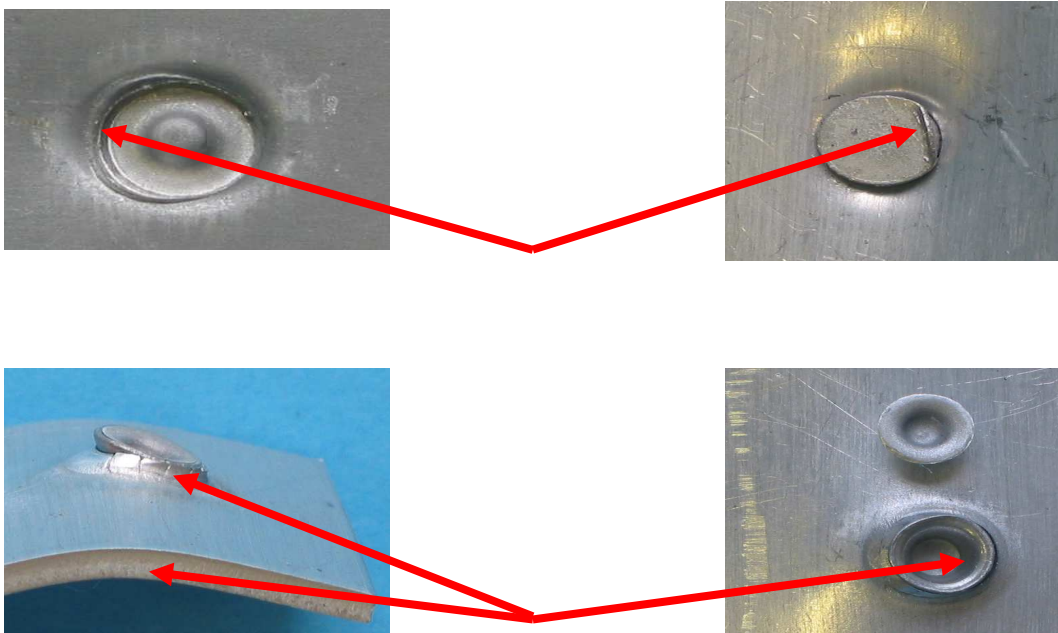
Fig.41 - Lap shear failure mechanism for the Al 5754 on top + IF Steel on bottom
        configuration

The lap shear failure mechanism for the (Al 5754 on top + IF Steel on bottom) samples was by means of rivet pull-out. Fig. 41 shows that the Aluminium acting as the pierced sheet suffered a significant amount of bending prior to failure. In addition, minor cracks were observed around the rivet hole of the pierced sheet.

IF Steel on top + Aluminium 5754 on bottom:
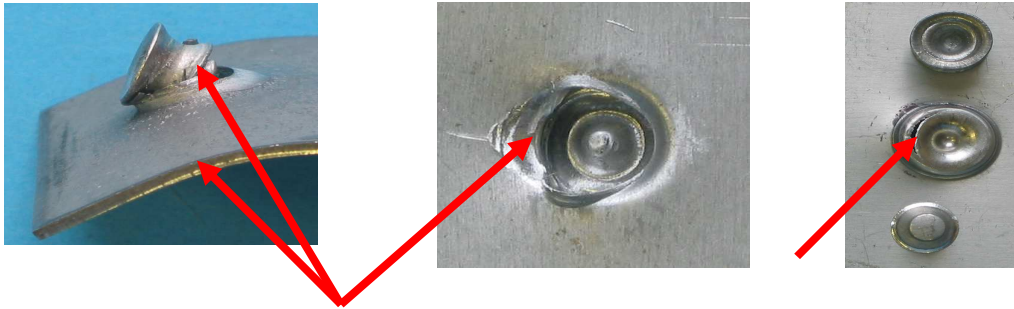
Fig.42 -   Lap shear failure mechanism for the I.F. Steel on top + Al 5754 on bottom
           configuration

From Fig. 42 it can be seen that there is a significant deformation around the aluminium buttonhole. In addition, fracture around the buttonhole has been observed. The pierced hole also experienced a significant amount of deformation and there is more deformation on the top material. Final failure was by rivet pull-out. However, there is not much deformation of the rivet and there are some scratches on the top of the buttonhole, which took place during the final stages of pull out. Since I.F. Steel is a harder material than Aluminium 5754, it is more difficult to be pierced.

4.7 Fatigue studies

The fatigue behaviour of the (1.2mm I.F. steel top + 1.5mm 5182 bottom) and (1.5mm 5182 top + 1.2mm I.F. steel bottom) modifications is displayed in Fig.43 and 44 respectively. The (1.2mm I.F. steel top + 1.5mm 5182 bottom) samples exhibited a higher fatigue life at the higher loads, but, at lower loads, they displayed a much lower fatigue life than the (1.5mm 5182 top + 1.2mm I.F. steel bottom) samples. This observation was rather surprising when taking into consideration the fact that the (1.2mm I.F. steel top + 1.5mm 5182 bottom) samples exhibited a lap shear strength that was significantly higher (by about 29%) compared to the (1.5mm 5182 top + 1.2mm I.F. steel bottom) samples. The relatively low fatigue life of the (1.5mm 5182 top + 1.2mm I.F. steel bottom) samples at a maximum load of 4kN was most likely due to the fact that this value was close to the lap shear fracture load of 4.85kN for this sample modification. Fig.45 shows a graph comparison of the average best fit lines of the above two joint configurations.

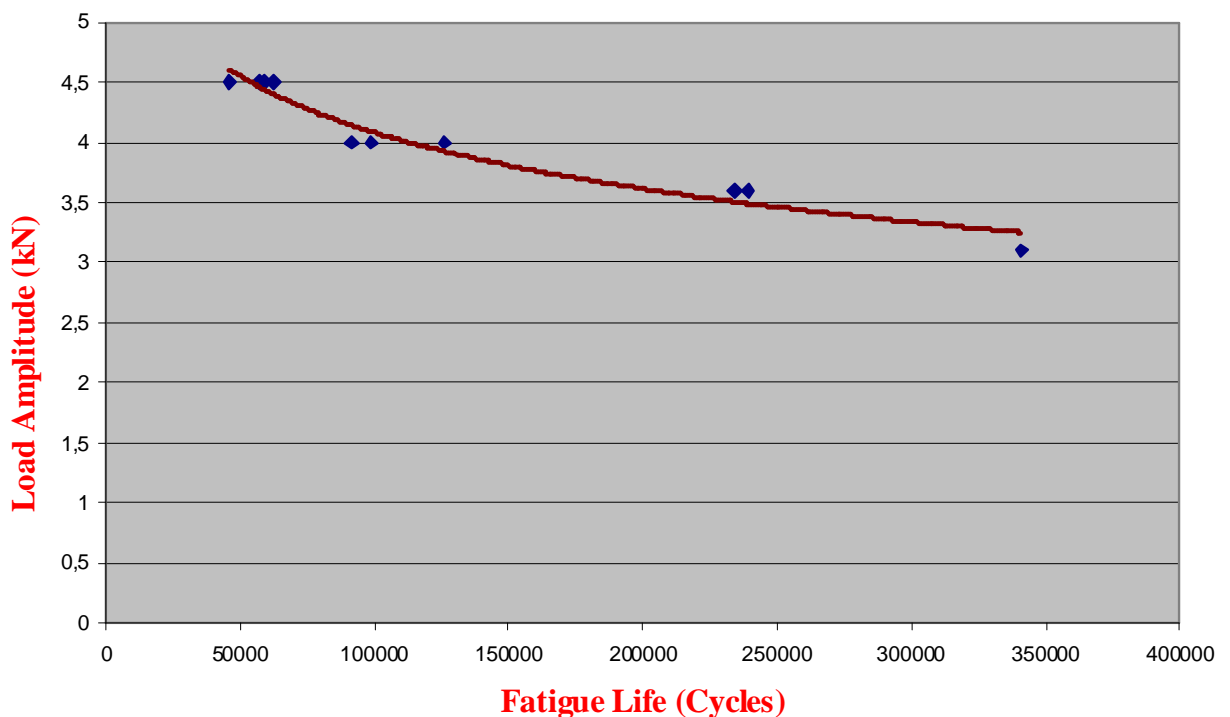Fig.43 – S-N response for I.F. steel on top + Aluminium 5182 on bottom joint
          configuration with 6.26 kN average shear strength
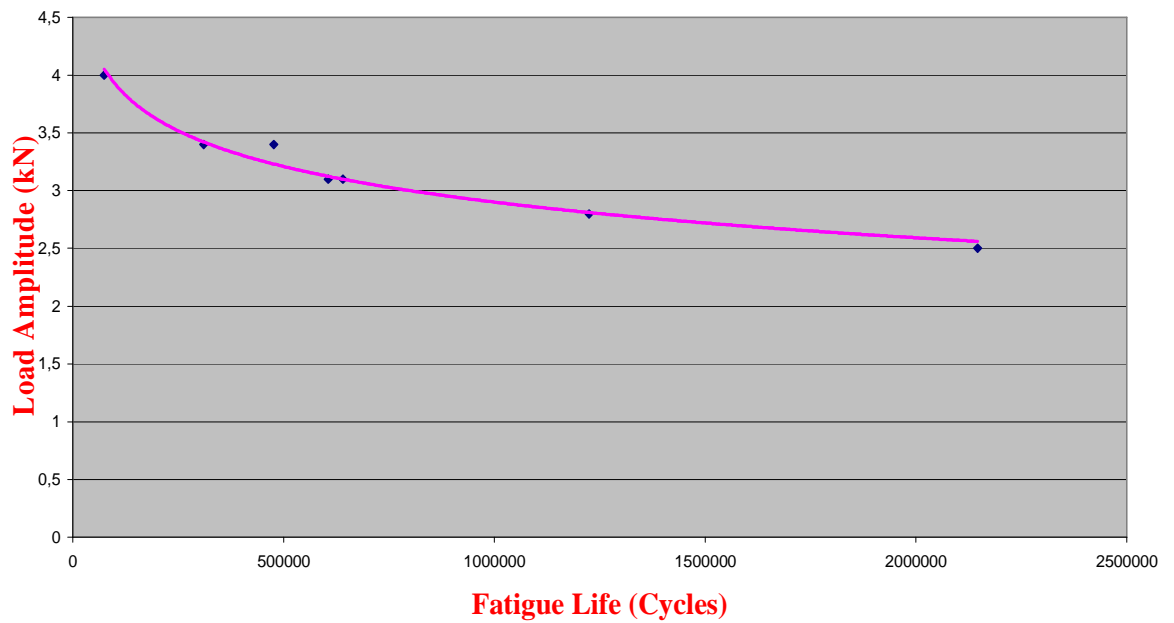
Fig.44 – S-N response for Aluminium 5182 on top + I.F. Steel on bottom joint
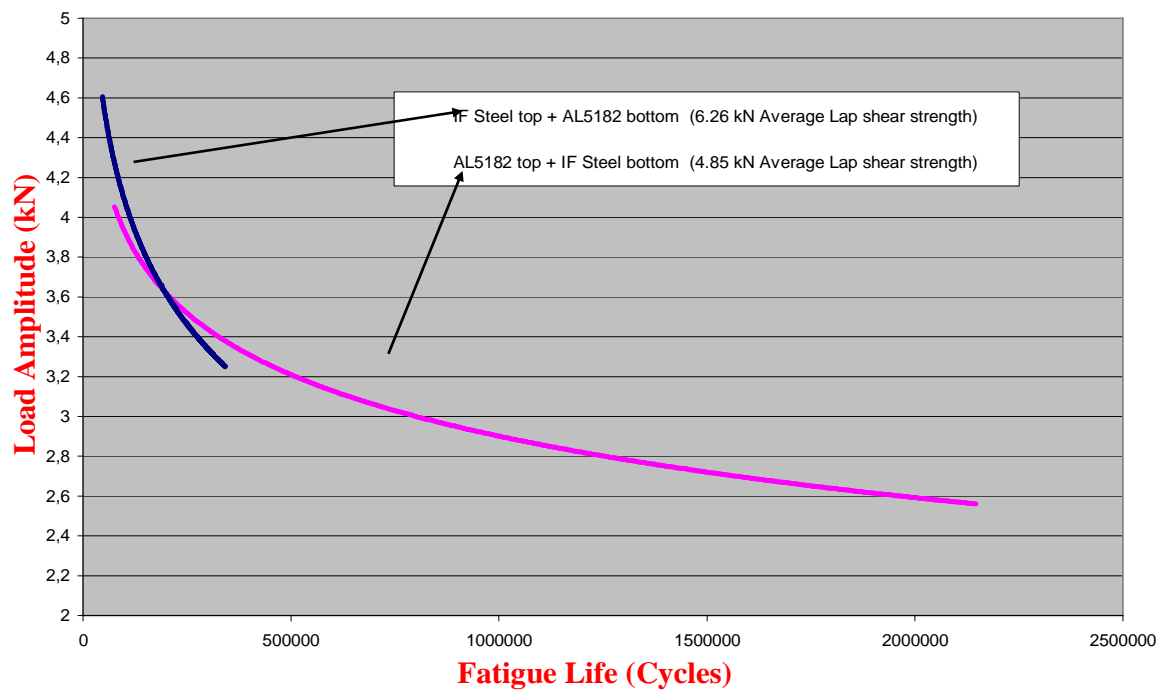configuration with 4.85 kN average shear strength

Fig.45 – A comparison of the fatigue life the I.F. steel on top + Al 5182 on bottom and Al
5182 on top + I.F. Steel on bottom joint configurations

Examination of fatigue fractured samples indicated that the failure mechanisms of the two types of samples differed as presented in Fig. 46(a), 46(b) and 47(a), 47(b) and 47(c). The failure of the (1.2mm I.F. steel top + 1.5mm 5182 bottom) samples involved fatigue crack formation in the 5182 buttonhole at roughly the 3 and 9 o'clock positions. The crack formation in the buttonhole originated due to friction between the rivet and the buttonhole. These cracks led to eventual failure of the samples by means of rivet pull-out. In addition, there was crack initiation in the I.F. steel sheet, but this did not propagate to failure. It was rather surprising to observe two cracks initiating in the sample, one in I.F. steel and one in the aluminium alloy. In all previously reported investigations, cracks were only observed in one material (normally aluminium). SEM examination revealed that fretting occurred at the interface between the mating sheets (this is further analysed in the next section). The initiation of cracks in the I.F. steel was observed to take place initially due to the effect of fretting. As the crack propagated, the I.F. steel was observed to bend as can be observed in Fig. 46a. The propagation of the crack then ceased; instead the load was then transmitted to the rivet and this was followed by the initiation of cracks at the 3 and 9 o'clock positions of the buttonhole. It was surprising to observe a crack initiating and propagating in the I.F. steel. It was also surprising to observe the propagation of the crack cease. Initially it was thought that perhaps there was a problem with the alignment of the equipment, but that was not so. In fact, even after changing the sample orientation by 180° or by turning over the sample, the same behaviour mode was observed. These cracks gradually propagated resulting in final failure due to pull-out of the rivet. By contrast, the (1.5mm 5182 top + 1.2mm I.F. steel bottom) samples failed by eye-brow type of fracture that initiated at the 6 o'clock position of the 5182 top sheet, while the rivet and buttonhole remained intact. A substantial amount of bending of both sheets was noticeable.
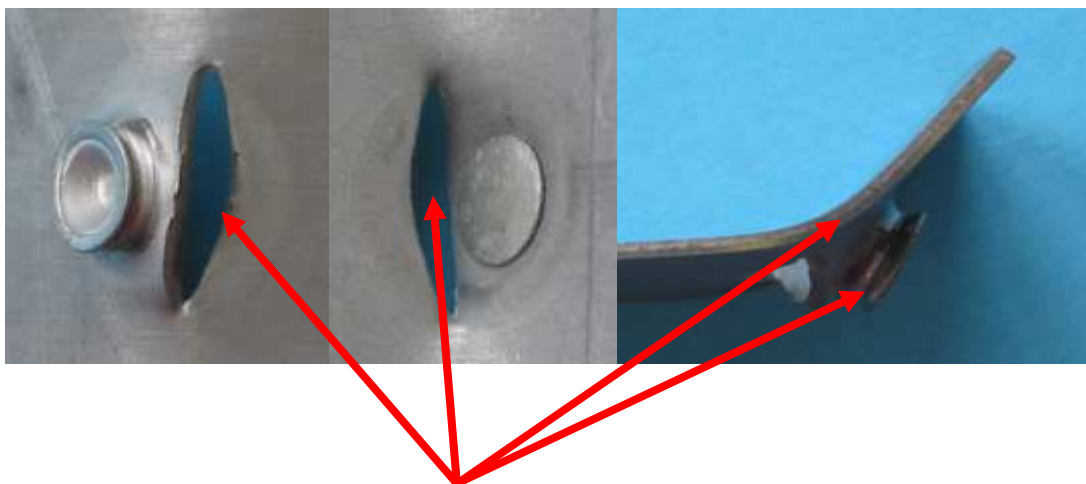

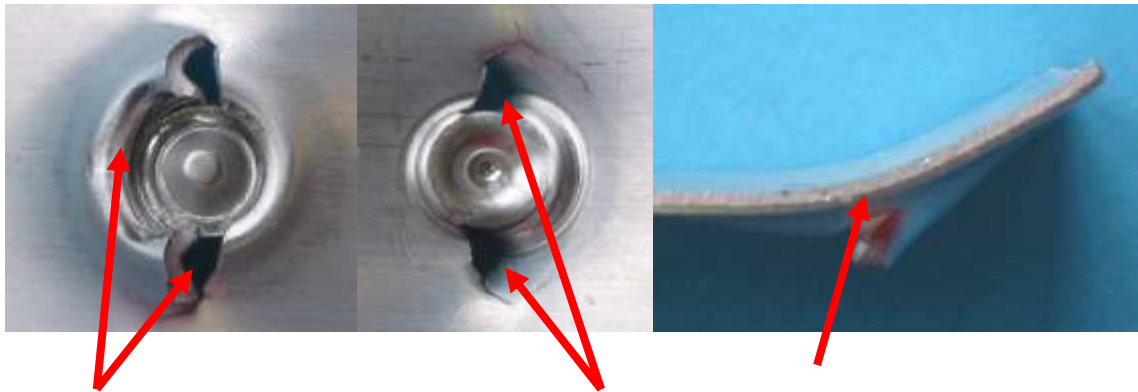Fig.46a – IF Steel on top (pierced sheet) after the fatigue test

Fig.46b – Aluminium 5182 on bottom (locked sheet) after the fatigue test

Fig.47a – Fatigue failure of (Aluminium 5182 top + IF steel bottom) joint
configuration with 4.85 kN average shear strength

Fig.47b – Fatigue failure of (Aluminium 5182 top + IF steel bottom) joint
configuration with 4.85 kN average shear strength

Fig.47c – Substantial bending of both Aluminium 5182 and I.F. Steel

In previous work, it has generally been observed that the greater the mechanical interlock the higher the static lap shear strength and higher fatigue resistance. As explained in the previous section, the static lap shear strength of SPR is dominated by a number of factors including plastic deformation of the rivet and the buttonhole. On the other hand, the fatigue behaviour is dominated by elastic stress concentration. In the present work it is evident that for both sets of samples, the stress concentration was acting on the aluminium 5182 alloy and therefore that was where the crack propagation was focused. However, observation of the failure behaviour of the (I.F. steel top + 5182 bottom) samples showed that crack initiation started on the surface of the steel initially. It was only after bending of the steel that crack initiation and propagation occurred at the 5182 buttonhole. Factors that might contribute to stress concentration include damage that may occur during (i) the piercing and/or locking operations especially if the rivet material is much stronger than the materials to be joined, (ii) by fretting between the two sheets. In conclusion, the interlock distance may be used as a guide of the strength and fatigue behaviour of a SPR joint. However, it is clear that this factor on its own is not sufficient to predict the strength and fatigue of the joint.   In addition, the sheet material combination must be considered together with the development of the deformation characteristics of the materials to be joined.

4.8 Observation of fretting for IF steel – Aluminium 5182 samples

The following photographs have been taken using the JEOL 5700 scanning electron microscope for the IF steel on top + Aluminium 5182 on bottom joint configuration after fatigue failure. Fig. 48 shows evidence of fretting scars on the surface of 5182 together

with delamination of material. The mating surface of the I.F. steel also suffered from fretting as shown in Fig. 49 together with evidence of delamination.
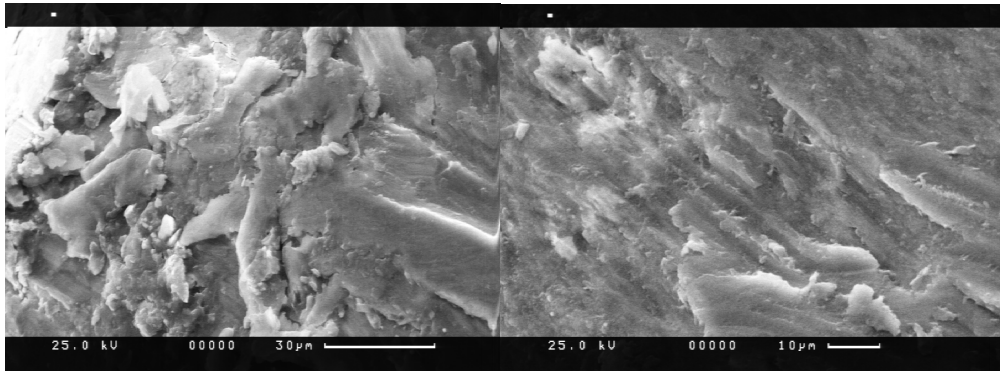
Fig.48 – Fretting on the surface of Aluminium 5182 for the (I.F. steel on top + Aluminium 5182) sample
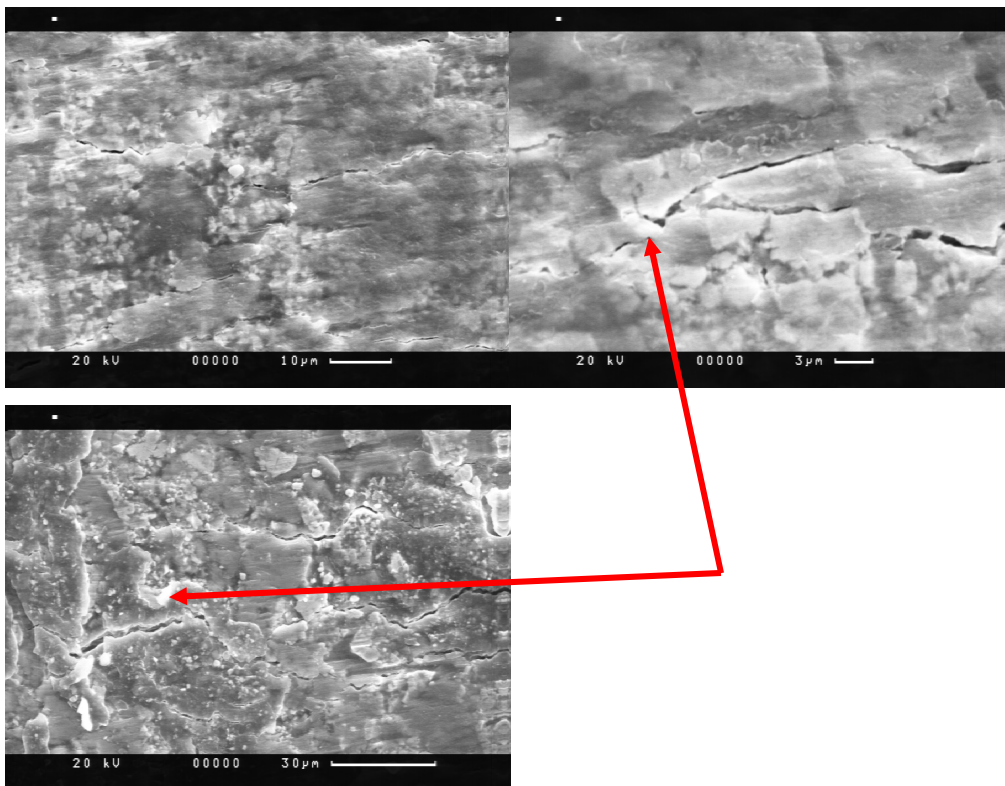
Fig.49 – Fretting scars on the surface of I.F. Steel for the (I.F. steel on top + Aluminium 5182 bottom) sample

Further investigation has shown the presence of fatigue striations near the fatigue crack that developed in the I.F. steel as shown in Fig. 50.
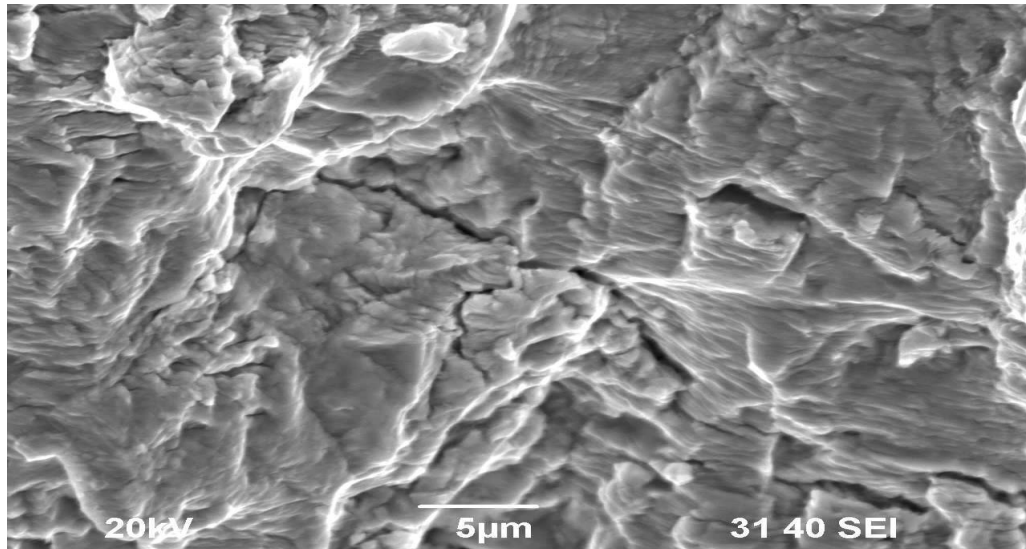
Fig.50 – Presence of fatigue striations near the fatigue crack in I.F. steel
        for the (I.F. steel on top + Aluminium 5182 bottom)

In addition, Fig.51 shows the emergence of fatigue cracks from within the area where fretting was observed. This suggested that the fatigue cracks initiated as a result of fretting between the I.F. steel and the aluminium alloy. Final failure of this sample was due to failure of the buttonhole at around the 3 and 9 o'clock positions.
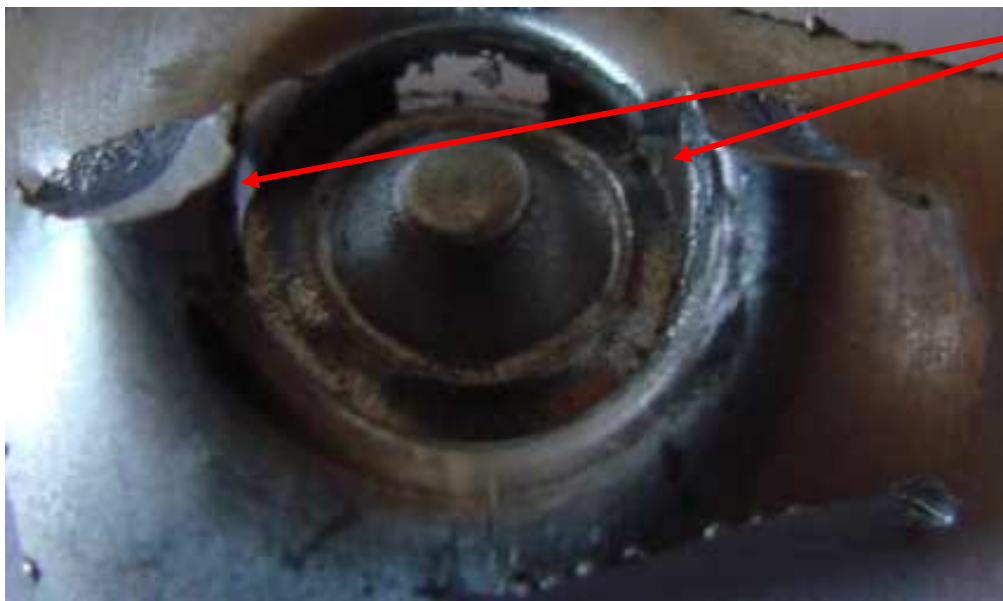
Fig.51 – Emergence of fatigue cracks at the button hole of the (IF steel on top +
        Aluminium 5182 bottom) sample

SEM examination of the failure of the aluminium alloy in Fig.52 showed striations at the fractured area indicating fatigue failure.
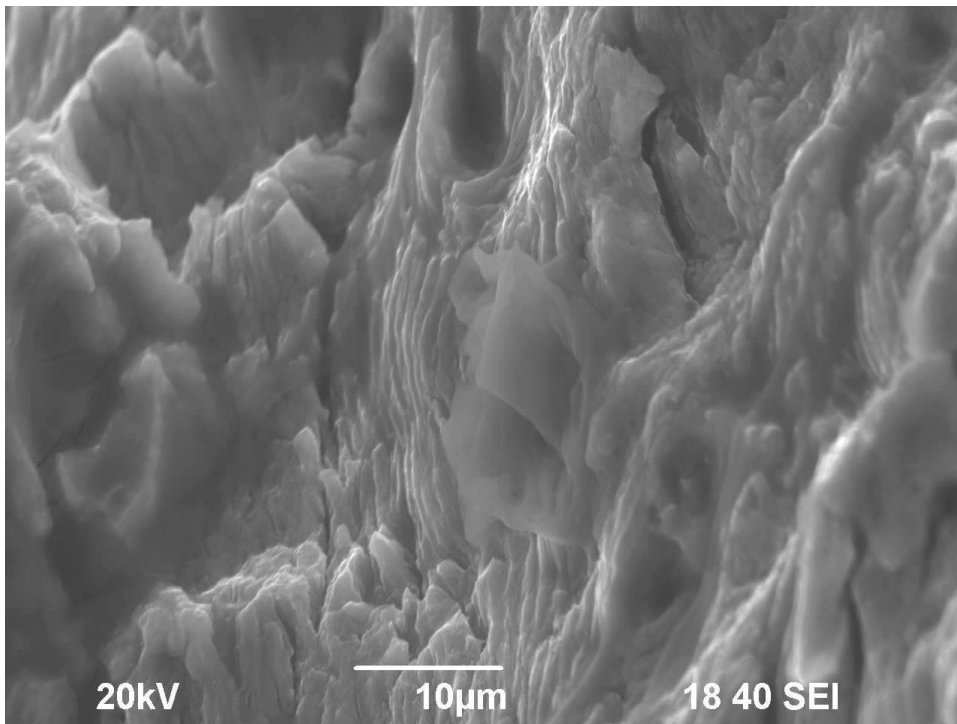
Fig.52 – Striations at the fractured area of 5182 for a (I.F. steel on top +
    Aluminium 5182 bottom) sample

Further examination revealed the presence of fretting scars close to the fractured areas as presented in Fig.53a. EDAX analysis revealed the presence of mainly Al_2O_3 with smaller amounts of MgO, ZnO and Fe_2O_3 (Fig. 53b).
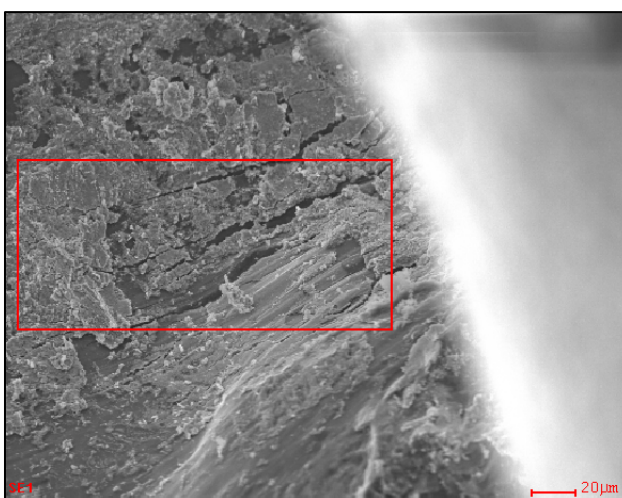
Element	Wt%	At%
OK	10.33	18.64
MgK	04.49	05.33
AlK	60.42	64.65
FeK	05.94	03.07
ZnK	18.83	08.31
Matrix	Correction	ZAF

Fig.53a – Presence of fretting scars close to the fractured areas in aluminium 5182 for a
    (I.F. steel on top + Aluminium 5182 bottom) sample
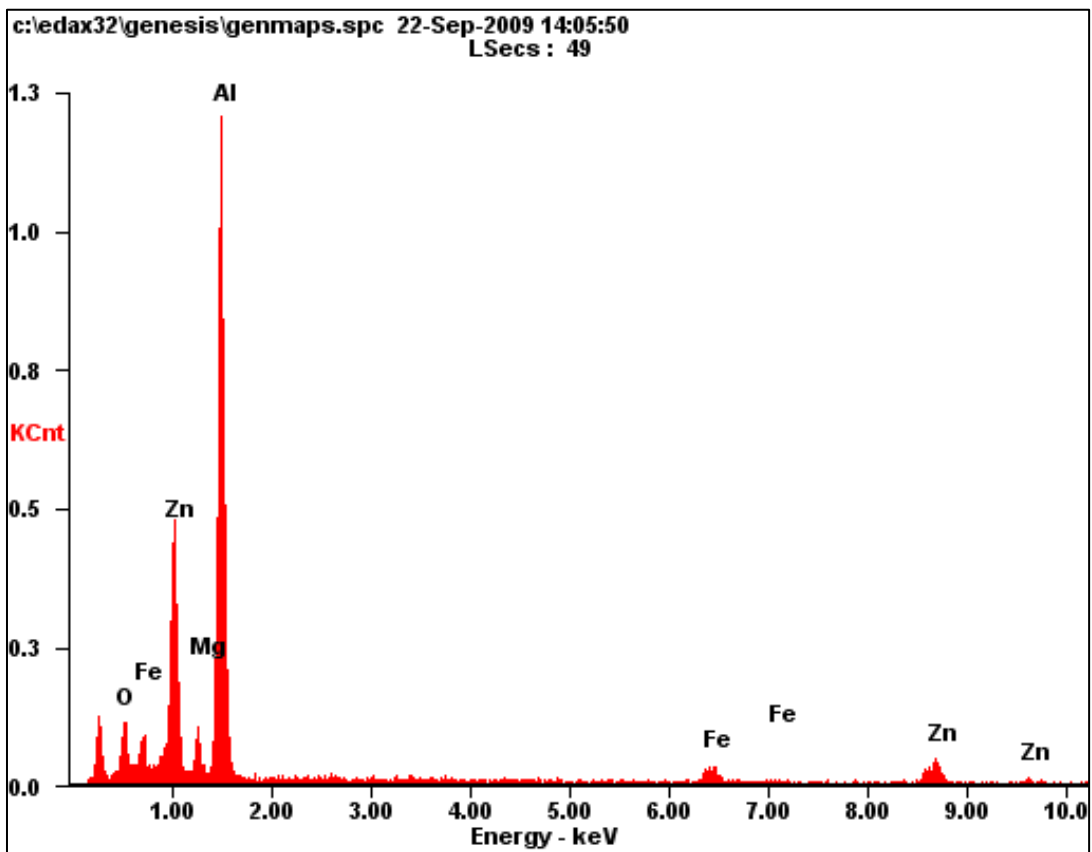
Fig.53b - EDAX analysis revealed the presence of mainly Al_2O_3 with smaller amounts of MgO, ZnO and Fe_2O_3

Inspection very close to the fracture in the 5182 alloy, revealed the presence of fretting scars as well as cracks and delamination of the fretting product as shown in Fig. 54.
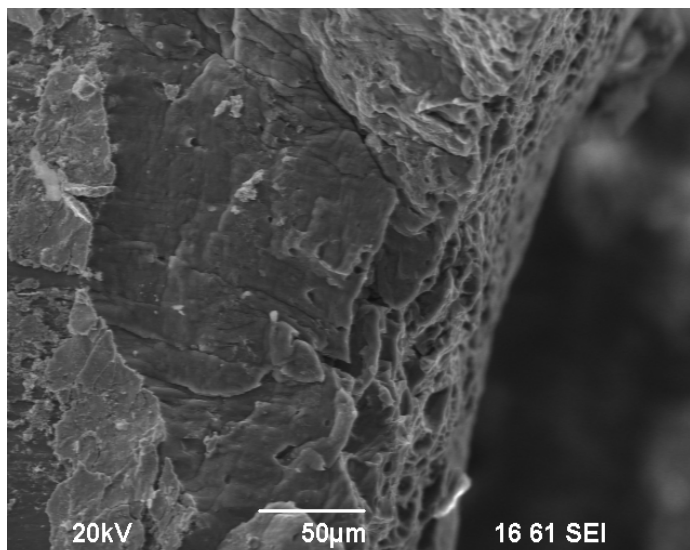
Fig.54 – Presence of fretting scars as well as cracks and delamination of the fretting product

Examination of the fatigue fractured (Aluminium 5182 on top + I.F. steel bottom)) samples also showed evidence of fretting scars and are shown in Fig. 55.
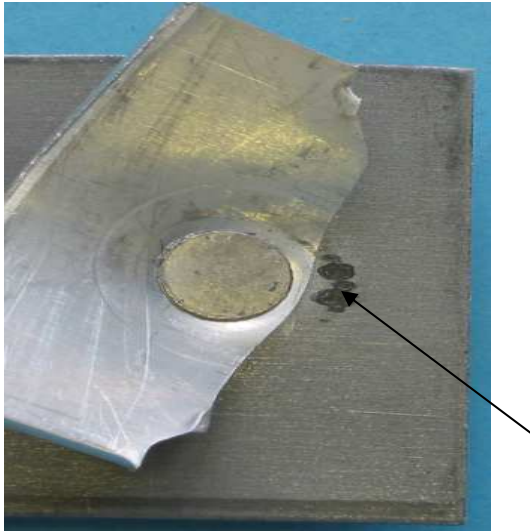
Fig.55 – Evidence of fretting scars after the fatigue tests

The position of the fretting area clearly shows that the sample failure arises as a result of fretting between the two sheets of material.

Fretting creates wear and oxidation at the same time. The above SEM micrographs show that the oxide is broken at some areas to form fretting debris. In addition, delamination was observed to take place. When examining the fretting scars on the surface of the 5182 alloy, the main product was Al_2O_3. Small amounts of MgO were also detected. This was to be expected as aluminium is the base metal in alloy 5182, while magnesium is the main alloying element. It appears, that there is also material transfer from the Zn-rich coating on the I.F. Steel into the fretting debris at the periphery of the buttonhole of the aluminium alloy. In addition, small amounts of iron were also detected that were transferred from the steel rivet.

Analysis of the fretting scars on I.F. Steel showed a high concentration of ZnO and minor amounts of MgO, Al_2O_3, SnO, and Fe_2O_3 due to friction between the two sheets of materials. In both cases, the Al_2O_3 and MgO come from the Aluminium 5182, while the ZnO and SnO come from the I.F. Steel coating and finally the Fe_2O_3 comes from the I.F. Steel.

Examination of the fretting debris at the initial stages indicated that the oxides of aluminium (from 5182) and zinc (from the corrosion protective coating on the I.F. steel) were formed. During the initial stages two-body fretting wear between the two sheets was taking place. Following the formation of the Al_2O_3 and ZnO debris, three-body fretting wear started to take place. By the time fatigue failure had taken place, oxides of magnesium (from the 5182 alloy) and iron were also detected. While the amount of iron oxide present within the debris on the surface of the 5182 alloy was very low, significant amounts of Al_2O_3 were observed within the debris on the surface of the steel. This observation was to be expected because the 5182 alloy is softer and is expected to suffer more severe fretting wear than the I.F. steel.

4.9 Fatigue behaviour of (DP600 top + Al 5182 bottom)

SPR samples of (DP600 top + Al 5182 bottom) underwent fatigue testing and results are presented in Fig.56.
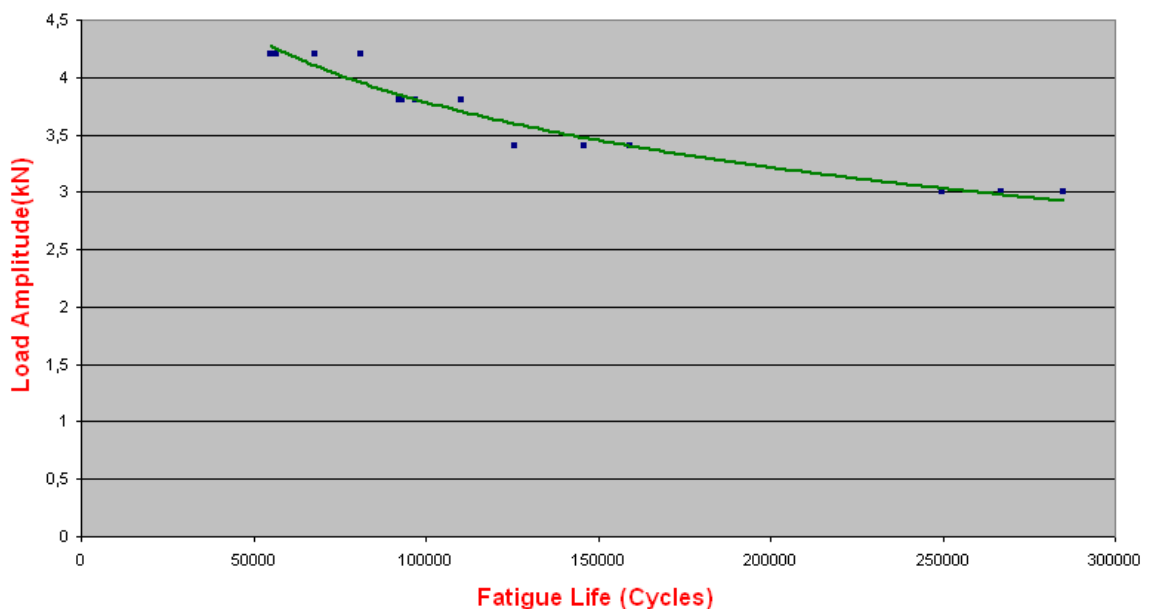
Fig.56 – S-N Response for the DP600 on top + 5182 on bottom joint configuration after the fatigue tests

Photographs of the fractured samples (four different applied loads) from the fatigue tests are presented in Figs.57(a-d).

Fig.57a (3kN)   Fig.57b (3.4 kN)

Fig.57c (3,8 kN)   Fig.57d (4,2 kN)

Final failure of the samples was observed to be due to fracture of the Al5182 locked sheet. It is obvious from Figs. 57(a-d) that the position of fracture of the samples was different as the maximum applied load changed. The position of fracture for the four different maximum applied loads that were used is summarised in Fig.58.

4   kN (3 and 9 o'clock positions)
3.8 kN (4 and 8 o'clock positions)
3.4 kN (5 and 7 o'clock positions)
3.2 kN (6 o'clock position)

Points of fracture initiation
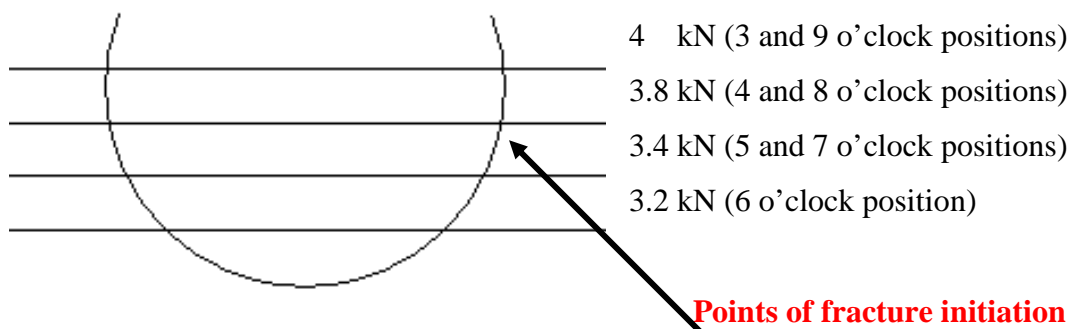
Fig.58 – Positions of fractured points as the maximum load changed

The fractured samples were examined by using light microscopy and SEM. Fretting scars were observed on the surface of DP600 as shown in Fig.59.

Fig.59 – Fretting scars on the bottom surface of DP600

SEM investigation also confirms that fretting scars occurring on the surface of the DP600 steel close to the periphery of the rivet. An SEM micrograph showing evidence of this is presented in Fig.60.
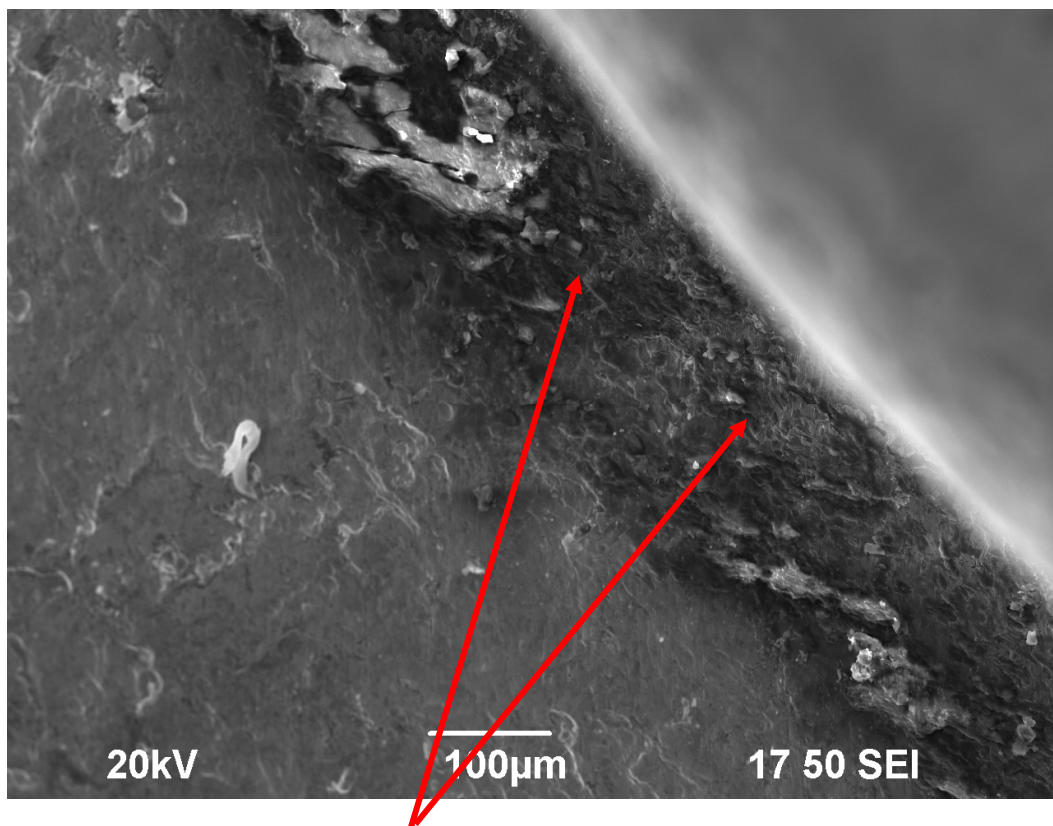
Fig.60 – Fretting scars on the surface of the DP600 steel close to the periphery
        of the rivet

In addition, elemental mapping was obtained using EDAX analysis and the results are
presented in Fig.61.
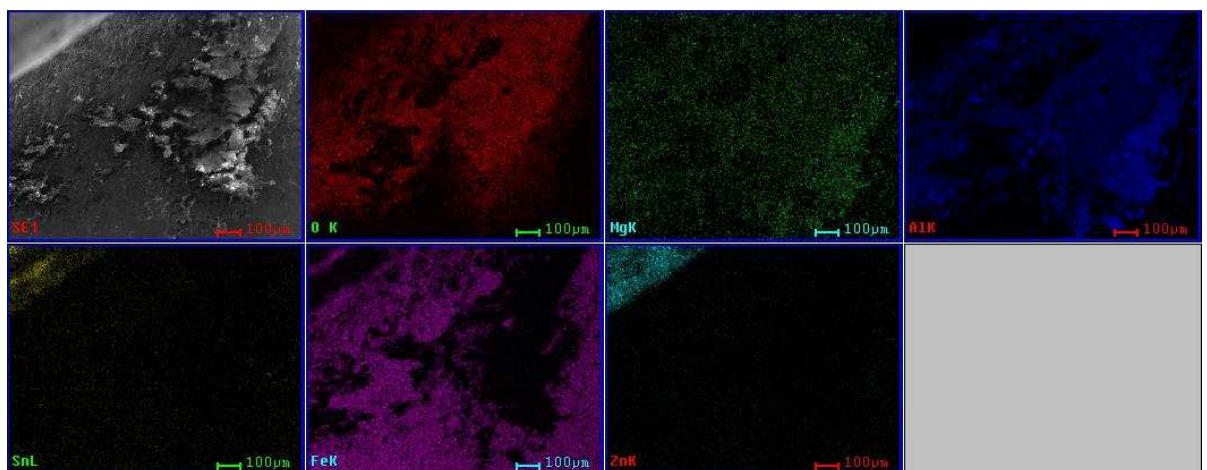
Fig.61 – Element mapping of the DP600 using EDAX analysis

The results show the presence of the oxides of iron, aluminium and magnesium 62b. The areas showing zinc and tin are from the surface of the rivet. As a result of fretting, there was transfer of aluminium and magnesium from the 5182 alloy. Fretting was also observed to occur on the mating side of the 5182 and evidence of it is shown in Fig.62a.
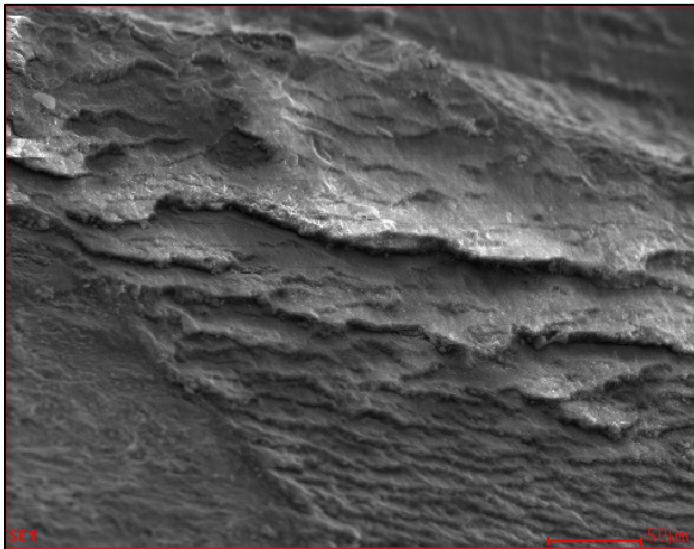
Element	Wt%	At%
OK	22.07	32.21
MgK	03.86	03.71
AlK	74.06	64.08
Matrix	Correction	ZAF

Fig.62a – Fretting occurred on the mating side of the Al 5182
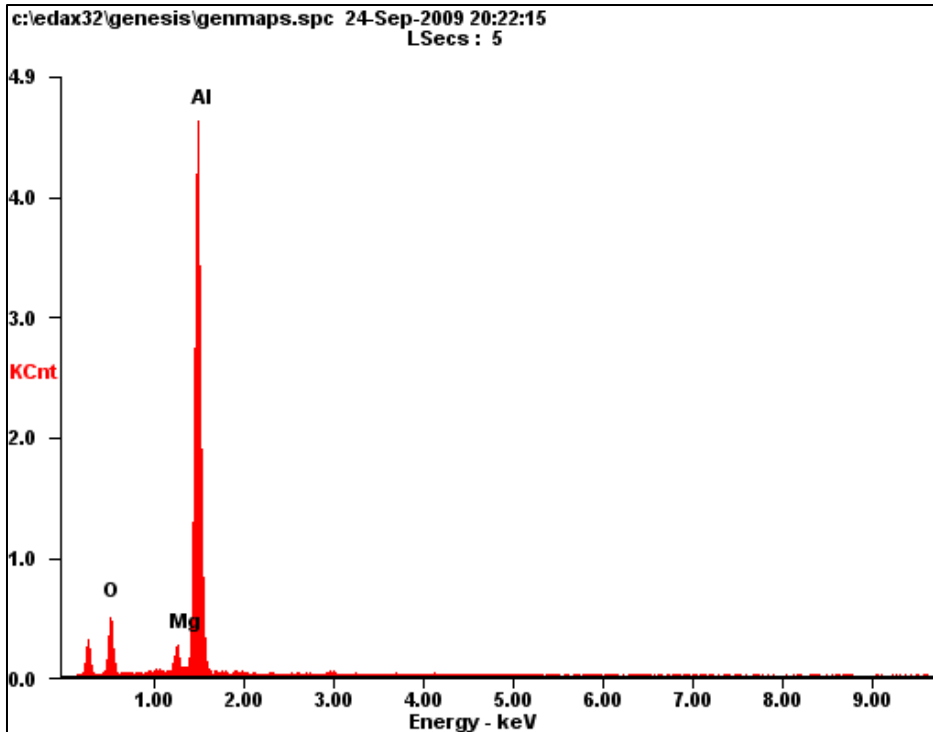
Fig.62b – EDAX analysis show the presence oxides of iron, aluminium and magnesium

A significant amount of fretting scars was also observed at the periphery of the buttonhole of the 5182 alloy. This is shown in Figs.63 and 64a.

Fig.63 – Fretting scars at the periphery of the buttonhole of the Al 5182
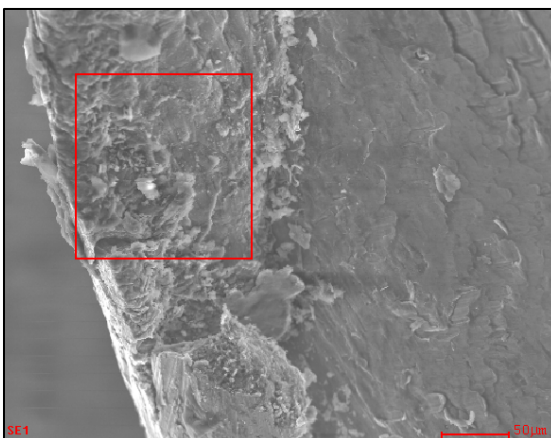
Element	Wt%	At%
OK	28.61	56.13
MgK	00.94	01.22
AlK	15.54	18.08
SnL	11.56	03.06
FeK	07.78	04.37
CuK	04.53	02.24
ZnK	31.04	14.90
Matrix	Correction	ZAF

Fig.64a – Fretting scars at the periphery of the buttonhole of the Al 5182
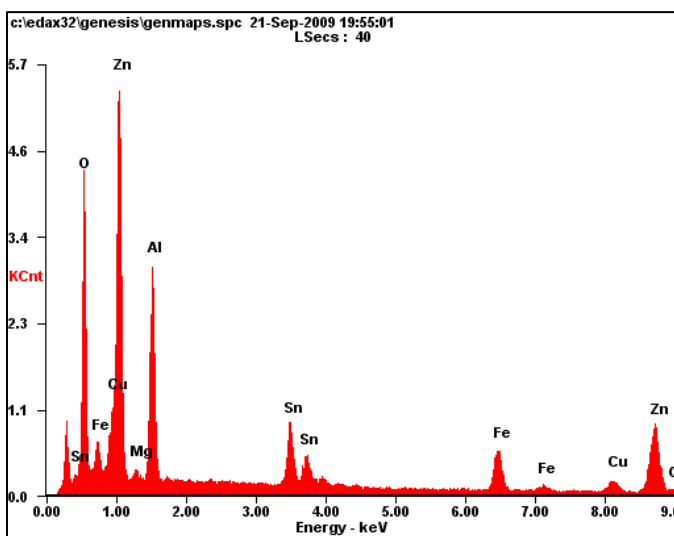
Fig.64b – EDAX analysis show the presence of the oxides of aluminium, magnesium, copper, zinc, tin and iron

EDAX analysis has revealed the presence of the oxides of aluminium, magnesium, copper, zinc, tin and iron (Fig.64b). Aluminium is the base metal of 5182 alloy, while magnesium and copper are the main alloying elements. Zinc and tin are the elements present in the coating of the steel rivet. Clearly there was fretting at the mating area between the 5182 alloy and the rivet. This was more severe in the areas below the 3 and 9 o'clock positions. It was also observed that the fretting scars in the 5182 buttonhole led to fatigue crack initiation as presented in Fig.65.
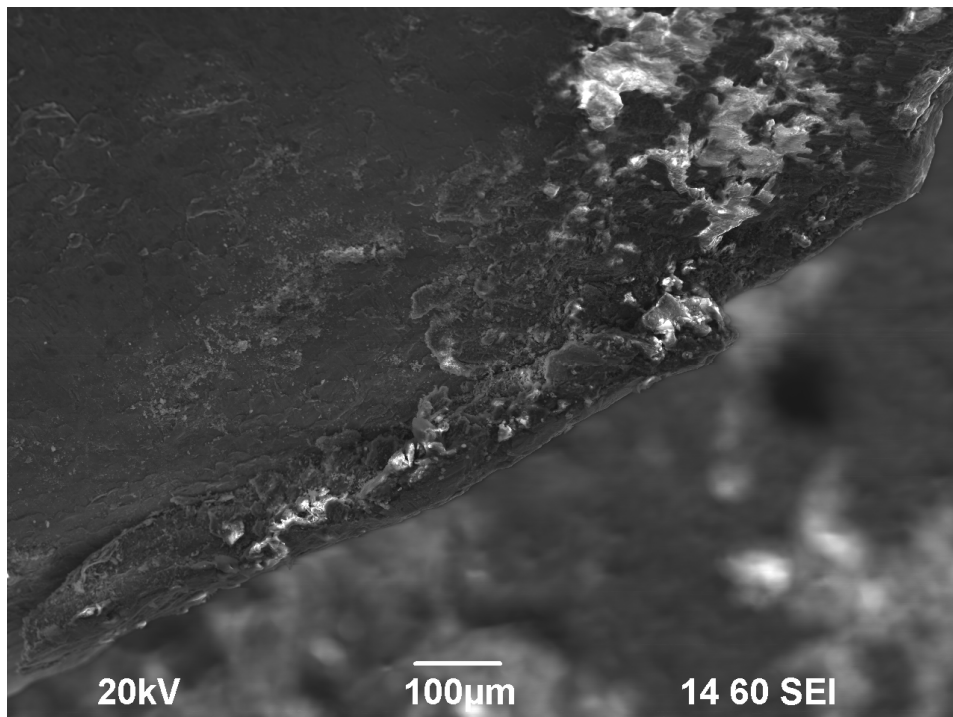
Fig.65 – Fretting scars in the 5182 buttonhole led to fatigue crack initiation

4.10 Discussion of the mechanism of fatigue failure of DP600 Steel + Al 5182

The fatigue failure for all the (DP600 steel + 5182) samples that were tested was by means of fracture of the 5182 locked sheet as presented in Figs. 57(a-d). Close observation of the fractured samples also showed evidence of fretting scars on the surface of both the DP600 and the 5182 aluminium alloy as shown in Figs. 59, 60 and 61. This was further confirmed by examination using SEM that also revealed evidence of fretting scars on the surface of the steel around the periphery of the rivet and below the larger and thicker scars. Fretting damage typically occurs on the contacting surfaces of components that are fastened or clamped together. Fretting is caused by repeated alternating slipping of the

mating surfaces over part of their mutual contact. Based on the examination of the fractured samples, it was apparent that the position of fatigue fracture changed with the maximum applied load as can be observed in Figs.57(a-d) and 58. For example, the fracture position for the samples tested to a maximum load of 4.2kN was close to the 3 and 9 o'clock positions at the periphery of the buttonhole of the 5182 locked sheet. As the maximum applied load decreased, the position of the fatigue fracture shifted lower down the periphery of the buttonhole. For example, for the sample that was tested at a maximum load of 3 kN, the position of fracture approached the 6 o'clock position. For rivets of optimum quality, the rivet setting force must be high enough to produce a joint with a high interlock distance. The rivet works in such a way as to tighten the two sheets together. In such a situation, when a load is applied to the joint, the load will be transmitted primarily by surface friction between the two mating sheets. As a result, the rivet plays a lesser role for transmitting the load. Under such conditions, deformation around the buttonhole will be restricted. However, as a result of a combination of the applied load and of the number of fatigue cycles, the joint can gradually become less tight and this can promote fretting between the rivet and the buttonhole. Inspection of the periphery of the buttonhole of the 5182 alloy using light microscopy and SEM has shown the presence of fretting scars in Figs.63 and 64 a-b. The SEM investigation has also shown that the fatigue cracks initiate from the fretting scars in the buttonhole area as shown in Fig. 65. In the case of the lower applied loads of 3 and 3.4kN, it was observed that during the fatigue tests, the 5182 alloy would tilt against the mating surface of the rivet and fracture would occur at an angle as shown in Fig. 57a. The amount of fretting was observed to be higher at the positions below the centre of the joint, that is, at between the 4 and 8 o'clock positions. These positions gradually experienced a higher stress concentration and fatigue crack initiation started at these positions. Final failure at the two lower applied load values was observed to occur with the 5182 sheet tilted at an angle in relation with the rivet as presented in Fig.57a. On the other hand at the higher applied loads of 3.8 and 4.2 kN, after loosening of the samples, initiation and propagation of the fatigue cracks was relatively fast with very little or with no tilting of the 5182 sheet as shown in Fig.57d. In such a situation, the fatigue cracks tended to initiate near the central areas of the periphery of the buttonhole.

4.11 Corrosion Studies

An investigation of the corrosion behaviour of (I.F. Steel + Aluminium 5182) samples was conducted using a salt spray test according to the ASTM B117-97 standard for 1000 hrs. Five samples were tested and the results of %weight change for each sample with corrosion time are presented in Fig.66.
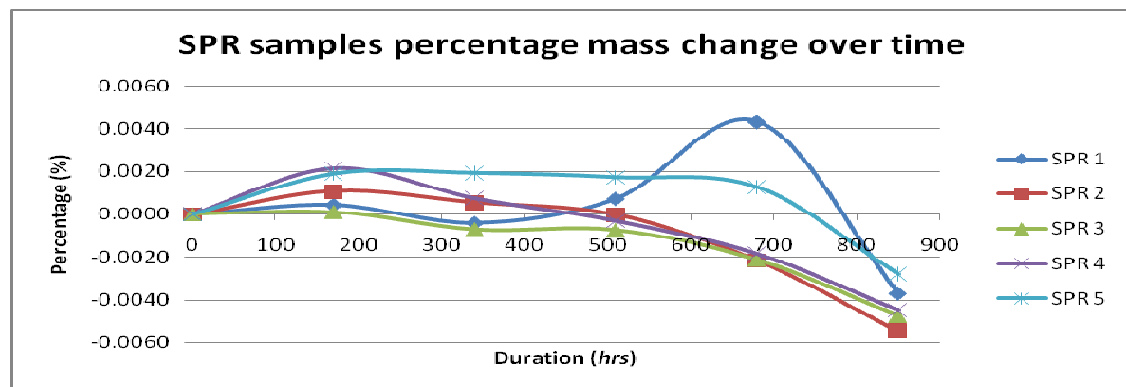
Fig.66 – The % weight change of I.F. Steel + Aluminium 5182 SPR joints with time

During the initial stages of corrosion and in particular during the first 187 hrs, a small weight gain was recorded. The latter part of the salt-spray corrosion treatment was characterized by a weight loss. Inspection of the samples at this stage showed that the weight gain was primarily due to the result of the corrosion of the zinc-rich (Zn-Sn) coating on the surface of both the steel sheet and the rivet. The alloys that were involved in making these samples (I.F. steel, aluminium 5182, the rivet alloy or its coating) were in contact with each other. As a result of the contact between these materials, the initial signs of corrosion were due to galvanic corrosion. The function of the Zn-Sn coating that was to provide corrosion protection by shielding the steel sheet or the rivet material from exposure to water/moisture and oxygen. The Zn-Sn coating for both of these materials was therefore in direct contact with the aluminium alloy.

In other words, zinc is more electronegative than aluminium and will be expected to preferentially corrode in the current sample set up. Fig.67a shows an SEM micrograph of the corrosion product on the surface of the rivet after 187 hours. EDAX analysis shown in the figure indicated that the corrosion deposit was mainly zinc oxide (ZnO) (Fig.67b).

Element	Wt%	At%
OK	36.20	69.35
ClK	01.85	01.60
ZnK	61.96	29.05
Matrix	Correction	ZAF
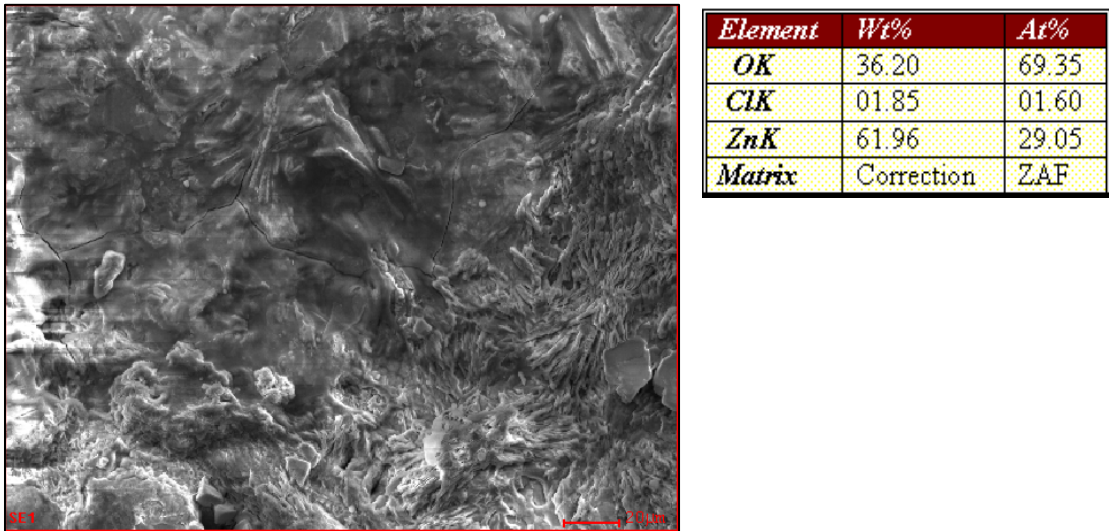
Fig.67a – Corrosion product on the surface of the rivet after 187 hrs of exposure
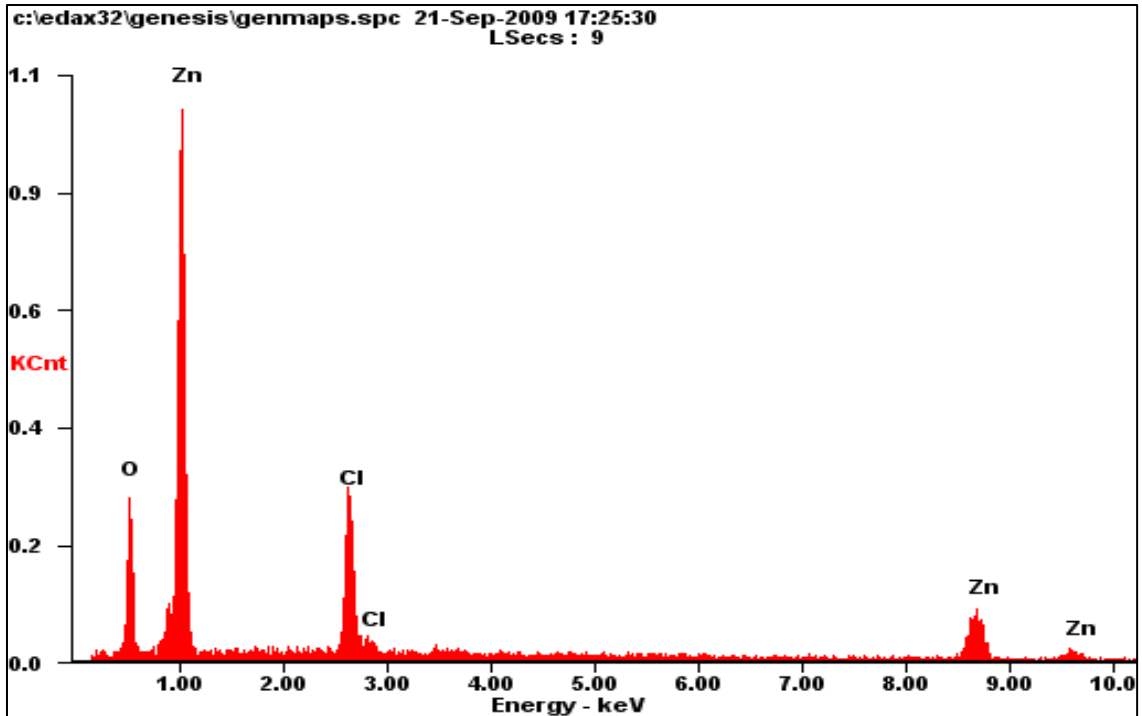
Fig.67b – EDAX analysis show that the corrosion deposit was mainly zinc oxide (ZnO)
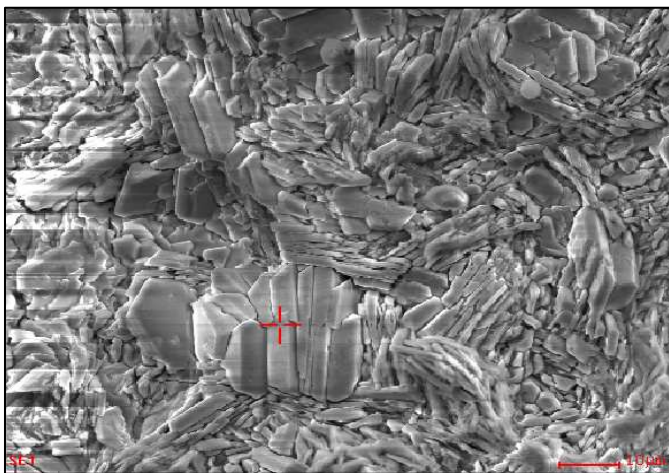
Element	Wt%	At%
OK	14.27	37.42
ClK	13.95	16.51
ZnK	71.78	46.07
Matrix	Correction	ZAF

Fig.68a – Presence of chlorine on the rivet surface
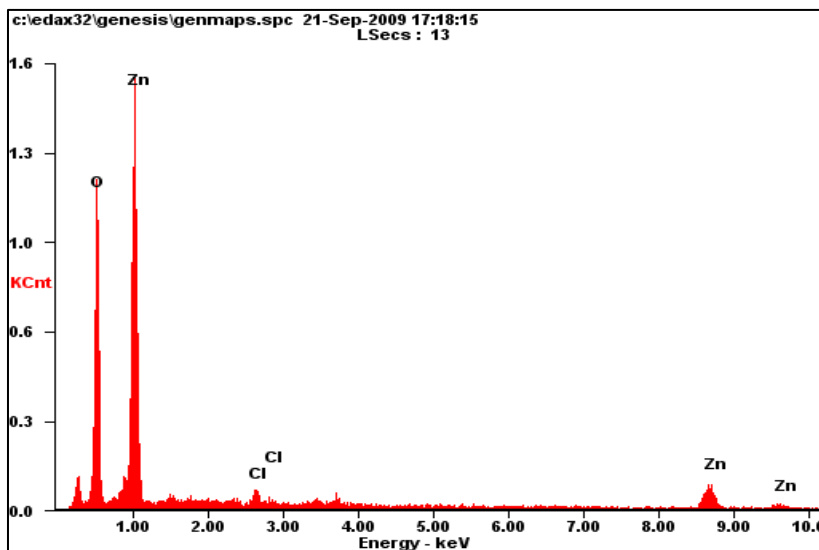
Fig.68b – Presence of chlorine on the rivet surface indicating the formation of
simonkolleite $(Zn_5(OH)_8Cl_2.H_2O)$ rod-like particles

In some parts of the rivet surface, small amounts of chlorine were also detected suggesting the presence of traces of simonkolleite $(Zn_5(OH)_8Cl_2.H_2O)$ particles as shown in Figs.68 (a-b). The observation of ZnO and $(Zn_5(OH)_8Cl_2.H_2O)$ in the corrosion product is in agreement with the results reported by Almeida and Morcillo [104] who studied the corrosion of automotive steels coated with zinc in chloride media. In addition, it was observed that tin (from the zinc-rich coating) also corroded and formed a solution of zinc-tin oxide. The highlighted particles in Figs. 69 (a-b) are evidence of particles of this solution of oxides as shown by the EDAX analysis. The production of ZnO, $(Zn_5(OH)_8Cl_2.H_2O)$ and Zn-Sn oxides were associated with the weight gain that was observed during the initial stages of corrosion.

Element	Wt%	At%
OK	36.98	75.95
SnL	33.76	09.35
ZnK	29.26	14.71
Matrix	Correction	ZAF

Fig.69a – Particles of zinc-tin oxide solution
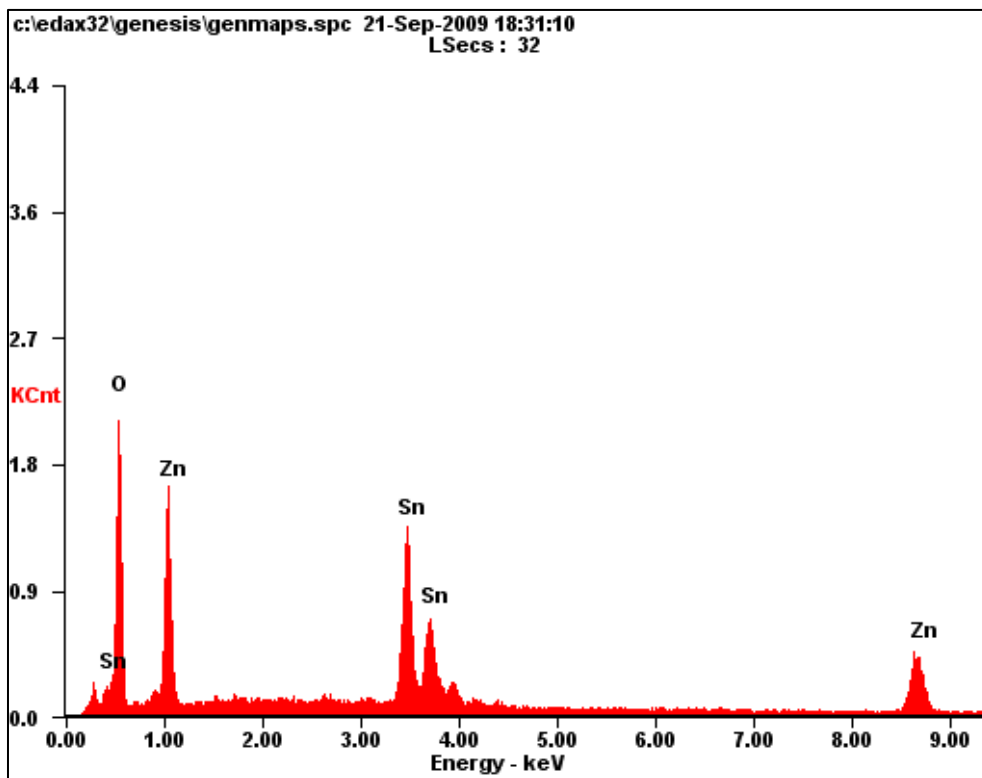
Fig.69b – EDAX results indicating the formation of a solution of zinc-tin oxide

Essentially the corrosion reaction during the early stages was the oxidation of zinc as a result of galvanic corrosion to form ZnO and the associated corrosion products:

$$Zn_{(s)} + \tfrac{1}{2}\, O_{2(g)} \rightarrow ZnO_{(s)}$$
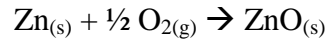
In addition, interaction of ZnO with chlorine (from NaCl) was observed to form small amounts of simonkolleite. Fig. 70 shows a photograph of the samples after corrosion treatment for 187 hrs indicating that the samples were covered with a white corrosion product.

Fig.70 – Samples after 187 hrs of corrosion treatment

During this initial period, corrosion was also observed to occur at the overlap between the two riveted sheets. The corrosion products were the same as reported above due to corrosion of the zinc-rich coating on the surface of the I.F. steel. At the sides of the I.F. steel (where it was cut in preparing the samples), the steel was exposed and there was evidence of corrosion of iron. A typical example of corrosion at the overlap after 351 hrs is presented in Fig.71.
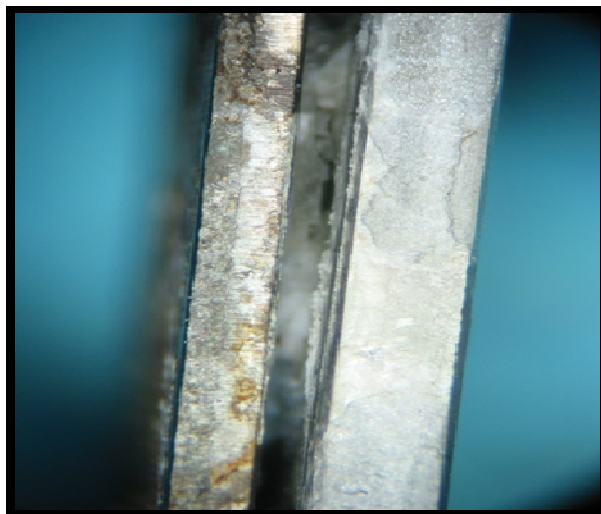
Fig.71 - Corrosion at the overlap of I.F. Steel + 5182 SPR samples after 351 hrs
          of exposure

This observation of corrosion that had occurred within the overlap was the result of differential aeration corrosion, sometimes also referred to as crevice corrosion. The factor that gives this type of corrosion is the fact that there is a differential in the concentration of oxygen between the electrolyte (water, moisture and steam in the salt spray) within the overlap and the electrolyte in the surrounding area. The oxygen concentration in the electrolyte in the surrounding areas is higher and this makes the area within the overlap anodic to the surrounding area which becomes cathodic. The anodic reaction, in the case of zinc, can be presented as:

$$Zn \rightarrow Zn^{2+} + 2e^-$$
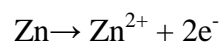
while the cathodic reaction is presented as:

$$2H_2O + O_2 + 4e^- \rightarrow 4OH^-$$
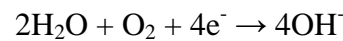
As a result, the area within the overlap corroded and the corrosion products piled up within the overlap and contributed more to the weight gain during the initial stages of corrosion. Corrosion in this area was observed to initiate at the outer regions of the overlap and gradually moved inwards towards the rivet. The corrosion affected area within the overlap increased with time as the electrolyte gradually moved further towards the centre of the overlap. Fig.72 presents two sectioned samples after 660 hrs of treatment showing progression of the corroded areas almost to the centre of the joint. It must be noted that in Fig.72 there is evidence of corrosion of I.F. steel progressing from the side of the sheet towards the centre. Similarly there seems to be evidence of corrosion the aluminium sheet.

Fig.72 – Progression of the corrosion progressing towards the centre of the overlap after 660 hrs of corrosion

The progression of differential aeration corrosion with time at the interface between the two sheets is also presented in Figs.73(a-d). These figures show that the build up of the corrosion products within the overlap increased with time. After sufficient build up of the zinc corrosion products, a loss of direct contact between the metal was lost and this gave rise to the corrosion of iron (from steel) and aluminium within the overlap. In the case of two samples, the build up of the corrosion product within the overlap generated stresses and led to failure of the rivet. The corrosion of the rivet probably gradually progressed in the areas below the rivet head and into the crevice that was produced by the piercing process. Figs.74 (a-b) show the corrosion on the surface of the steel rivet that has fractured.
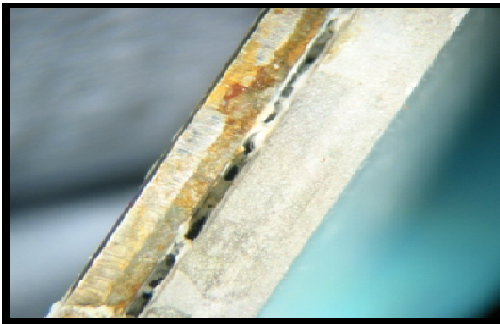
Fig.73a – Oxide build-up after 351 hours exposure
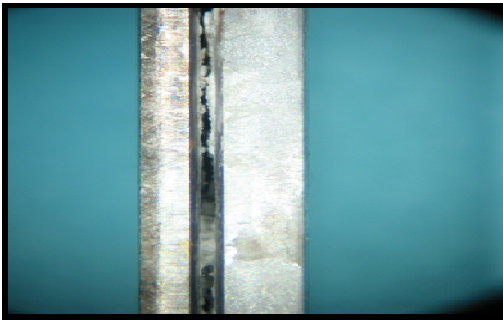
Fig.73b – Oxide build-up after 496 hours exposure
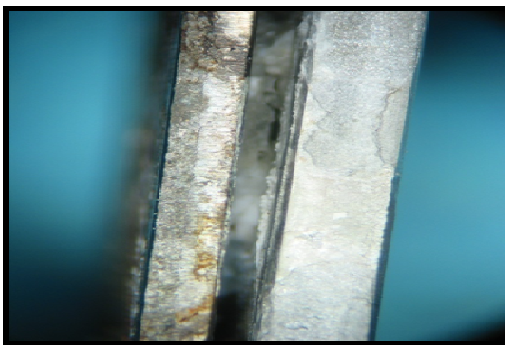
Fig.73c – Oxide build-up after 660 hours exposure
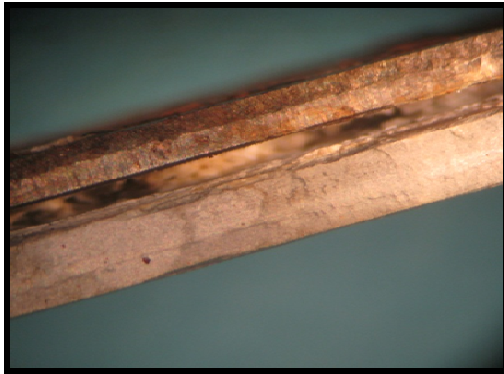
Fig.73d – Oxide build-up after 845 hours exposure
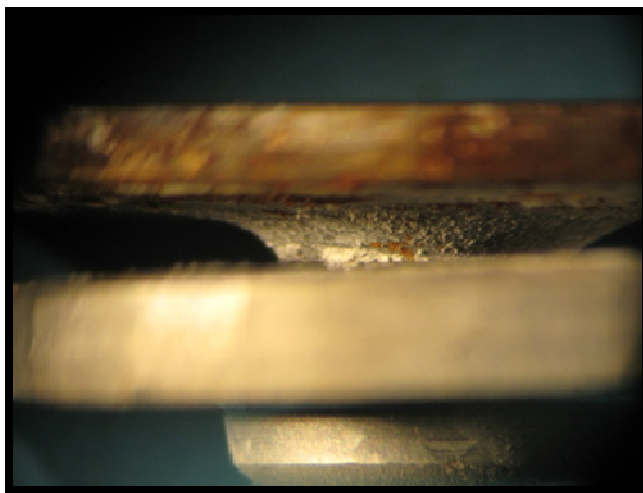
Fig.74a – Failure at the overlap of I.F. Steel + 5182 SPR samples after 660 hrs
            of exposure
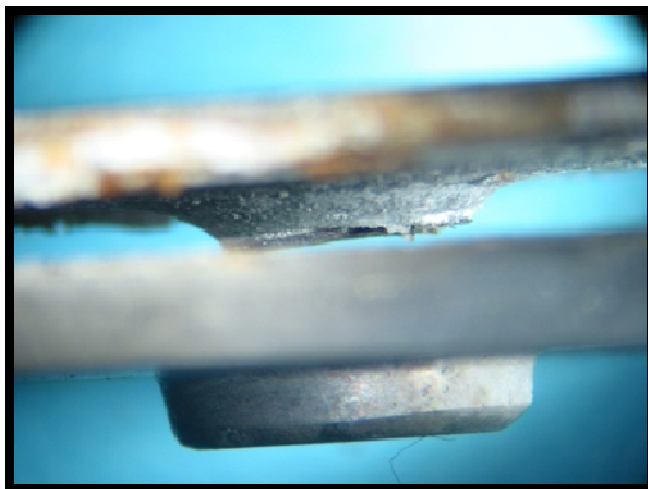
Fig. 74b – Failure at the overlap of I.F. Steel + 5182 SPR samples after 660 hrs
            of exposure

Examination of the fracture surface as shown in Fig.75 also revealed evidence of corrosion in some areas where fracture took place. It was therefore concluded that a combination of two factors led to the failure of these samples during the corrosion test; the build up of the corrosion products within the overlap provided high enough tensile stresses, while the corrosion of the rivet led to weakening of the rivet surface.
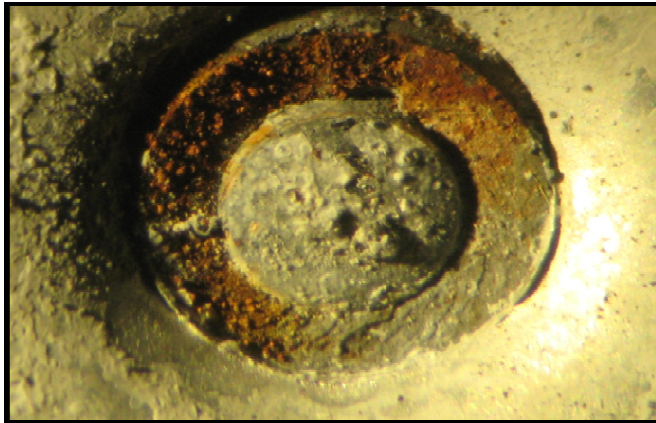
Fig.75 – Rivet fracture surface, 5182 side, after corrosion treatment for 660 hrs

Examination of the area around the rivet-head periphery as presented in Figs.76 (a-d), showed corrosion of the Zn-Sn coating from both the rivet and the I.F. steel. In Fig.76(a) it was evident that after 351 hrs of the salt-spray treatment, the gap between the rivet and the I.F. steel sheet was covered with the zinc corrosion product. As corrosion progressed, the zinc corrosion products gradually became detached away from the area at the top of the sample around the rivet-head and the I.F. steel sheet. At this point the steel surface started to become exposed and began to suffer from corrosion as shown in Figs.76 (b-d). In addition, there was also evidence of corrosion of iron around the periphery of the I.F. steel.
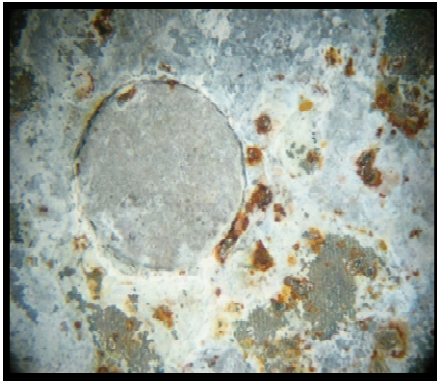
Fig.76a – SPR after 351 hours of exposure
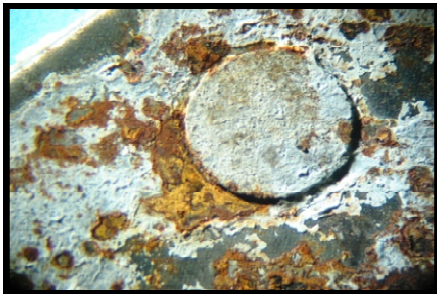
Fig.76b – SPR after 496 hours of exposure

Fig.76c – SPR after 660 hours of exposure

Fig.76d – SPR after 845 hours of exposure

After about 660 hrs of exposure, a significant amount of zinc had been lost from the I.F. steel surface thus exposing in many regions, areas steel that no longer had the protection of zinc. This observation which is presented in Fig.77 was followed by a weight loss as iron began to corrode very fast. During the initial part of corrosion, a weight gain was recorded for all the samples. This was mainly due to the corrosion of zinc, where the zinc took up oxygen thus increasing the weight of each sample. There was also a contribution   to the weight gain by the differential aeration corrosion within the overlap between the two sheets.

Fig.77 – Significant amount of zinc which had been lost from the I.F. steel surface after
        660 hrs

However, with time, the accelerated corrosion test led to removal of the zinc corrosion products and exposed the I.F. steel, whereupon, corrosion of iron commenced. The product of the corrosion of iron was Fe_2O_3. The quality of an oxide with regard to its ability to provide corrosion protection can be assessed by the value of its Pilling-Bedworth ratio. The Pilling-Bedworth ratio is defined as:

$$R_{PB} = \frac{V_{oxide}}{V_{metal}} = \frac{M_{oxide} \cdot \rho_{metal}}{n \cdot M_{metal} \cdot \rho_{oxide}}$$

Where:

R$_{PB}$ is the Pilling-Bedworth ratio,

M - the atomic or molecular mass,

n - number of atoms of metal per one molecule of the oxide,

ρ - density and

V - the molar volume

Using values for iron and Fe_2O_3, the Pilling-Bedworth value was calculated to be 2.14. A value greater than 2 implies that the volume ratio between the oxide and the metal is rather high and therefore the high amount of oxide that forms is under compression and as a result cracks are unable to adhere well enough onto the metal surface to provide protection from corrosion. Thus, the Fe_2O_3 layer on the surface of steel is non-adherent and continuously flakes off giving rise to a fast weight loss as shown in Fig.77. On the other hand, using the relevant values for aluminium and Al_2O_3 [29], the value of the Pilling-Bedworth ratio was calculated to be 1.27 and this value, being between 1 and 2, is expected to adhere onto the surface of the metal and to provide it with corrosion protection. As a result only the iron was expected to contribute to the weight loss of the samples. On the other hand, the oxidation of aluminium was expected to lead to a weight gain, but since Al_2O_3 is a protective oxide, the rate of weight gain for aluminium is expected to be very slow in comparison to the weight loss due to the removal of iron.

At this point of the study, it was decided to also examine the corrosion behaviour of HSLA steel and Aluminium 5182 separately i.e. as individual samples and not in the form of riveted joints. This was decided in order to further examine the individual contribution of each alloy to the corrosion behaviour of the riveted joints. In addition, it was decided to explore in this part of investigation, the ability of pulse current treatment to improve the corrosion resistance of the samples.

Table 9 – Regimes of PEC treatment

No.	Steel HSLA	Aluminum alloy 5182
	Current amplitude, kA	
1	19	24
2	19	24
3	29	35
4	29	35
5	41	52
6	41	52
Remark: specimens No.1, 3, 5 were treated using three pulses with 1 min. interval, specimens No. 2, 4, 6 were treated using three pulses with 3 min. interval		

Account must be taken of the different corrosion behaviour of steel and aluminum alloys; in the case of steel the corrosion product (Fe_2O_3) flakes off and causes the reduction of specimen weight after the corrosion tests, while in the case of aluminium alloys an increase of specimen weight was observed after the corrosion tests because Al_2O_3 has a high adhesion to the base metal (aluminium).

The estimation of the influence of PEC treatment on the corrosion behaviour of specimens was fulfilled in two steps. The percentage change of the weight of each specimen δ_m after tests was estimated in the first stage:

$$\delta_m = \frac{m_c - m_0}{m_0} \cdot 100\% \,,$$

where m_0 and m_c are the weights of the initial specimen and the same specimen after the corrosion tests respectively. In the second stage the influence factor of the PEC treatment on the specimen corrosion, k, was determined as presented below:

$$k = \frac{\left|\delta_m^{untreat}\right| - \left|\delta_m^{treat}\right|}{\left|\delta_m^{untreat}\right|} \cdot 100\% \,,$$

where $\delta_m^{untreat}$ is the percentage change of the weight of untreated specimens (mean for 6 specimens) and δ_m^{treat} is the percentage change of the weight of each specimen treated by PEC (Table 10).

The values of k for all the HSLA samples had a positive value (except for sample 6) and suggested that the PEC treatment extended the corrosion resistance of the steel. The uncharacteristic k value for HSLA sample 6 is likely to be due to experimental error and it would best be ignored. Examination of the k values for 5182 show that the overall effect of the PEC treatment was to extend the corrosion resistance of the material.

Table 10 – Results of corrosion tests

No.	HSLA Steel		Aluminum alloy 5182	
	After PEC treatment			
	δ_m, %	k, %	δ_m, %	k, %
1	-0.5224	+26	+0.1217	+15
2	-0.5310	+25	+0.1571	-9
3	-0.2706	+62	+0.1188	+17
4	-0.6010	+15	+0.0614	+57
5	-0.6890	+2	+0.1640	-14
6	-1.2729	-81	+0.1426	+1
Without PEC treatment				
Mean for 6 specimens	δ_m, %		δ_m, %	
	-0.7050		+0.1437	

Macrophotographs of the surface appearance of the investigated metal specimens after the corrosion tests are presented on Fig.78.
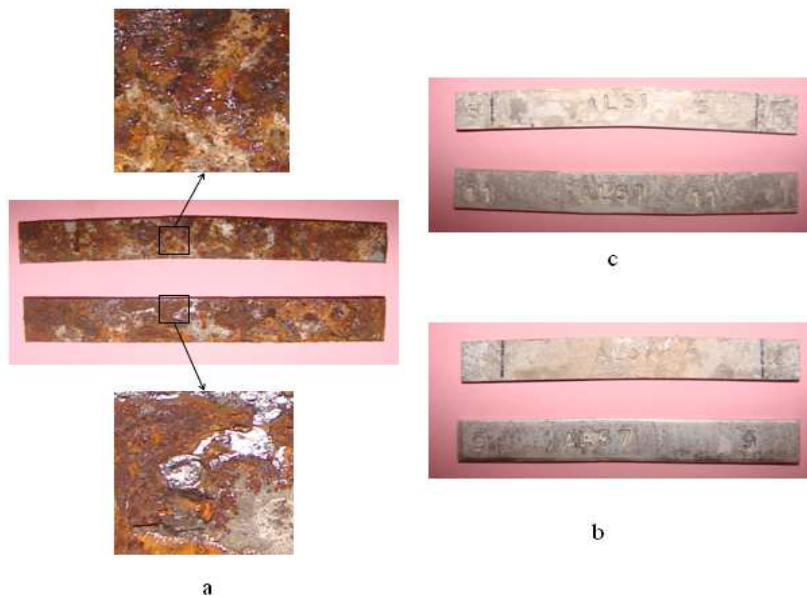
Fig.78 – Surface appearances of investigated metal specimens after corrosion
        tests (specimens after PEC treatment are located on top of each picture,
        specimens without treatment are located on bottom): (a)HSLA steel,
        (b) aluminium alloys 5754 and (c) aluminium alloys 5182

The visual difference in the appearance of treated and untreated specimens in the case of aluminium alloy specimens is insignificant. However, in the case of the HSLA steel specimens, a substantial difference in the corrosion damage of the alloy surface takes place; PEC treatment causes uniform, homogeneous corrosion on the whole surface of specimen. In the case of the specimens without PEC treatment, zones with selective, localized corrosion are visibly clear (Fig.78a). This observation may be to be due to the likelihood that these samples exhibit higher structural and surface heterogeniety. Such heterogeinity may arise during the production of the sheet by means of cold working that builds up non-uniform residual stresses. On the other hand, the PEC treatment may relieve these stresses thus providing a more homogeneous material. However, it must be stressed that research on the effects on PEC treatment is still in its relative "infancy" stages and more research studies are reguired in order to substantiate these results and to understand the reasons for such behaviour. The overall results of this part of the study substantiated the suggestion that once uniform corrosion of the samples starts to take place, iron will contribute to a weight loss of the samples and aluminium to a weight gain.

The corrosion tests results suggest that the PEC treatment with the above regimes influences the behaviour of the investigated metals. The treatment causes deceleration of the corrosion processes for both the HSLA steel and aluminium 5182. The results of k versus current density are presented in Fig.79. The results show that regimes of PEC treatment with maximum effect exist. These regimes are the ones showing the maximum values, that is, for samples 3 and 4 with a current amplitude of 29 kA for HSLA steel and 35 kA for Aluminium 5182 (or current density of 2 kA/mm^2 for both).
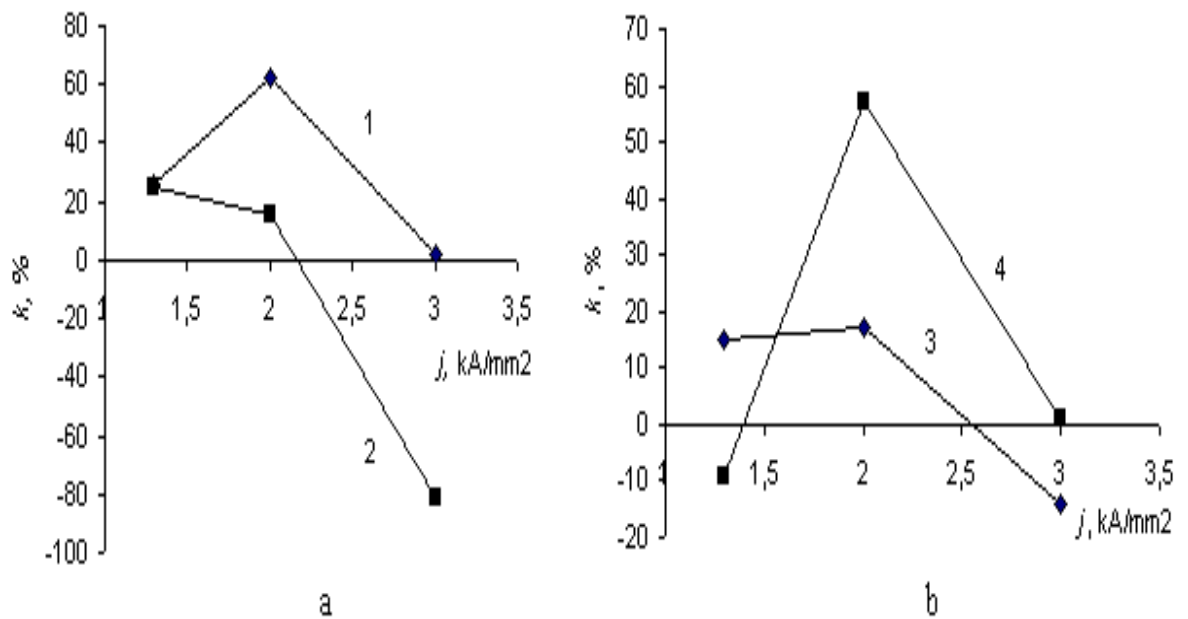
Fig.79 – The change of influence factor of PEC treatment on specimen corrosion (*k*)
against the metal (a – HSLA steel and b –Aluminium 5182 alloy), density of PEC,
and interval between electric current pulse (1, 3, 5 with 1 min. interval and 2, 4,
6 with 3 min. interval)

4.11.1 Effect of corrosion on the lap-shear strength of (I.F. steel top + Aluminium 5182 bottom) SPR joints

The lap-shear strength of (I.F. steel top + 5182 bottom) SPR joints with corrosion time was
monitored by taking samples out of the salt-spray rig at various times and testing them.
The results are presented in Fig.80 and are the average values of three test samples for each
corrosion test time. The results show that there was a small drop in the lap shear strength
followed by a small increase and then by a drop thereafter.
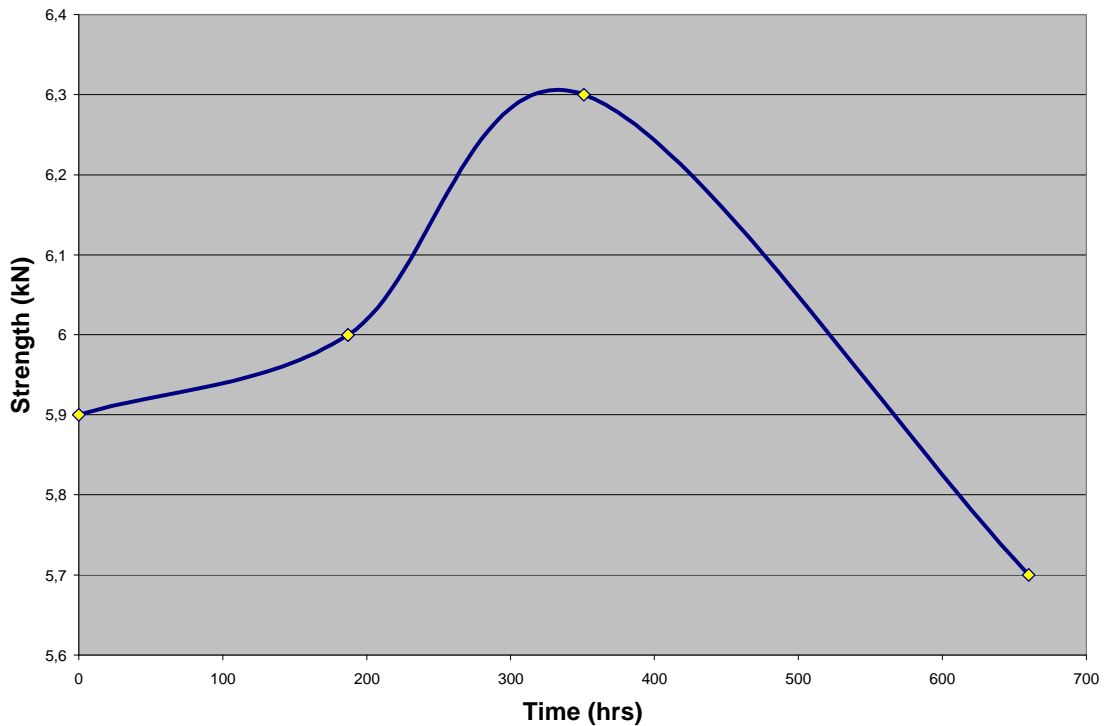
Fig.80 – Effect of Corrosion time on the lap-shear strength of I.F. steel top + 5182 bottom

In order to understand the behaviour of the samples, it is necessary to first consider the mechanism of failure by the lap shear test. In lap shear tests, all the samples were observed to fail by the rivet pulling out of the locked sheet with some deformation of the two sheets also taking place. Rivet pull-out is related to the load transfer mechanism of the joint. During the shear test, shearing of the rivet and bearing of the riveted sheets are expected to take place, similar to the behaviour of a conventional rivet as reported by Kulak [105]. In addition, for a rivet with a countersunk head, tilting of the rivet also took place. By considering the sketch in Fig.81, when a shear force S was applied, two shear components, S_1 and S_2, were created and formed a couple that acted on the rivet as shown.
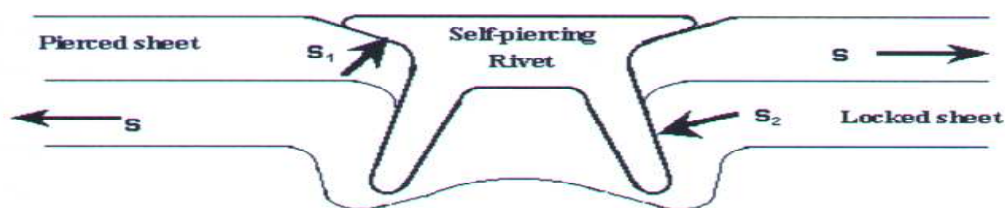
Fig.81 – The two components which are acted on the rivet by applying a shear force

As a consequence, the rivet tilted up by overcoming the frictional force between the rivet and the two riveted sheets. At the same time, bending also tended to pull the rivet out. During shear testing, both the pierced and the locked sheets were in bearing against the rivet, while the rivet was subjected to a shear and a pull-out force due to tilting and due to the effect of bending. As the loading process proceeded, the riveted sheets suffered localised yielding. The shear force was not sufficient to fracture the rivet, while the increase in the pull-out force enabled the rivet to overcome the frictional force at the interface between the rivet shank and the riveted sheets. Failure therefore occurred by the rivet being pulled out with some deformation of the riveted sheets. Part of the loading force was also taken up by friction between the two rivet sheets. During the early stages of corrosion, an increase in the lap shear strength was recorded. This observation was associated with the gradual build up of the corrosion products within the overlap between the two sheets. During the test, the frictional force that had to be overcome at the overlap therefore increased and this led to an increase in the lap shear strength of the samples. There was probably also a contribution by the corrosion products at the contact points between the rivet and the locked sheet by increasing the frictional force that had to be overcome at that area. After corrosion treatment for 351 hours, a decrease in the lap shear strength was observed. This was associated with the build up of stresses within the overlap and this also led to failure of some samples during the corrosion test. Also by this point, some of the steel began to be exposed leading to corrosion of iron. As explained earlier, the volume of the Fe_2O_3 product was much higher than that of the base metal and as a result it flaked off. The resulting material loss was therefore expected to lead to weakening of the samples once Fe_2O_3 began to flake off.

CHAPTER FIVE

5. CONCLUSIONS

Based on the investigation that was conducted, the following conclusions were drawn:

1. For the I.F. steel to 5182 joints that were examined, there was an inter-correlation between the rivet head height, the interlock distance and the lap shear strength. A high interlock distance provided a joint of higher strength, while a low head height was indicative of a higher interlock distance. The measurement of the head height can therefore be used as a non-destructive method to assess whether the strength of a SPR joint will be satisfactory or not. When joining 1.2mm I.F. steel to aluminium alloy 5182, it was concluded that for a higher joint strength, it is preferable to use the steel as the top sheet as this results in a greater interlock distance.

2. Even though the (I.F. steel top + 5182 bottom) modification exhibited a higher lap shear strength and a higher interlock distance than the (5182 top + I.F. steel bottom) modification, the latter was observed to have a better fatigue resistance at lower loads. This observation was attributed to the fact that the lap shear strength of SPR is dominated by a number of factors including plastic deformation of the rivet and the buttonhole, while the fatigue behaviour is dominated by elastic stress concentration. As a result caution needs to be exercised when the interlock distance is considered as a factor to predict fatigue behaviour.

3. During fatigue testing of (I.F. steel top + 5182 bottom) samples, a crack was observed to initiate and propagate in the I.F. steel. However, this did not propagate to failure as the sample underwent bending in such a way to transmit the load to the rivet. Eventual failure was due to cracks in the buttonhole and rivet pull-out.

4. Fretting scars and were observed to form in all the samples that were tested. These were subsequently observed to lead to the initiation of fatigue cracks and failure of the joints.

5. The position of fatigue crack initiation for the (DP600 + 5182) samples was observed to be dependent on the maximum applied load. For the higher loads, fatigue cracks initiated at the central areas of the periphery of the 5182 buttonhole (the 3 and 9 o'clock positions). Fatigue cracks under lower applied load values were observed to initiate lower down the periphery of the buttonhole. This observation was attributed to tilting of the 5182 in relation to the rivet.

6. The corrosion investigation showed that the samples underwent various types of corrosion; galvanic and differential aeration corrosion were observed in the initial stages followed by uniform corrosion in the latter stages. The strength of the (HSLA 350 + 5182) corroded samples initially increased as a result of the corrosion product at the lap interface providing an increase in the friction at the overlap. As a result a higher load was required to overcome the increasing frictional force. After 660 hrs of corrosion treatment, the lap shear strength of the samples began to decrease. In fact some samples had failed during the corrosion treatment. This was due to excessive build up of the corrosion product within the overlap. As a result, high stresses were built within the overlap leading to sample failure.

7. PEC treatment was observed to increase the corrosion resistance of HSLA steel. This was attributed to the reduction of residual stresses in the material giving rise to a more uniform structure.

CHAPTER SIX

6. FUTURE RECOMMENDED WORK

On the basis of the achievements of the current investigation, the following recommendations for future work are suggested:

1. The current study has contributed to the state-of-the-art knowledge of the fatigue behaviour of SPR joints between steel and aluminium alloys. However, the author believes that fundamental knowledge of this behaviour is still lacking. Considering that it is desirable for the automotive industry to develop modelling capability to predict the fatigue behaviour, it is necessary for further and more focused studies to be conducted on the fatigue behaviour. In particular, the effects of fretting and   of bending of samples need to be further studied.

2. The corrosion study has shown details of the corrosion mechanisms that take place for SPR. It is now to extend this to further examine corrosion protection at a fundamental level. In addition, PEC treatment appeared to be promising as a new means to extend the corrosion resistance of automotive materials and joints. Since the method is still in its infancy, it is recommended that further studies are required in order to fully understand its effects on the properties and behaviour of materials.

CHAPTER SEVEN

7. REFERENCES

1. J. Mortimer. International Robot: An International Journal. Volume 28, Number 3-2001,2001, p 192-198.

2. L. Han, "Mechanical Behaviour of Self-Piercing Riveted Aluminium Joints", Ph.D Thesis, University of Hertfordshire, 2003.

3. http://www.henrob.de/pages/frames.htm, (20 November 2005).

4. J. Hulbert, 1972, "Riveting Without Pre-punching", Machine Design, April 6.

5. R. Doo, 1993, "Automotive Body Construction Using Self-Piercing Rivets", Automotive   Manufacturing International 1993, 1-4.

6. H. Hill, 1994, "Introduction to the Self-Pierce Riveting Process and Equipment", IBEC 1994 - Body Assembly and Manufacturing, 1-9.

7. K. Edwards, 1992, "Pierce and Roll Riveting" – The Alternative to Spot Welding, Aluminium Industry, 11, No. 5, 24-26.

8. E. P. Patrick, M. L. Sharp, 1992, "Joining Aluminium Body Structure", Automotive Engineering, 100, No.5, 31-33.

9. J. Mortimer, 1994, Bonding: Sticking Points, Vehicle Engineering & Design, June, 9.

10. http://www.twi.co.uk/j32k/protected/band_3/kschjg002.html, (20 January 2006).

11. R.P. King, "Analysis and Quality Monitoring of a Self-Pierce Riveting Process", Ph.D. Thesis, University of Hertfordshire, 1997.

12. E.P. Patrick, J. R. Auhl and T.S. Sun, "Understanding the process mechanisms is key to reliable resistance spot welding aluminium autobody components", SAE Technical Paper, 840291, 1984.

13. J.R. Auhl and E. P. Patrick, " Afresh look at resistance spot welding of aluminium automotive components",SAE Technical Paper, 940160, 1994.

14. I. J. Polmear, "Light alloys", Third edition, Edward Arnold, 1995.

15. A. B. D. Gingell and T. G. Gooch, "Review of factors influencing porosity in aluminium arc welds", TWI Report, 625/1997.

16. T. A. Barnes and I. R. Pashby, "Joining technigues for aluminium spaceframes used in automobiles, Part I, II – solid and liquid phase welding", Journal of Materials Processing Technology, 99 (2000), 62-79.

17. L. Jones, "Laser make advances in welding of automotive aluminium alloys", TWI Bulletin 2 March 1995.

18. Stephan W. Kallee, Wayne M. Thomas and E. Dave Nicholas, "Friction stir welding of lightweight materials", International conference on magnesium alloys and their applications, 26-28 September 2000, Munich.

19. D. J. Warldron, R. W. Roberts, C. J. Dawes, P. J. Tubby, "Friction stir welding – A Revolutionary new joining method", SAE Technical Paper, 982149, 1998.

20. Stephan Kallee and Dave Nicholas, "Application of friction stir welding to lightweight vehicles", SAE Technical Paper, 982362, 1998.

21. S. M. Tavakoli, "Durability of structural adhesives and adhesively bonded joints and mechanisms of environmetal attack – A review", TWI, 1993.

22. http://www.henrob.de/pages/frames.htm, (14 March 2006).

23. G. S. Booth, C. A. Olivier, S.A. Westgate, F. Liebrecht and S.Braunling, "Self-Piercing Riveted Joints and Resistance Spot Welded Joint in Steel and Aluminium", SAE Papers 2000-01-2681, 2000.

24. http://www.findarticles.com/cf_dls/m3MKT/185_108/65542863/p1/article.html, (06 May 2006).

25. MSc Automobile Engineering – "Technical developments of Materials".

26. http://www.istc.ru/istc/db/projects.nsf/we/2664, (04 July 2006).

27. Llewellyn, D. T. "Steels:metallurgy and applications"/ D.T. Llewellyn and R. C. Hudd

28. http://www.steelforge.com/infoservices/matoverview/mo_hsla_steel.asp, (24 October 2006).

29. D.R. Askeland, "The science and Engineering of Materials", 3rd Edition, Stanley Thornes Ltd.

30 Hill, H., 1994. Introduction to the self-pierce riveting process and equipment. In:IBEC'94 Body Assembly and Manufacture, vol.8, Warren, pp. 1–9.

31. Budde, L., Lappe, W., 1991. Riveting without pre-punching; self pierce riveting has a future in the sheet metal processing industry. Bander Bleche Rohre 32, 94–100.

32. Budde, L., Lappe, W., Liebrecht, F., 1992. Further developments in the self-piercing rivet technology. Bleche Rohre Profile 39, 310–314.

33. Bokhari, N., 1995. Self-piercing riveting—process and equipment. Weld. Met. Fabrication 63 (5), 186–188.

34. King, R.P., O'Sullivan, J.M., Spurgeon, D., Bentley, P., 1995. Setting load requirements and fastening strength in the self-pierce riveting process. In: Proceedings of the 11th National.

35. Taylor, G., 1997. Self pierce riveting in automotive assembly. In: Proceedings of the 30th ISATA Materials for Energy Efficient Vehicles Conference, Florence, Italy, June 16–19, pp. 229–240.

36. ETI, 2002. Self-piercing rivet (SPR) specifications. Emhart Teknologies Inc.

37. Henrob Group, http://www.henrob.co.uk, (15 February 2007).

38. Hou, W., Mangialardi, E., Hu, S.J., Wang, P.C., Menassa, R., 2004. Characterization for quality monitoring of a self-piercing riveting process. In: Proceedings of the Sheet Metal Welding conference XI, Sterling Heights, MI, 2004, Paper No. 8-3.

39. Westgate S.A., Razmjoo G.R., 1999. Static and fatigue performance of mechanically fastened and hybrid joints in steel metals, TWI Report 691/1999.

40. Fu, M., Mallick, P.K., 2001. Effect of process variables on the static and fatigue properties of self-piercing riveted joints in aluminium alloy 5754, SAE Technical paper 0825; pp. 117–129.

41. Fu, M., Mallick, P.K., 2003. Fatigue of self-piercing riveted joints in aluminium alloy 6111. Int. J. Fatigue 25, 183–189.

42. Chen, Y.K., Han, L., Chrysanthou, A., O'Sullivan, J.M., 2003. Fretting wear in self-piercing riveted aluminium sheet. Wear 255, 1463–1470.

43. Han, L., Chrysanthou, A., O'Sullivan, J.M., 2006a. Fretting behaviour of self-piercing riveted aluminium alloy joints under different interfacial conditions. Materials Design 27,(3), 200–208.

44. Razmjoo, G.R., Westgate, A., 1999. Fatigue properties of clinched, self-piercing riveted and spot welded joints in steel and aluminium alloy sheet, TWI Report, 680/1999.

45. Howard, R.M., Sunday, S.P., 1983. The Corrosion performance of steel self-pierce rivets when used with aluminium components, SAE Technical Paper Series 831816.

46. Bazdresch R.Z., 2001. Aluminium self pierce rivets for use in the construction of aluminium vehicles. MS Dissertation. University of Warwick.

47. Krause, A.R., Chernenkoff, R.A., 1995. A comparative study of the fatigue behaviour of spot welded and mechanically fastened aluminium joints, SAE Technical Paper 950710.

48. Riches, S.T., Westgate, S.A., Nicholas, E.D., Powell, H.J., 1995. Advanced joining technologies for lightweight vehicle manufacture. In: Proceedings of the Materials for Lean Weight Vehicles Conference, Institute of Materials, pp. 137–146.

49. Miller, K.W., Chao, Y.J., Wang, P.C., 1998. Performance comparison of spot-welded, adhesive bonded, and self-piercing riveted aluminium joints. In: ASM Proceedings of the International Conference: Trends in Welding Research, pp. 910–915.

50. Stegemann, T., Hahn, O., Schulte, A., 1998. Advanced joining techniques for modern lightweight steel construction. La Revue de M/etallurgie-CIT 95 (1), 95–107.

51. Sun, X., Stephens, E.V., Khaleel, M.A., Shao, H., Kimchi, M., 2004. Resistance spot welding of aluminium alloy to steel with transition material – from process to performance—Part I. experimental study. Weld. J. (Miami, FL) 83 (6), 188-S–195-S.

52. Sun, X., Khaleel, M.A., 2005. Strength estimation of self-piercing rivets using lower bound limit load analysis. Sci. Technol. Weld. Joining 10 (5), 624–635.

53. Lennon, R., Pedreschi, R., Sinha, B.P., 1999. Comparative study of some mechanical connections in cold formed steel. Constr. Build. Mater. 13, 109–116.

54. Bonde, N., Grange-Jansson, S., 1996. Self-piercing riveting in high strength steel—a way to increase fatigue life. In: Advanced Technologies & Process. IBEC, pp. 16–20.

55. Olivier, C.A., 2000. Comparison of static properties of point and hybrid joints in steel sheets, TWI Report, 695/2000.

56. Booth, G., Olivier, C., Westgate, S., Liebrecht, F., Braunling, G., 2000. Self-piercing riveted joints and resistance spot welded joints in steel and aluminium, Proceedings of the International Body Engineering Conference. Detroit, MI, October 3–5. SAE Paper 2000-01-2681.

57. Cai, W., Wang, P.C., Yang, W., 2005. Assembly dimensional prediction for self-piercing riveted aluminium panels. Int. J. Machine Tools Manuf. 45, 695–704.

58. Hahn, O., Meschut, G., Peetz, A., 1999. Mechanical properties of punch-riveted and adhesive-bonded aluminium sheets. Weld. Cutting 51 (7), E130–E134.

59. Sunday, S.P., 1983. Self pierce rivets for aluminium components, SAE Technical Paper Series 830526.

60. Bonde, N., 1995. Choosing Henrob self-piercing rivet for the joint between the engine cover and fire wall of the new truck cab, Volvo internal report LM-500872.

61. Litherland, H., 1998. Self-piercing riveting for aluminium applications. In: Proceedings of the Seventh International Conference INALCO'98, Cambridge, April 15–17, pp. 135–147.

62. Tileli, F., O'Sullivan, J.M., Chen, Y.K., Andrew, J., Denham, K., 1999. Dynamic response of self-pierce riveted joints. In: Proceedings of the 15th National Conference on Manufacturing Research, pp. 3–7.

63. Li, B., Fatemi, A., 2006. An experimental investigation of deformation and fatigue behaviour of coach peel riveted joints. Int. J. Fatigue 28 (1), 9–18.

64. Agrawal, H., Li, W., Bollimunta, S., Potty, K., Blows, A., 2003. Fatigue life of self-piercing rivets (SPR) in car body, SAE Technical Paper Series 2003-01-914.

65. Mizukoshi, H., Okada, H., 1997. Fatigue properties of mechanical fastening joints. Mater. Sci. Forum 242, 231–238.

66. Jin, Z., Mallick, P.K., 2002. Enhancement of fatigue life of self-piercing riveted joints by coining. In: Proceedings of the ASME IMECE 2002-MED-323368.

67. Neugebauer, R., Mauermann, R., Grutzner, R., 2005. Combination of hydroforming and joining. Steel Res. Int. 76 (12), 939–944.

68. Iyer, K., Hu, S.J., Brittman, F.L., Wang, P.C., Hayden, D.B., Marin, S.P., 2005. Fatigue of single-and double-rivet self-piercing riveted lap joints. Fatigue Fracture Eng. Mater. Struct. 28, 997–1007.

69. Olivier, C.A., 1999. Comparison of static properties of point and hybrid joints in steel sheets. TWI Report 88254.01/99/1039.1.

70. Madasamy, C., Faruque, O., Tyan, T., Thomas, R., 2001. Static and impact behaviour of self-pierced rivet connections in aluminium. In: Proceedings of the ASME International Mechanical Engineering Congress and Exposition IMECE 2001, November 11–16, New York, pp. 73–79.

71. Madasamy, C., Faruque, O., Tyan, T., 2002. Experimental study on the crash performance of aluminium and steel rails. In: Proceedings of the ASME International Mechanical Engineering Congress and Exposition IMECE 2002, 17–22 November, New Orleans, LA, pp. 223–231.

72. Weber, A., 2004. A new look at an old technology. Assembly 47 (6), 38–45.

73. Hahn, O., Wibbeke, T., 2005. Application of low-heat hybrid joining technologies for the joining of thin-walled sheet materials. Weld. Cutting 4 (4), 208–214.

74. Anon., 2005. School bus learns adhesives lesson. Assembly 48 (3), 20–23.

75. Whitworth, B., 2006. Lotus highlights flexibility with VVA modular build. Automotive Eng. (London) 31 (3), 40.

76. Iyer, K., Brittman, F.L., Hu, S.J., Wang, P.C., Hayden, D.B., Marin, S.P., 2002. Fatigue and fretting of self-piercing riveted joints. In: Proceedings of the ASME International Mechanical Engineering Congress and Exposition IMECE 2002, November 17–22, New Orleans, LA, pp. 401–415.

77. He, X., Pearson, I., Young, K.W., 2007b. Finite element analysis of self-pierce riveted joints. Key Eng. Mater. 344, 647–654.

78. Hahn, O., D olle, N., 2001. Numerische simulation des ¨f¨ugeprozesses beim stanznieten mit halbhohlniet vonduktilen blechwerkstoffen. Universit¨at Paderborn, LWF journal of materials processing technology 199 (2008) 27–36 Schriftreihe 48, Shaker Verlag, Aachen, ISBN3-8265 -9427-4.

79. S. A. Westgate, R. Doo, F. Liebrecht, S. Braeunling, T. Mattsin and K-O. Stromberg, "The Development of lightweight self-piercing riveting equipment", SAE World Congress Detroit, Michigan, March 5-8, 2001.

80. Khezri, R., 2000. Finite element simulation of crash testing of self-piercing riveting of deep drawing and rephosphorized sheet steel, Swedish Institute for Metal Research Report No.IM-2000-25.

81. Westerberg, C., 2002. Finite element simulation of crash testing of self-piercing rivet joints, peel specimen, MS Dissertation. Lund University, Sweden.

82. Stromstedt, E., 2002. Finite element simulation of crash testing of self-piercing rivet lap shear joint specimens, Swedish Institute for Metal Research Report No. IM-2002022.

83. Tang, D., Barthelemy, B., Yuan, H., 2002. Self-pierced rivet (SPR) modelling in aluminium structure crash analysis. In: Proceedings of the ASME International Mechanical Engineering Congress and Exposition IMECE 2002, November 17–22, New Orleans, LA, pp. 207–222.

84. Sui, B., Du, D., Chang, B., 2004. Finite element analysis of self-piercing riveting process. In: Proceedings of the ASME International Mechanical Engineering Congress and Exposition IMECE 2004, November 13–20, Anaheim, CA, USA, pp. 149–160.

85. Kim, M.G., Kim, J.H., Lee, K.C., Yi, W., 2005. Assessment for structural stiffness and fatigue life on self-piercing rivet of car bodies. Key Eng. Mater. 297–300, 2519–25.

86. Atzeni, E., Ippolito, R., Settineri, L., 2003. Analysis of the self-piercing riveting process. In: Proceedings of the Sixth AITEM Conference, Gaeta, Italy, pp. 281–292.

87. Atzeni, E., Ippolito, R., Settineri, L., 2004. Numerical and laboratory experiments on self-piercing riveting. In: Proceedings of the fourth CIRP International Seminar on Intelligent Computation in Manufacturing Engineering, Sorrento, Italy, pp. 305–309.

88. Atzeni, E., Ippolito, R., Settineri, L., 2005. Experimental and numerical investigation on self-piercing riveting, SME Technical Paper TP05PUB94.

89. Porcaro, R., Hanssen, A.G., Aalberg, A., Langseth, M., 2004. Joining of aluminium using self-piercing riveting: testing, modelling and analysis. Int. J. Crashworthiness 9 (2), 141–154. journal of materials processing technology 199 (2008) 27–36.

90. Porcaro, R., Hanssen, A.G., Langseth, M., Aalberg, A., 2006a. The behaviour of a self-piercing riveted connection under quasi-static loading conditions. Int. J. Solids Struc. 43, 5110–5131.

91. Porcaro, R., Hanssen, A.G., Langseth, M., Aalberg, A., 2006b. Self-piercing riveting process: an experimental and numerical investigation. J. Mater. Process. Technol. 171 (1), 10–20.

92. Patrick, E.P., Sharp, M.L., 1992. Joining aluminium auto body structure, SAE Technical paper 920282, pp. 1–8.

93. The Welding Institute TWI. http://www.twi.co.uk, (27 August 2007).

94. Varis, J., 2006. Economics of clinched joint compared to riveted joint and example of applying calculations to a volume product. J. Mater. Process. Technol. 172 (1), 130–138.

95. Corrosion protection of oil-field equipment // E.M. Gutman, K.R.Nizamov, M.D.Getmansky, E.A. Nizamov. – Moscow: Nedra, 1983, 152 p. (in Russian)

96. Emi H, Kumano A, Baba N, Yamamoto N, Nakamura Y, Shihara H. A study on life assessment of ships and offshore structures (Part 1: basic study)// J. Soc. Nav. Archit. Jpn. - 1991, No.169.- p. 443–454.

97. Emi H, Yuasa M, Kumano A, Arima T, Yamamoto N, Umino M. A study on life assessment of ships and offshore structures (3rd report: corrosion control and condition evaluation for a long life service of the ship)// J. Soc. Nav. Archit. Jpn. – 1993, No. 174. – p. 735–744.

98. Theory of corrosion processes // Isaev N.I. – Moscow: Metallurgy, 1997. – 361 p. (in Russian).

99. http://www.cathedral.ru/cathedra/num2/demidov, (13 April 2008).

100. Y.V.Baranov, O.A.Troitskiy, et al. Physical bases of electro-impulse and electro-plastic treatments and new materials. – Moscow: MGIU, 2001. – 844 p. (in Russian).

101. G.Stepanov, A. Babutsky and L. Krushka. Metal behavior under passage of impulse electric current.-J.Phys.IV France 110 (2003), p.577-582.

102. G.V.Stepanov, A.I.Babutsky, G.V.Chyzhyk Estimation of impulse electric current influence on strength of metallic materials // Metals science and treatment (Metaloznavstvo ta obrobka metaliv) – 2005, №2.- P. 64-68 (in Ukrainian).

103. G. V. Stepanov, A. I. Babutskii, I. A. Mameev High-density pulse current-induced unsteady stress-strain state in a long rod // Strength of Materials. - Vol. 36, No. 4, 2004. – p. 377-381.

104. Elisabete Almeida, Manuel Morcillo, "Lap-joint corrosion of automotive coated materials in chlorine media. Part 1 – Electrogalvanized steel", Surface Coatings Technology 124 (2000) 169-179.

105. Kulak. G. L, Fisher. J. W and Struik. J. H. A, *"Guide to design criteria for bolted and riveted joints",* Second Edition, John Wiley & Sons, Inc., ISBN 0-471-83791-1, 1987.

106. http://autoweb.autospeed.com/cms/A_110770/article.html, (16 June 2008).

LIST OF PUBLICATIONS

1. A.I. Babutskii, A. Chrysanthou, J. Ioannou, "Effect of pulsed electric current treatment on corrosion of structural metals" (2009), Strength of Materials 41 (4), 387-393.

2. A.I. Babutskii, A. Chrysanthou, J. Ioannou and I, Mamuzic, "Correlation between of corrosion resistance and hardness scattering of structural metals treated by pulse electric current", Materiali in Technologije, (2010),44,99-102.

3. A. Chrysanthou, L. Han, J. Ioannou and J.M. O' Sullivan, "Self-Piercing Riveted Joints Between Aluminium 5182 And Interstitial-Free Steel" Proceedings of the 3rd International Conference on Manufacturing Research Ed. JX Gao, DI Baxter and PL Sackett, Cranfield University, 6-8 September 2005.